ABSTRACT

Title of Thesis:	RUTTING PERFOMANCE OF RECYCLED ASPHALT PAVEMENTS
	Azadeh Farzaneh, Master of Science, 2016
Thesis directed by:	Professor Charles Schwartz, Department of Civil and Environmental Engineering

Cold in-place recycling (CIR) and cold central plant recycling (CCPR) of asphalt concrete (AC) and/or full-depth reclamation (FDR) of AC and aggregate base are faster and less costly rehabilitation alternatives to conventional reconstruction for structurally distressed pavements. This study examines 26 different rehabilitation projects across the USA and Canada. Field cores from these projects were tested for dynamic modulus and repeated load permanent deformation. These structural characteristics are compared to reference values for hot mix asphalt (HMA). A rutting sensitivity analysis was performed on two rehabilitation scenarios with recycled and conventional HMA structural overlays in different climatic conditions using the Mechanistic Empirical Pavement Design (MEPDG). The cold-recycled scenarios exhibited performance similar to that of HMA overlays for most cases. The exceptions were the cases with thin HMA wearing courses and/or very poor cold-recycled material quality. The overall conclusion

is that properly designed CIR/FDR/CCPR cold-recycled materials are a viable alternative to virgin HMA materials.

RUTTING PERFORMANCE OF ASPHALT PAVEMENTS

by

Azadeh Farzaneh

Thesis submitted to the Faculty of the Graduate School of the
University of Maryland, College Park, in partial fulfillment
of the requirements for the degree of
Master of Science
2016

Advisory Committee:
Professor Charles Schwartz, Chair
Associate Professor Dimitrios G. Goulias
Professor M. Sherif Aggour

Dedication

To my beloved parents.

Acknowledgements

I would like to thank to those who helped me getting this work done.
First of all, I want to thank to my advisor Dr. Charles Schwartz, who constantly guided me through this learning journey and provided the support during my studies at University of Maryland.
I also like to thank National Cooperative Highway Research Program and prestigious A. James Clark dean fellowship of School of Engineering, University of Maryland that provided the funding.
I am thankful to civil engineering faculty member Dr. Dimitrios G. Goulias and Dr. M. Sherif Aggour whom I had the opportunity to learn a lot from.
I want to thank my dear friend Ali Asadabadi who his precision and delicacy helped completing my thesis.
I want to thank dear Dr. Al-Sheikhly who supported me as well in my studies.

Table of Contents

List of Tables

List of Figures

Chapter 1: Introduction

Pavement recycling using asphalt-stabilized cold-recycling processes has become increasingly popular in recent years. Cold recycling reuses the existing asphalt layer to construct a new layer using the old materials plus a stabilizer. The reasons for this increased popularity are: cold-recycling costs less than constructing new pavements; it is environmental friendly and sustainable; it reduces construction waste materials; and it reduces the need for virgin materials.

This study considers cold-recycling processes using asphalt stabilizers, often with additional additives. The specific cold-recycling processes considered in this study are cold in-place recycling (CIR), cold central-plant recycling (CCPR), and full-depth reclamation (FDR). In the CIR process, the upper portion of the asphalt layer is milled, mixed with an asphalt stabilizer (foamed asphalt or asphalt emulsion), and then placed back onto the roadway. It is then covered with a thin hot mix asphalt (HMA) wearing course. CIR has been performed in many states across the US, especially in the central and western areas of the country. A set of equipment called a CIR train performs all of the required procedures: milling, grading, crushing, mixing, paving, and compacting. Technology improvements over time have made these trains smaller and more versatile. Additives are often used to enhance the performance of the CIR layer. These additives include lime, fly ash, cement, lime kiln dust (ARRA, 2001).

CCPR is a similar cold-recycling method in which the milled asphalt material is transported to a nearby (usually mobile) production plant for mixing with stabilizer and additives. The cold-recycled material is then transported back to the project site and placed using conventional paving techniques. One advantages of the CCPR method is that the recycled materials can be stored while the underlying layer is enhanced. The stockpiled materials can also be used for constructing new pavements, reducing the need for virgin materials.

FDR is used when there is a deep-seated deficiency in the pavement section that cannot be repaired by only recycling a few inches on top. The FDR process removes the full asphalt layer along with some portion of the underlying unbound layer and/or subgrade. This material is then mixed with asphalt stabilizer and optional additives and then placed back on the excavated surface and compacted. An asphalt overlay (either CCPR or HMA) and an HMA wearing course are then placed on top of the FDR layer.

All of the projects in this study used either foamed asphalt or asphalt emulsions as the stabilizing agents. Foamed asphalt is formed by injecting cold water and compressed air into hot liquid asphalt binder. The water turns into vapor and creates bubbles in the asphalt. The foamed asphalt is then sprayed over the cold aggregates. Asphalt emulsions use water to emulsify the liquid asphalt binder. The emulsified asphalt is mixed with the cold aggregates. Numerous studies have described the satisfactory performance of both foamed asphalt and asphalt emulsion stabilization (Kim et al., 2012, L Mohammad et al., 2003, Diefenderfer et al.,2011).

1.1 Study Objectives

The lack of quantitative values for the engineering properties of CIR/FDR/CCPR materials that can be used with confidence in pavement structural design is the greatest impediment to more widespread usage of these fast, cost-effective, and sustainable rehabilitation strategies. Laboratory measurement of relevant structurally-related properties during design is problematic, both due to the difficulties of simulating field mixing, compaction, and curing conditions in the laboratory and because of the practical infeasibility of performing sophisticated material property testing for routine production design. The purpose of this study is to assess CIR/FDR/CCPR structural properties from laboratory test data of field cores from the cured layers. This study, which is part of the larger National Cooperative Highway Research Program (NCHRP) Project 9-51, analyzes test data measured by the Virginia Center for Transportation Research (VCTR) to derive the material property inputs for CIR/FDR/CCPR materials required by the Mechanistic-Empirical Pavement Design Guide (MEPDG). The study also evaluates the rutting behavior of these materials and their performance in comparison to conventional HMA materials.

1.2 Literature Review

The structural material properties required by the MEPDG are the dynamic modulus (DM) and the repeated load permanent deformation (RPLD) characteristics.

1.2.1 Dynamic Modulus:

Cold-recycled materials behave similarly to conventional HMA in that their stiffness varies with temperature and loading rate. Therefore, dynamic modulus is used to characterize the stiffness of cold-recycled materials. Diefenderfer at al (2015) performed statistical tests on measured dynamic moduli from different projects and found that there is no significant difference in the range of dynamic moduli for different types of recycling processes (CIR, CCPR, FDR).

1.2.2 Permanent Deformation

Permanent deformation or rutting is the plastic deformation of the pavement. Rutting can be due to insufficient subgrade support, inappropriate compaction, substandard materials, or improper structural design.

Long and Ventura (2004) performed a triaxial test at 4Hz on good-quality granular material stabilized with cement and variable foam asphalt content. They performed the test with different confining pressures and relative densities. They concluded that for stress-to-strength ratios below 0.6, permanent deformation is small and mostly dependent on aggregate skeleton and material type and strength. However, for ratios greater than 0.6 permanent deformations increases significantly. The study also showed an increase in permanent deformation by increasing foam content.

Fu *et al*. (2010) investigated role of cement content on rutting resistance of foam stabilized RAP. The study showed that cement improved the material's rut-resistance even in soaked conditions.

Mohammad *et al*. (2006) investigated rutting susceptibility of three groups of materials: (1)non-stabilized 100% RAP, (2) a blend of 50% foamed stabilized RAP plus 50% soil cement, and (3) a foam stabilized 100% RAP. The RLPD test was performed to 10,000 cycles at 10 Hz with a cyclic 15 psi deviatoric stress at a constant 5 psi confinement pressure. The final permanent deformation of the materials was 3000, 5000, and 21,000 $\mu\varepsilon$, respectively. Thus the 100% foam-stabilized RAP had the highest and the non-stabilized had the lowest measured permanent deformation. The authors did not state reasons for such behavior.

Kim *et al*. (2009) performed uniaxial RLPD tests on seven different RAP sections in Iowa at 10Hz and 104°F. They again showed that higher foam contents result in increased permanent deformation.

1.2.3 Recycled Pavement Performance:

Cold-recycling is a relatively new technology, and thus there is little in the literature on the performance of these pavements over long periods. The Nevada DOT performed a long-term performance analysis on CIR sections built on low and medium traffic volume roads. In these sections, the CIR layer was covered with a thin HMA wearing course. All of the sections showed excellent performance under field and laboratory tests (Sebaaly et al., 2004). Bemanian et al. (2006) performed a life-cycle analysis of CIR and FDR sections constructed in Nevada and concluded that they showed good long-term performance and saved more than $600M over a 20 year period. Jahren at al. (1998) documented the performance of CIR pavements in Iowa in another study. They showed that for low-volume traffic the sections had an average predicted life-time of 16-25 years and field investigation showed little rutting during the five years of performance modeling. Morian et al (2004) also demonstrated that CIR is a cost-effective rehabilitation method. They investigate four sections with different resurfacing strategies over 21 years. Among the different strategies, the life cycle performance of sections rehabilitated using cold-recycling was not significantly different from sections rebuilt with conventional HMA materials. Kazmierowski *et al*. (1999) proved after 10 years of studying Ontario pavements that CIR has the same degradation rate as conventional HMA. Sebaaly et al. (2004) showed that rehabilitation of a heavily rutted pavement using a CIR overlay and a thin HMA wearing course exhibited no significant rutting after five years of evaluation.

Chen et al. (2010) studied the long-term performance of CIR asphalt roads based on the PCI (Pavement Condition Index) and Falling Weigh Deflectometer. It showed that the CIR layers with smaller modulus values and higher void ratios resulted in better performance and concluded that less stiff CIR layers prevent cracks from propagating from underlying layers to the HMA. In another study, Sanjeevan et al (2014) compared CIR with HMA overlays followed only by a surface treatment. They found the HMA overlay resulted in a much better performance. They also concluded that climate condition, CIR thickness, and surface treatment type do not influence the road serviceability.

Other literatures relevant to specialized topics in this thesis are covered in context in the subsequent chapters.

Chapter 2: Test Sites

This chapter provides a brief description of each rehabilitation project. The total of 26 projects were included in the NCHRP Project -51 study: 16 were CIR, 6 FDR, and 4 CCPR. Seventeen of these projects were stabilized with emulsion and 9 with foam. Table 2.1 summarizes the projects and their assigned identification numbers. The projects will be referenced by their assigned identification numbers throughout this thesis. Figure 2.1 presents the geographical distribution of these 26 projects.

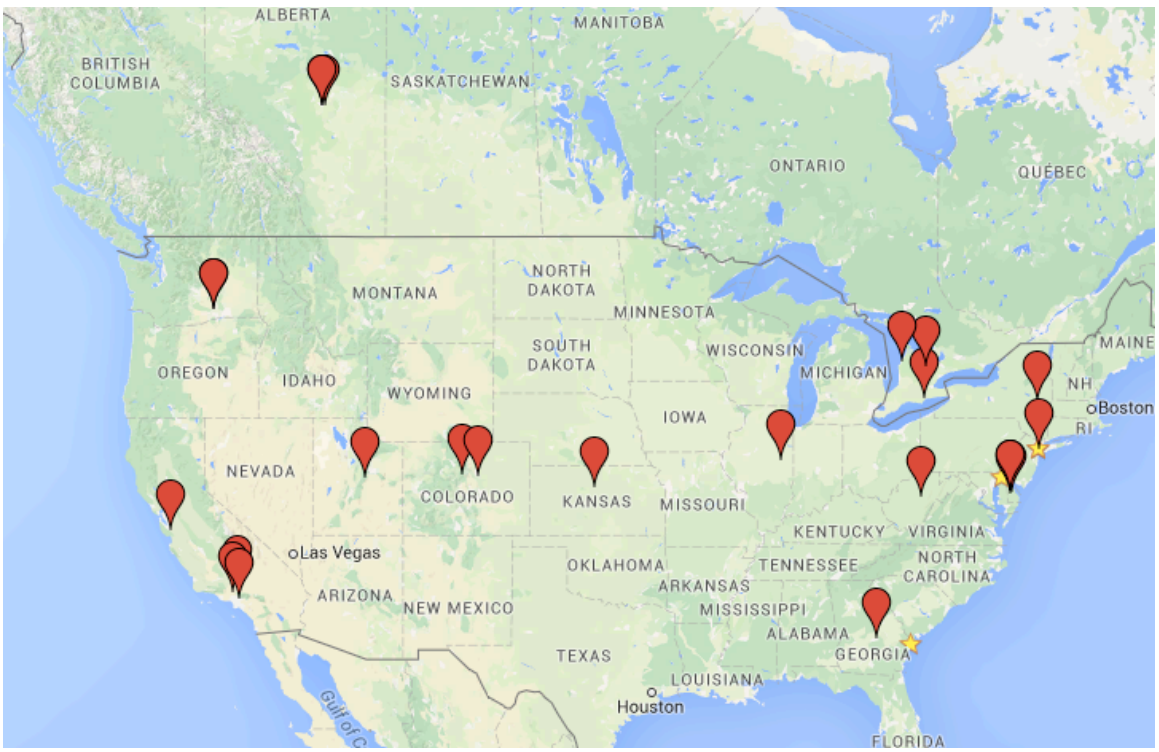

Figure 2.1- Geographical distribution of projects across the USA and Canada

Table 2.1. NCHRP 9-51 projects.

Project Name	Location	Route	Type	Stabilizer Content
13-1093	Kansas, USA	Scott county, KS 96	CIR	2.5% Emulsion
13-1111	Ontario, Canada	Hwy 10/89	CIR	1% Foam
13-1112	Ontario, Canada	Hwy 21 / Tiverton to Port Elgin	CIR	1.2% Foam
13-1113	Ontario, Canada	Hwy 24	CIR	1% Emulsion
13-1114	Ontario, Canada	Hwy 21 / Amberley to Kincardine	CIR	1.2% Emulsion
13-1115	Edmonton, Canada	Dovercourt, 141 Street	FDR	2.5% Foam
13-1116	Edmonton, Canada	Windsor Park 1, 92 Avenue	FDR	2% Foam
13-1117	Edmonton, Canada	Windsor Park 2, 117 Street	FDR	2.5% Foam
13-1124	California (San Jose), USA	Redmond Avenue	CIR	2.2% Foam
13-1127	Colorado, USA	State Highway 83	CIR	2.5% Emulsion
14-1001	California (LA County), USA	50th Street West	CCPR	3% Emulsion
14-1002	California (LA County), USA	Vasquez Canyon Road	CIR	3% Emulsion
14-1003	California (LA County), USA	Altadena Drive	CIR	3% Emulsion
14-1011	West Virginia, USA	Fort Martin Road	CIR	3.4% Emulsion
14-1025	Delaware, USA	Seashore Hwy (Lewes/Georgetown Hwy)	CIR	3.5% Emulsion
14-1026	Delaware, USA	Gravel Hill Road	CIR	3.5% Emulsion
14-1027	Delaware, USA	Springfield Road	FDR	3.5% Emulsion
14-1028	Delaware, USA	Sussex Pine Road	FDR	3.5% Emulsion
14-1055	Utah, USA	SR 32	CIR	Emulsion
14-1057	Georgia, USA	Kelly Mill Road	FDR	2% Foam
14-1058	Washington, USA	SR 14	CIR	2% Emulsion
14-1062	Colorado, USA	SH-160, Cortez	CIR	3% Emulsion
15-1002	Maine, USA	Corinna, Exeter	CCPR	3% Emulsion
15-1003	Maine, USA	Lyman	CCPR	3.5% Emulsion
I-81CIR	Virginia, USA	Southbound Hwy I-81	CIR	2% Foam
I-81CCPR	Virginia, USA	Southbound Hwy I-81	CCPR	2% Foam

2.1 *HMA Mixtures*

Several HMA mixtures are employed in this study as a reference for comparison with the cold-recycled materials. These mixtures were produced and tested in the Maryland State Highway Administration asphalt laboratory. The names of these mixtures and their main characteristics are summarized in Table 2.2.

Table 2.2. HMA mixtures names

Mix Name	NMAS	Binder Grade	Mix Method
H077A09A2C03	9.5	64-22	Hot mix
H083A12C2C02	12.5	64-22	Hot mix
H127A12R2C02	12.5	64-22	Hot mix
H135A12H2C02	12.5	64-22	Hot mix
H135A19G4F01	19	76-22	Hot mix
H151B19R2C02	19	64-22	Warm mix
H160A09R1C03	9.5	64-22	Hot mix
H168A09R2C03	9.5	64-22	Hot mix

Chapter 3: Structural Properties

The material structural properties required by the MEPDG for asphaltic materials, including asphalt-stabilized cold-recycled materials, are the dynamic modulus and repeated load permanent deformation characteristics. Dynamic modulus (DM) and repeated load permanent deformation (RLPD) tests were performed as part of NCHRP Project 9-51 by the Virginia Transportation Research Council (VTRC) on field cores collected from rehabilitation projects. All VCTR tests were performed using an IPC Asphalt Mixture Performance Tester (AMPT). Brief descriptions of the AMPT device and the DM and RLPD test protocols are provided in the following sections. HMA mixtures used for comparison were tested at the Maryland State Highway Administration (MSHA) by Intikhab Haider, also using an IPC AMPT. This chapter describes the tests performed on the cores and explains how these test data were processed. The "Raw Data" section describes the test apparatus and procedures while the "Processed Data" section examines how test data were manipulated for the research purposes of this study.

3.1 Raw Data

3.1.1 AMPT Apparatus

AMPT device was the offshoot of research from NCHRP 9-19 *Superpave Support and Performance Models Management* (*1*) and 9-29 *Simple Performance Tester for Superpave Mix Design*. The AMPT provides a simplified method for characterizing asphalt mixtures for the purposes of constructing dynamic modulus master curves and determining repeated load permanent deformation properties for input into MEPDG. The AMPT tests specimens having a 100 mm (4 in) diameter and 150 mm (6 in) height. These are prepared from larger gyratory compactor specimens according to AASHTO TP 60 Provisional Standard Practice for Preparation of Cylindrical Performance Test Specimens Using the Superpave Gyratory Compactor (SGC). For dynamic modulus testing, the apparatus applies sinusoidal loads at different frequencies and temperatures. It reports the dynamic modulus value as the ratio of peak stress over peak strain (Equation 3.1). This apparatus also measures the rutting susceptibility of a mixture. It applies a repetitive haversine load at a constant 0.1 sec load cycle and 0.9 sec rest period at various temperatures and records the permanent strains at each cycle. A schematic of the device and applied load is illustrated in Figure 3.1.

$$|E^*| = \frac{\sigma_{\max}}{\varepsilon_{\max}} \qquad \text{Equation 3.1}$$

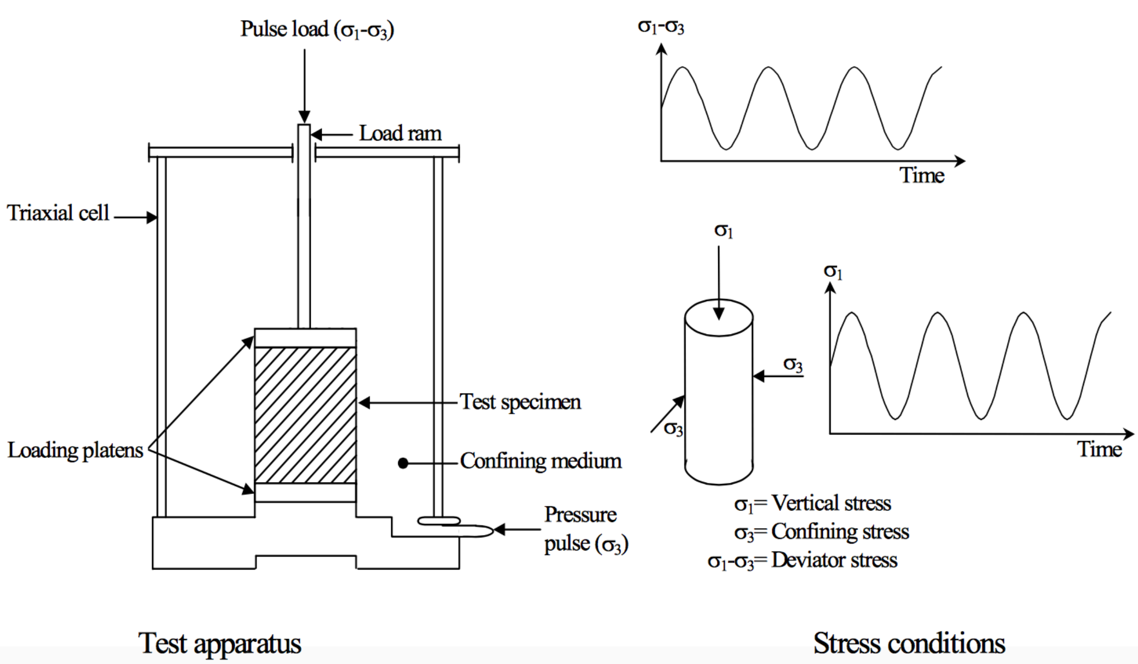

Figure 3.1. AMPT apparatus, DM and RLPD test (Brown et. al., 2001)

3.2 Dynamic Modulus Test

3.2.1 Test on cores from Rehabilitated projects

Cores were tested according to AASHTO TP 79 Standard Method of Test for Determining the Dynamic Modulus and Flow Number for Hot Mix Asphalt (HMA) Using the Asphalt Mixture Performance Tester (AMPT). Some modifications were made to AASHTO TP 79 for this study. These included performing the test at fewer temperatures (4.4,21.1 and 37.8°C) and performing the test on small-scale specimens. Obtaining a core with 150 mm height is not practical in CIR projects since the thickness of the layer is usually much less than the required 150 mm. A study was conducted by Diefenderfer et al. (2015) to evaluate the feasibility of measuring dynamic modulus from samples having smaller diameters and heights cored horizontally from the field. Four sample sizes with 2 different diameters (38 and 50 mm) and two heights (110 and 135 mm) were evaluated. The evaluation testing was conducted on HMA mixtures having four different Nominal Maximum Aggregate Sizes (NMAS) of 9.5, 12.5, 19 and 25 mm. The measured dynamic moduli at for the small-scale and conventional-sized specimen were essentially the same for the 9.5 and 12.5 mm mixtures. The differences for the 19 and 25 mm mixtures were larger. Consequently, it was recommended that the small sized specimens be used only for the 9.5 and 12.5 mm mixtures and that testing for larger NMAS mixtures be conducted on conventional-sized specimens. The results from this study provided justification for using small-scale specimens for testing the cold-recycled materials.

The cold-recycled materials in NCHRP Project 9-51 were tested at three temperatures (4.4, 21.1 and 37.8°C) and six frequencies (0.1, 0.5, 1, 5, 10 and 25 Hz). Testing started from the lowest temperature and highest frequency to minimize damage to the test specimens.

3.2.2 Tests on HMA Cores

Dynamic modulus tests of HMA mixtures were performed at the Maryland State Highway Administration Office of Material Technologies. The replicates were prepared according to AASHTO PP 60-09. The specimens had the standard 150 mm height and 100 mm diameter. The dynamic modulus test was performed in the AMPT at three temperatures (4.4,21.1 and 37.8°C) and 3 frequencies at each temperature (0.1, 1, 10) with an additional frequency of 0.01 at 37.8°C. Detailed information on these mixtures is provided in Appendix III.

3.3 Repeated Load Permanent Deformation Test

The repeated load permanent deformation (RLPD) test is used to evaluate the rutting potential of asphaltic materials. In this test, the permanent deformations are measured after each load cycle, producing a plot similar to Figure 3.2. The RLPD behavior has three stages:

1. Primary zone (1): There is a rapid accumulation of strains in this stage as the sample densifies.
2. Secondary zone (2): The accumulation rate is reduced in this stage and the graph has a constant slope in log-log space. The RLPD behavior in the secondary zone can be characterized by the slope (b) and intercept (a). This stage is the most

important part of the RLPD test, as it corresponds to most of the service life of a real pavement.

3. Tertiary zone (3): In this stage the accumulation rate accelerates again and the sample goes into a tertiary flow.

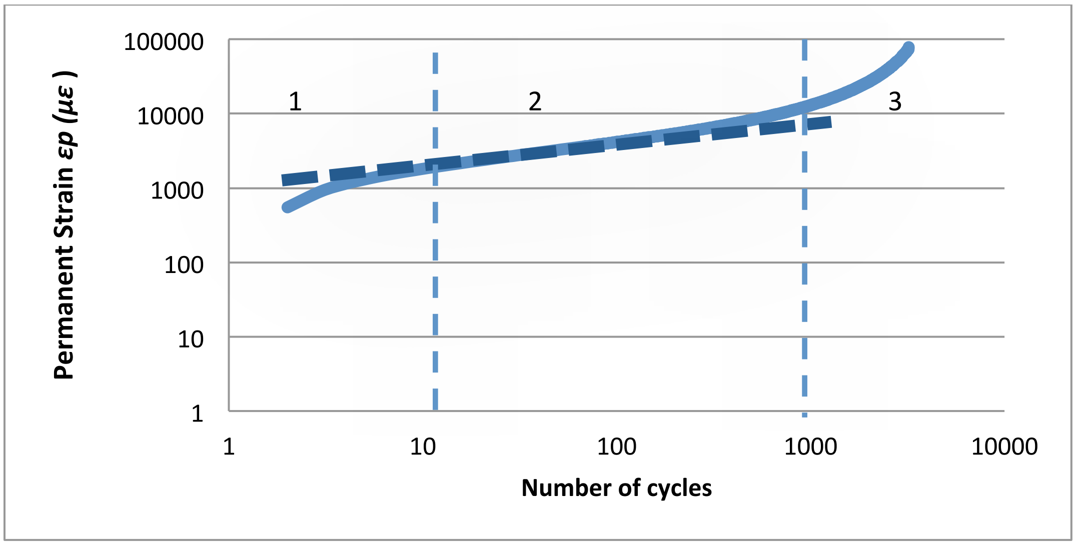

Figure 3.2. Schematic of permanent strain vs. cycle. The numbers above the curve indicate the stage of the response.

3.3.1 Test on cores from rehabilitated projects

Repeated load permanent deformation tests in this study were performed using the IPC AMPT device at 10 psi confining pressure and 70 psi deviator stress. For the cold-recycled materials, small-scale specimens 50 mm in diameter and 110 mm in height were tested. The test was performed at a single temperature of 45°C.

3.3.2 Tests on HMA cores

Nine test specimens were prepared for each HMA mixture. Three of these were used for the dynamic modulus test. The RLPD test was performed on all 9 specimens, including the re-use of the three specimens from the dynamic modulus test. The RLPD test was performed at three temperatures (20, 40 and 58°C); three replicate specimens were tested at each temperature. The test procedure was similar to that for the cold-recycled materials except for the size of the specimen. The HMA specimens were the conventional 150 mm in height and 100 mm in diameter.

3.4 Processed Data

3.4.1 Dynamic Modulus Master Curve

A dynamic modulus master curve was constructed from the laboratory-measured test data. The reference temperature for the master curve was selected as 21.1°C. The sigmoidal function employed in the MEPDG was used to fit the data (Equation 3.2).

$$\log|E^*| = \log(\min) + \frac{\log(\max) - \log(\min)}{1 + e^{\beta + \gamma \log \omega_r}} \qquad \text{Equation 3.2}$$

in which

$|E^*|$ = dynamic modulus

ω_r = reduced frequency at reference temperature, Hz

$|E^*|_{max}$ = limiting maximum mixture dynamic modulus, ksi

$|E^*|_{min}$ = limiting minimum mixture dynamic modulus, ksi

$\beta, and\ \gamma$ = fitting parameters

The reduced frequency is computed as:

$$\log \omega_r = \log \omega + \log[a(T)] \qquad \text{Equation 3.3}$$

in which

ω= frequency at the test temperature

$a(T)$ = the temperature shift factor at the test temperature

The Arrhenius equation was used as the temperature shift function:

$$\log[a(T)] = \frac{\Delta E_a}{19.14714}\left(\frac{1}{T} - \frac{1}{T_r}\right) \qquad \text{Equation 3.4}$$

in which

T_r = reference temperature, °K

T = test temperature, °K

ΔE_a = activation energy (treated as a fitting parameter)

A Matlab code was developed to fit the master curves. The code used a multidimensional unconstrained nonlinear minimization function (fminsearch) to determine β, γ, EA, $|E^*|_{min}$, $|E^*|_{max}$. Each material had at least 3 specimens that were tested for dynamic modulus and some projects had up to 16 specimens. A single master curve was fit to the entire set of replicates for each material. More than 65% of the fitted master curves had R^2 values greater than 0.8 and only 11% had R^2 values less than 0.5. The materials with the lower goodness-of-fit statistics was usually had a higher number of specimens and high specimen-to-specimen variability. For example, two materials having 12 and 18 specimens each had the lowest R^2 values. A typical fitted master curve is depicted in Figure 3.3. Rest of master-curves are added in Appendix I.

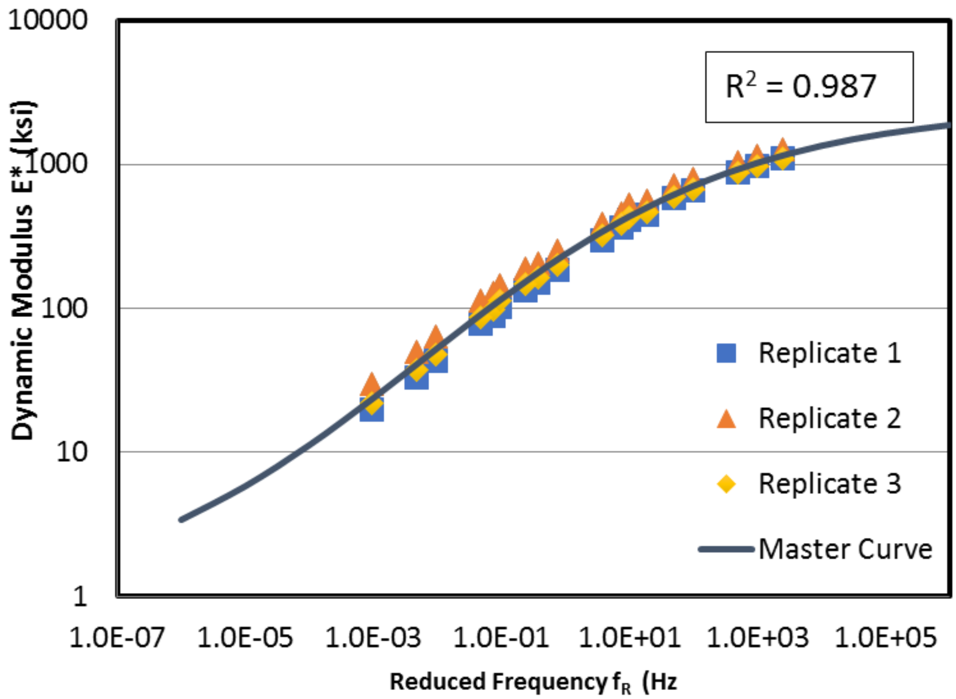

Figure 3.3. Fitted dynamic modulus master curve for Delaware CIR material.

3.4.2 RLPD Properties

The log-log RLPD characterization model in the MEPDG was fit to the laboratory RLPD test data Equation 3.5).

$$\frac{\varepsilon_p}{\varepsilon_r} = k_z \beta_{r1} 10^{k_1} T^{k_2 \beta_{r2}} N^{k_3 \beta_{r3}} \qquad \text{Equation 3.5}$$

$$k_z = (C_1 + C_2 * depth) * 0.328196^{depth}$$

$$C_1 = -0.1030 * H_\alpha^2 + 2.4868 * H_\alpha - 17.342$$
$$C_2 = 0.0172 * H_\alpha^2 - 0.7331 * H_\alpha = 27.428$$

in which:

ε_p = plastic strain

ε_r = resilient strain

T = layer Temperature(°F)

N = Number of load repetitions

The Excel Solver tool was used initially to find the RLPD coefficients but the fitted models had large errors. Thus another approach was taken. Multiple regression was used to fit a single linear model to the data. The strain ratio ($\frac{\varepsilon_p}{\varepsilon_r}$) was set as the dependent variable and temperature *T* and number of cycles *N* were set as the independent variables. The depth function k_z was set to 1, as it is not relevant for interpreting laboratory test data having homogeneous stress conditions. The resilient strain is not measured or recorded by the IPC AMPT and thus was estimated using the deviator stress and dynamic modulus E* at the RLPD test temperature and frequency (10 Hz). The k_1, k_2, and k_3 material coefficients were fitted to MEPDG rutting model and β_{r1}, β_{r2}, β_{r3} field calibration coefficients were assumed to be equal to 1.

The RLPD tests on the cold-recycled materials were performed at only a single temperature. The MEPDG rutting model is dependent on temperature, so plastic strain data at at least two other temperatures are needed. The technique developed by Khosravifar et al. (2014) was used to predict plastic deformations at other temperatures. The process is similar to fitting a master curve; after a reference temperature is picked, the Arrhenius temperature shift function (Equation 3.4) determined from the dynamic modulus testing is used to shift the permanent strain data to the desired temperature (Figure 3.4). This is done using the concept of reduced load cycles and reduced intercept, similar to the concept of reduced frequencies in dynamic modulus testing:

$$\log(N_R) = \log(N) - \log[a(T)]$$
$$\log A' = \log A + B \log a(T)$$

in which

A = Intercept of secondary zone, described in RLPD Test section

B = Slope of secondary zone

The HMA materials were tested at three temperatures, so there was no need to predict the permanent deformations at other temperatures for these materials. A typical fitted RLPD model for a cold-recycled material is depicted in Figure 3.5. RLPD graphs of materials are added in Appendix II.

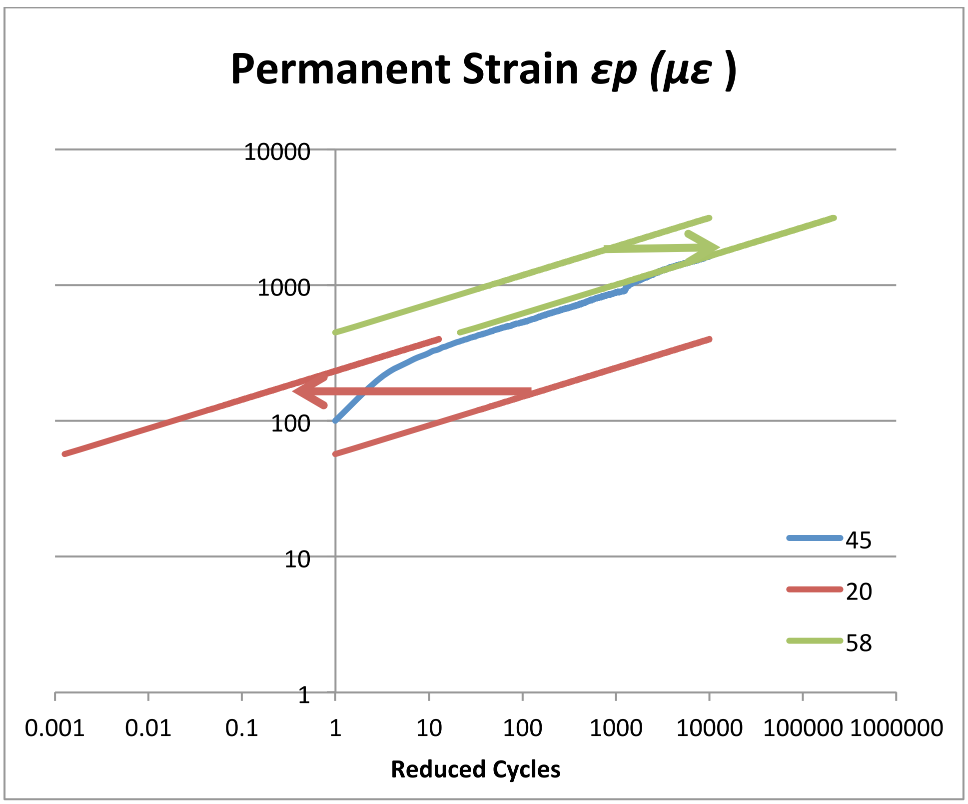

Figure 3.4. Time-temperature shift factor to form a RLPD master curve using Khosravifar et al. (2014) method.

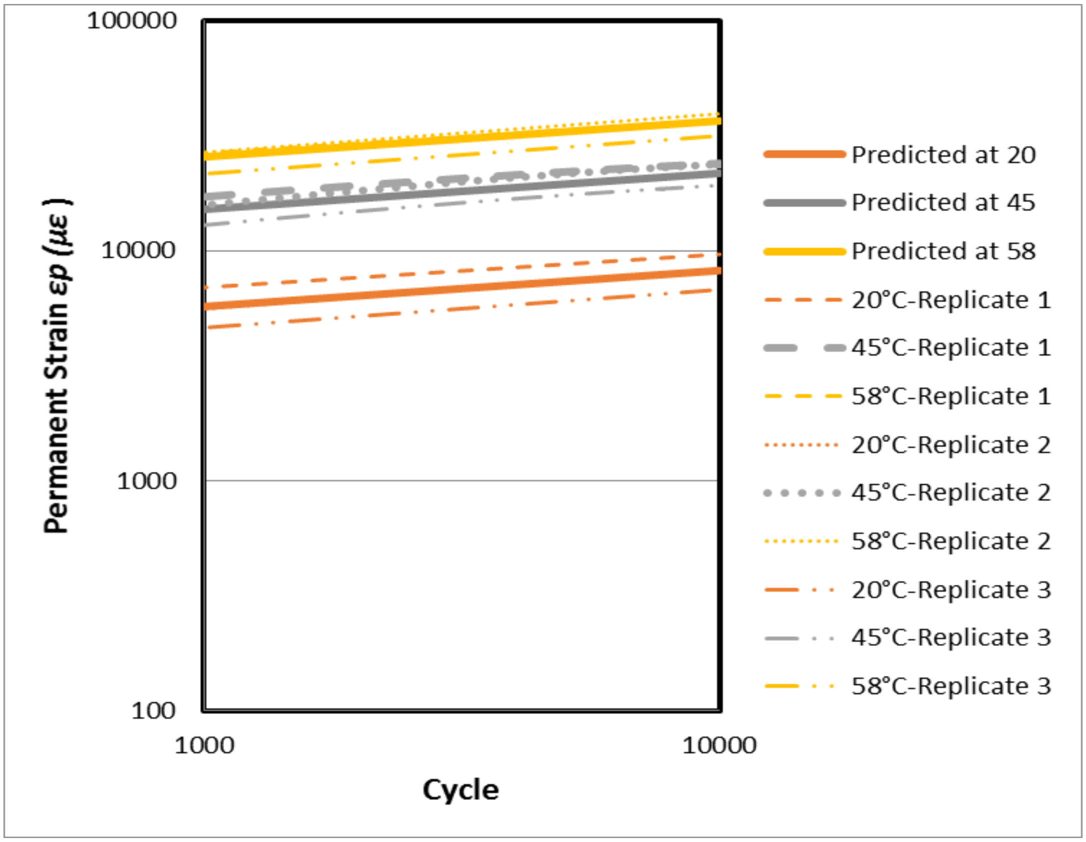

Figure 3.5. Typical RLPD fitted model to Project 15-1003.

During the fitting procedure for some mixes, negative values were obtained for the temperature coefficient, which suggests that resilient strains are more sensitive to temperature than permanent strains. Figure 3.3.6 shows the rates of change for plastic strains and resilient strains at the 10,000th cycle. Each group of strains is normalized by its respective strain at 20°C; in other words, the plastic strains at each temperature are divided by the plastic strain at 20°C and the resilient strains are divided by the resilient strain at 20°C. These negative coefficients were due to the fact that Dynamic modulus tests on samples were performed in unconfined conditions that lead to lower stiffness at higher temperature. Thus confined modulus curves were produced to estimate appropriate resilient strains values. After calculation of true resilient strain values all βr_2 values were positive.

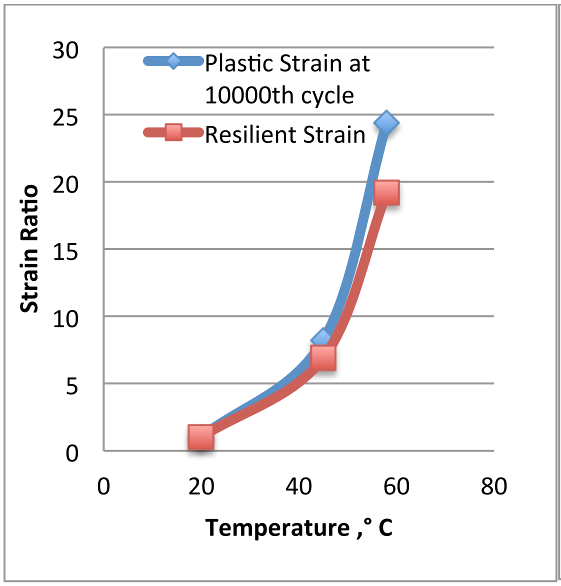

a.

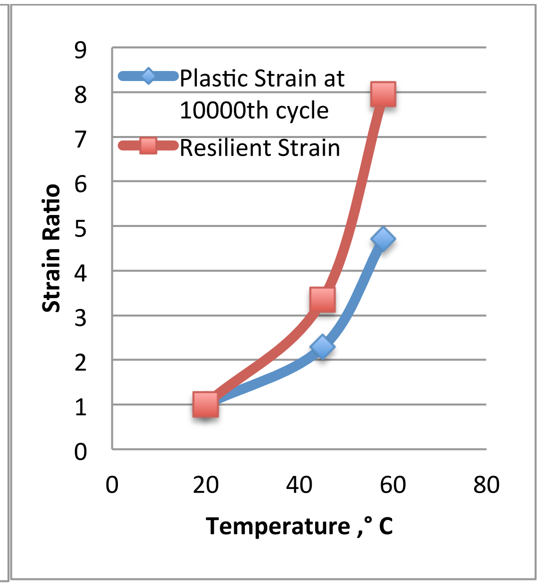

b.

Figure 3.3.6. Strain Ratio $\frac{\varepsilon}{\varepsilon_{at\,20C}}$: (a) Delaware CIR with positive temperature coefficient β_{r2}. (b) San Jose CIR with negative temperature coefficient.

Since resilient strains were not measured in the IPC AMPT they had to be calculated from the applied stresses and the dynamic modulus of the material. However, the RLPD test is performed under confined conditions while the dynamic modulus test is performed under unconfined conditions. Previous researchers (Zhao et al., 2012, Seo et al., 2007, Yun et al., 2010) have shown that there can be significant differences between confined and unconfined dynamic modulus values, especially at the high temperatures in the RLPD test.

In order to calculate resilient strains, confined dynamic modulus values are required. Zhao et al. (2012) proposed a model to derive confined dynamic modulus values at different confining pressures.

$$\ln(E) = \log(\min) + \frac{\log(\max) - \log(\min)}{1 + e^{\beta + \gamma(\ln(w_r))}} + \frac{C_5(e^{-C_6 P_0} - e^{-C_6 P})}{1 + e^{C_3 + C_4 \ln(w_r)}} \quad \text{Equation 3.6}$$

in which

C_3, C_4,C_5,C_6 = Fitting parameters

P_0 = Test Confining pressure

P = desired confining pressure

The model needs to be calibrated with confined dynamic modulus data. Zhao et al. (2012) performed the calibration for 19 mm and 25 mm Superpave HMA mixtures. For lack of any better approach, Zhao et al.'s calibrated coefficients for the 19 mm mix were assumed to be representative for the materials tested in this study. The coefficients are represented in the following table:

Table 3.1-Calibration coefficients for confined master curve

C3	**C4**	**C5**	**C6**
1.632	0.421	4.031	3.259

In the absence of any better approach, these calibrated coefficients were therefore used to estimate the confined modulus values for the HMA and cold-recycled materials in this study at the 10 psi confining pressure in the RLPD test and thus to estimate the resilient strains for the confined conditions. Typical confined vs. unconfined dynamic modulus master curves for a cold-recycled material as determined using this procedure are depicted in Figure 3.7.

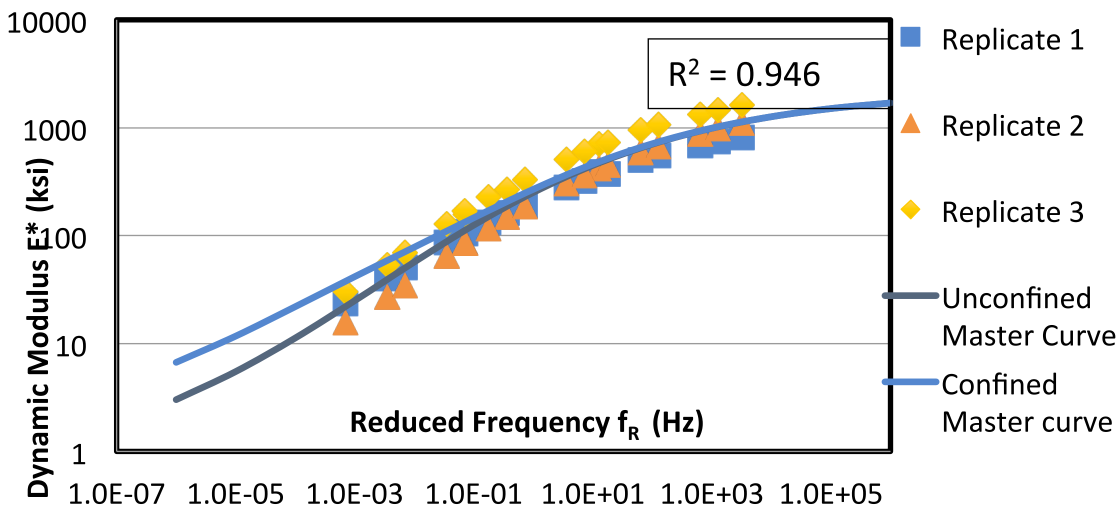

Figure 3.7. Confined vs. unconfined DM master curve of Project 13-1114

Summaries of the coefficients attained from applying these procedures to the cold-recycled and HMA materials are provided in Table 3.2 and Table 3.3, respectively.

Table 3.2. Fitting coefficients for HMA cores

	K1	K2	K3
H160A09	1.55E-01	0.821	0.163
H151B19	6.64E-01	0.407	0.228
H135A19	6.45E+00	0.101	0.117
H077A09	5.22E-01	0.610	0.130
H083A12	6.06E-02	1.018	0.138
H127A12	5.09E+00	0.100	0.144
H135A12	1.66E-01	0.787	0.124
H168A09	8.25E+00	0.0002	0.116

Table 3.3. Fitting coefficients of rehabilitated projects

	K1	K2	K3
13-1093	3.72E-07	3.3054	0.340
13-1111	1.61E-09	4.5055	0.530
13-1112	4.47E-03	1.5668	0.366
13-1113	5.62E-02	0.9332	0.304
13-1114	1.88E-01	0.7226	0.314

13-1115	1.59E+01	0.0687	0.027
13-1116	2.97E+00	0.2029	0.071
13-1117	6.06E-03	1.4279	0.126
13-1124	3.15E+00	0.1545	0.149
13-1127	2.11E+00	0.0968	0.155
14-1001	3.01E-04	2.1380	0.362
14-1002	1.73E-16	7.3551	0.705
14-1003	3.87E-03	1.5091	0.279
14-1011	2.92E-03	1.3187	0.183
14-1025	2.73E-02	1.1658	0.346
14-1026	3.03E-04	2.1724	0.413
14-1027	1.06E+00	0.5540	0.181
14-1028	3.17E-01	0.6648	0.118
14-1055	1.99E-08	4.0716	0.470
14-1057	2.39E-02	1.2063	0.140
14-1058	3.88E+00	0.2544	0.156
14-1062	5.58E-01	0.5587	0.168
15-1002	7.48E-05	2.3050	0.383
15-1003	4.47E+00	0.1373	0.159
I-81-CCPR	9.38E-06	2.7841	0.326

Chapter 4: Data Acquisition and Database Structure

A database containing all of the information for the NCHRP 9-51 projects was created with Microsoft Access 2010. The database consists of four parts. The first part contains pre-construction characteristics collected from State DOTs and contractors. Pre-construction data include mix design information and laboratory tests performed during mix design. The second part contains construction data collected from State DOTs or project contractors during recycling/paving operations. The third section contains test data from tests performed on cores extracted from project sites. Cores from each project were shipped to the Virginia Center for Transportation Research (VCTR) for testing. The last section contains the processed data—i.e., the material structural properties developed from the raw test data. A schematic of the database structure is presented in Table 4.1. The following subsections describe in more detail the information stored in the database. Complete documentation of the database and a listing of its contents are provided in Appendix III.

Table 4.1. Schematic of database structure

Data category	Info category	Detailed info
Pre- Construction data	Mix Design	Gradation
		Stabilizer type & content
		Dry additive type & content
		Strength & stability
		Moisture-Density relation
Construction data	Site Condition	Weather conditions & precipitation
		Pavement structural section & Traffic
	Equipment	Types
	QC/QA	Density control
Test data	Dynamic Modulus (DM) Repeated Load Permanent Deformations (RLPD)	
Processed data	DM master curve	Master curve fitted parameters
	RLPD fitted graphs	Permanent deformation calibration coefficients

4.1 Pre-Construction Characteristics

The project identification information and mixture design properties are the major component of the pre-construction characteristics. This includes all the information from the mix design in each project:

Mix Design Information

- Mix design type (CIR/CCPR/FDR)
- Gradation
- Stabilizer type
- Binder grade/emulsion type
- Stabilizer content
- Dry Additive type
- Dry additive content
- Moisture-Density relations (T99/T180)
- Strength and Stability Characteristics
    - IDT strength (T283)
        - Dry Indirect Tensile Strength
        - Wet Indirect Tensile Strength
        - Tensile Strength Ratio
    - Flow/stability (T245)
        - Soaked Stability
        - Unsoaked Stability
        - Flow Index $_{\text{soaked}}$
    - Flow Index$_{\text{Unsoaked}}$
- Raveling test

Not all data were available for all projects. Since the information was gathered from different agency, agencies performed different test protocols.

4.2 Construction Data

The construction information collected at the site included: type of recycling equipment, weather conditions before, during, and after construction, and the type of overlay. Information about the pavement structural sections before and after rehabilitation, expected traffic, and QC/QA (if performed) is also included here. Table elements for construction data are listed below:

- Average stabilizer content
- Average dry additive content
- Type of recycling equipment
- Depth of recycling
- Forward speed of equipment
- Roller characteristics
- Density control description
- Overlay thickness
- Pavement section before rehabilitation
- Pavement section after rehabilitation

Weather info

- Weather before construction
- Weather during construction
- Weather after construction
- Precipitation during construction

4.3 Test Data

Dynamic modulus test and repeated load permanent deformation test were performed on cores collected in this study. Data from these tests was stored in the database. The data elements stored for each test are provided below (these data were stored for each specimen for each project/material):

Modulus at 4.4°C

- E* at 4.4°C-0.1 Hz
- E* at 4.4°C-0.5 Hz
- E* at 4.4°C-1 Hz
- E* at 4.4°C-5 Hz
- E* at 4.4°C-10 Hz
- E* at 4.4°C-25 Hz

Modulus at 21.1°C

- E* at 21.1°C-0.1 Hz
- E* at 21.1°C-0.5 Hz
- E* at 21.1°C-1 Hz

- E* at 21.1°C-5 Hz
- E* at 21.1°C-10 Hz
- E* at 21.1°C-25 Hz

Modulus at 37.8°C

- E* at 37.8°C-0.1 Hz
- E* at 37.8°C-0.5 Hz
- E* at 37.8°C-1 Hz
- E* at 37.8°C-5 Hz
- E* at 37.8°C-10 Hz
- E* at 37.8°C-25 Hz

Phase angle at 4.4°C

- Phase angle at 4.4°C-0.1 Hz
- Phase angle at 4.4°C-0.5 Hz
- Phase angle at 4.4°C-1 Hz
- Phase angle at 4.4°C-5 Hz
- Phase angle at 4.4°C-10 Hz
- Phase angle at 4.4°C-25 Hz

Phase angle at 21.1°C

- Phase angle at 21.1°C-0.1 Hz
- Phase angle at 21.1°C-0.5 Hz
- Phase angle at 21.1°C-1 Hz
- Phase angle at 21.1°C-5 Hz
- Phase angle at 21.1°C-10 Hz
- Phase angle at 21.1°C-25 Hz

Phase angle at 37.8°C

- Phase angle at 37.8°C-0.1 Hz
- Phase angle at 37.8°C-0.5 Hz
- Phase angle at 37.8°C-1 Hz
- Phase angle at 37.8°C-5 Hz
- Phase angle at 37.8°C-10 Hz
- Phase angle at 37.8°C-25 Hz

RLPD test data reports the accumulated microstrains at each cycle. Since there is a large amount of data and each specimen goes through 10,000 cycles, the microstrain data are not stored in a table but they were linked with an excel file. But following information was stored in RLPD table for each test specimen for each material:

- Deviator stress
- Confining pressure

- Contact pressure
- Sample dimension
- Flow number

4.4 Processed Data

Measured DM test data were used to fit master curves to all specimens for each project/material. The procedure was described in Chapter 3. The processed DM master curve data stored in the database are as follows:

DM

- Lower limit of master curve
- Upper limit of master curve
- β (master curve fitting parameter)
- γ (master curve fitting parameter)
- EA (activation energy, also fitting parameter for master curve)

RLPD test data was used to fit the permanent deformation model to all specimens for each project/table. The processed RLPD data stored in the database are as follows:

RLPD

- K_1 (RLPD graph fitting parameter)
- K_2 (RLPD graph fitting parameter)
- K_3 (RLPD graph fitting parameter)
- Measured microstrain at each cycle (1-10,000) at three temperatures (20, 45, & 58°C)

Chapter 5: Measured Structural Properties

This chapter summarizes the laboratory-measured structural properties of the recycled materials evaluated in this study. The structural properties of the recycled materials are also compared to typical structural properties of virgin HMA materials.

5.1 Master curve parameters

As previously described in Chapter 3, master curves were fit to measured dynamic modulus data collected in the lab. Five parameters were optimized during fitting to construct a master curve for each mixture. These five parameters are: Min (limiting minimum mixture dynamic modulus), beta, gamma, EA, and Max (limiting maximum mixture dynamic modulus). These 5 parameters are summarized in Table 5.1 for all of the recycled materials. Also summarized in the table are "fingerprint" values of measured E* at three temperature and frequency combinations. These fingerprints are indicators of the range of dynamic modulus for each material. Similar data are provided in Table 5.2 for the HMA mixtures used as references for comparison in this study.

Table 5.1. Master curve parameters of recycled materials

Mix Name	Min,ksi	beta	gamma	EA	Max,ksi	E*@4C-25Hz, ksi	E*@20C-10Hz,ksi	E*@40c-1Hz,ksi
13-1093	0.002	-1.817	-0.214	2.52E+05	2534.300	1009.800	486.790	94.862
13-1111	0.084	-1.452	-0.339	2.24E+05	2329.000	1225.700	539.070	60.634
13-1112	0.038	-1.446	-0.328	2.13E+05	3047.300	1421.400	592.700	63.296
13-1113	0.126	-1.326	-0.337	2.06E+05	2385.200	1139.300	496.810	62.906
13-1114	0.560	-1.034	-0.400	2.11E+05	2200.500	1147.300	447.610	41.046
13-1115	11.941	1.449	-0.179	-9.39E+03	10627000	273.340	240.430	168.130
13-1116	12.424	-0.971	-0.532	1.52E+05	651.520	488.380	317.010	94.861
13-1117	1.982	-2.195	-0.253	2.02E+05	1638.100	1217.000	959.380	536.780

13-1124	0.085	-1.969	-0.344	2.10E+05	1444.700	984.510	601.000	137.700
13-1127	0.000	-2.387	-0.257	2.40E+05	1847.700	1092.900	640.840	152.260
14-1001	0.000	-2.781	-0.342	2.19E+05	2213.700	1552.000	938.890	167.310
14-1002	0.000	-2.538	-0.334	1.94E+05	840.090	570.360	364.070	91.747
14-1003	0.886	-1.574	-0.371	2.19E+05	1888.800	1278.600	723.650	136.630
14-1011	0.732	-1.581	-0.262	1.90E+05	1136.900	637.490	416.530	160.950
14-1025	0.782	-0.881	-0.398	1.98E+05	2525.100	1169.800	435.120	42.796
14-1026	0.523	-0.987	-0.364	1.96E+05	3549.600	1508.100	577.900	63.116
14-1027	2.135	-0.864	-0.264	1.89E+05	4430.100	1423.700	683.900	170.480
14-1028	81.242	-1.142	-0.581	1.97E+05	890.760	805.640	619.810	245.000
14-1055	0.575	-1.282	-0.336	2.13E+05	2669.300	1398.900	660.330	102.740
14-1057	1.169	-1.778	-0.250	2.15E+05	1345.800	855.920	592.830	252.560
14-1058	3.095	-1.542	-0.349	2.44E+05	2003.500	1433.400	857.730	193.660
14-1062	0.205	-1.560	-0.267	2.22E+05	1722.300	890.580	492.330	123.450
15-1002	0.007	-1.293	-0.243	1.71E+05	1610.500	399.840	182.030	37.575
15-1003	3.923	-0.662	-0.337	1.98E+05	1708.700	732.000	332.940	70.629
I-81CIR	0.162	-1.544	-0.333	1.69E+05	1850.900	964.420	535.980	125.040
I-81CCPR	21.902	-1.269	-0.467	1.79E+05	1017.700	813.430	572.590	202.130

Table 5.2. Master curve parameters of HMA mixtures

Mix Name	Min,ksi	beta	gamma	EA	Max,ksi	E*@4C-25Hz,ksi	E*@20C-10Hz,ksi	E*@40c-1Hz,ksi
H077A09A2C03	6.289	-0.932	-0.572	1.91E+05	3169.34	2178.834	936.265	89.571
H083A12C2C02	1.140	-1.396	-0.452	1.84E+05	3181.53	1518.972	1050.187	146.363
H127A12R2C02	5.103	-1.114	-0.518	1.88E+05	3160.10	2169.587	1078.172	130.292
H135A12H2C02	9.315	-0.829	-0.464	1.95E+05	3058.39	1893.986	878.363	126.830
H135A19G4F01	7.325	-0.864	-0.457	2.06E+05	3027.26	1890.125	850.479	109.629
H151B19R2C02	5.252	-1.390	-0.507	1.90E+05	3206.44	2425.895	1388.276	206.417
H160A09R1C03	13.010	-0.751	-0.588	1.77E+05	3144.96	2184.046	1006.260	112.842
H168A09R2C03	2.646	-1.251	-0.503	2.00E+05	3184.40	2267.760	1118.534	110.618

5.2 *RLPD Measured Properties*

The permanent deformation properties are summarized in Table 5.3 and Table 5.4 for recycled and virgin materials, respectively. The characteristic permanent deformation properties are the intercept and slope of the secondary region, the microstrain at the 1000th cycle, and the microstrain at the 10,000th cycle. Note that all recycled samples were tested at 45°C. Some recycled material test samples failed before 10,000th cycle or even 1000th cycle, and therefore values are not recorded in Table 5.3 for these samples.

RLPD testing of the HMA materials (Table 5.4) followed a different procedure. Nine samples were prepared for each mixture and the dynamic modulus test was performed on three of these. Then all nine samples were tested for RLPD. Three replicate samples were tested at each temperature.

Table 5.3. RLPD measured properties of recycled materials at 45°C. *Note that empty cells for microstrain denote sample failure before the 1000th or 10,000th cycle

Mixture Name	Replicate Number	Intercept	Slope	Microstrain @1000th cycle @ 45 C	Microstrain @10,000th cycle @ 45 C
13-1093	1	9.17E-04	0.2655	5817	10638
	2	8.33E-04	0.3908	12408	30397
	3	1.12E-03	0.3643	13923	32057
13-1111	1	1.16E-03	0.5596	53944	74216
	2	2.39E-03	0.4999	66233	
13-1112	1	5.18E-03	0.3245	46313	
	2	3.65E-03	0.4035	52059	
	3	4.18E-03	0.3682	59088	
13-1113	1	3.51E-03	0.3008	26092	55315
	2	1.63E-03	0.3134	12915	28859
	3	3.39E-03	0.2965	24802	51411
13-1114	1	4.33E-03	0.3116	35146	75493
	2	6.00E-03	0.3167	50247	
13-1115	3	2.74E-03	0.0257	12010	12899
	4	9.90E-03	0.0284	3314	3496
13-1116	1	2.73E-03	0.0640	4242	4933
	2	2.95E-03	0.0932	5568	6942
	3	2.45E-03	0.0506	3462	3897
	4	3.64E-03	0.0596	5465	6283
	5	1.19E-03	0.0891	2206	2707
13-1117	1	2.35E-04	0.2252	1346	1875
	2	3.07E-04	0.0969	702	757
	3	7.07E-04	0.1203	1623	2141

	4	6.70E-04	0.0617	1029	1181
13-1124	1	2.15E-03	0.1526	26092	55315
	2	1.30E-03	0.1468	3569	5023
	3	3.24E-03	0.0989	6361	8032
13-1127	1	8.89E-04	0.1545	2616	3764
	2	3.16E-03	0.0872	5752	7061
	3	1.99E-03	0.1043	4068	5182
14-1001	1	1.07E-03	0.2183	4770	7958
	2	3.92E-03	0.1617	11856	17294
	3	6.02E-03	0.1542	16375	24735
14-1002	1	9.90E-05	0.7049	12989	
	2	6.02E-03	0.1542	16375	24735
14-1003	1	2.08E-03	0.3256	19838	37290
	2	1.20E-03	0.2090	5100	7931
	3	1.02E-03	0.3027	8270	15385
14-1011	1	2.33E-04	0.2115	881	1636
	2	3.50E-03	0.0813	5877	7352
	3	4.10E-03	0.0588	6198	7097
	4	4.70E-04	0.2015	1684	2972
	5	2.21E-04	0.2077	922	1486
	6	4.71E-04	0.2015	4915	5938
	7	7.79E-04	0.1621	2339	3422
	8	4.78E-04	0.1300	1161	1574
14-1025	1	7.75E-03	0.3284	75249	
	2	5.36E-03	0.3184	45891	99564
	3	4.73E-03	0.3903	70493	
14-1026	1	1.44E-04	1.0624		
	2	8.11E-03	0.2964	60780	
	3	4.34E-03	0.3094	35745	74431
	4	8.18E-03	0.2912	60894	
	5	5.57E-03	0.2930	39789	81919
	6	5.06E-03	0.3612	61058	
	7	5.32E-03	0.2737	34849	65654
14-1027	1	2.60E-03	0.2997	20793	41068
	2	1.90E-03	0.3739	25222	58950
	3	3.65E-03	0.1120	7834	10178
	4	4.04E-03	0.1057	7909	10615
	5	4.33E-03	0.0685	6867	8079
	6	8.01E-03	0.0975	15310	19523
	7	4.52E-03	0.1177	10154	13327
	8	1.02E-03	0.2738	6708	12607

14-1028	1	5.28E-04	0.1744	1638	2601
	2	7.75E-04	0.1618	2363	3454
	3	2.95E-03	0.0714	4656	5672
	4	1.93E-03	0.0892	3331	4336
	5	7.28E-04	0.1746	2440	3623
	6	2.28E-03	0.0862	4095	4997
	7	4.91E-04	0.1237	1153	1533
	8	9.73E-04	0.1203	2213	2921
14-1055	1	1.79E-03	0.1924	6715	10458
	2	2.54E-04	0.8621	98089	
	3	1.02E-03	0.2473	5597	9857
	4	1.56E-03	0.4127	24852	68999
	5	1.34E-03	0.3364	13636	29452
	6	3.74E-03	0.3078	27568	63058
	7	3.28E-03	0.2326	15040	27575
	8	2.93E-03	0.1711	9459	14030
	9	8.95E-06	1.4627		
14-1057	1	6.48E-04	0.1295	1577	2124
	2	3.88E-04	0.1034	798	1009
	3	1.15E-04	0.1538	326	469
	4	5.48E-04	0.0688	883	1040
	5	9.26E-04	0.0719	1517	1788
	6	2.94E-04	0.1526	868	1202
	7	4.22E-03	0.2797	25855	54878
	8	9.88E-04	0.0978	1906	2421
	9	1.64E-03	0.3323	16155	34499
	10	1.09E-03	0.1290	2578	3541
	11	3.54E-03	0.3030	25028	56936
	12	1.99E-03	0.0546	2905	3285
	13	7.36E-04	0.1216	1706	2237
	14	2.48E-03	0.1287	5245	8030
	15	8.06E-04	0.1110	1730	2232
	16	1.45E-03	0.0941	2746	3421
	17	1.14E-03	0.0940	2094	2709
	18	5.72E-04	0.0988	1119	1408
14-1058	1	9.74E-04	0.2472	5354	9449
	2	2.32E-03	0.0922	4343	5398
	3	3.75E-03	0.1088	7920	10216
	4	3.41E-03	0.1108	7349	9474
14-1062	1	2.98E-03	0.2207	13411	22548
	2	4.96E-03	0.1054	10230	13058

	3	1.34E-03	0.2089	5450	9068
	4	1.52E-03	0.1374	3890	5362
15-1002	1	3.87E-03	0.4087	64877	
	2	5.15E-03	0.3573	60858	
15-1003	1	6.41E-03	0.1441	17121	23935
	2	5.12E-03	0.1679	15769	23725
	3	4.24E-03	0.1652	12903	19213
I-81-CCPR	1	1.40E-03	0.2462	7976	13572
	2	1.41E-03	0.3556	16417	37224
	3	5.24E-04	0.3768	7486	16888

Table 5.4. RLPD measured properties of HMA mixtures. *Note that values are measured for all samples @ 20C except for mixes 135A19G4F01 and H151B19R2C02, which were measured at 58°C. All other microstrain values are predicted with the model.

Mixture Name	Replicate #	Intercept	Slope	Microstrain @20C& 1000th cycle	Microstrain @45 1000th cycle	Microstrain @58 1000th cycle	Microstrain @20 10,000th cycle	Microstrain @45 10,000th cycle	Microstrain @58 10,000th cycle
H077A09	1	8.21E-04	0.121	1824	3981.27	5607.53	2481	5257.867	7405.59
	2	1.20E-03	0.094	2184	4115.00	5378.48	2840	5114.455	6684.80
	3	3.47E-04	0.174	1057	3366.02	5509.70	1705	5022.251	8220.73
H083A12	1	5.98E-04	0.147	1545	3929.78	5866.49	2288	5507.112	8221.18
	2	2.89E-04	0.162	849	2307.40	3589.48	1274	3347.756	5207.89
	3	5.43E-04	0.107	1124	2155.13	2889.81	1449	2759.112	3699.68
H127A12	1	2.15E-04	0.201	837	2893.19	5059.50	1357	4591.646	8029.70
	2	7.23E-04	0.121	1621	3470.62	4862.10	2190	4585.693	6424.25
	3	1.29E-03	0.109	2621	5273.12	7142.93	3479	6776.316	9179.16
H135A12	1	7.36E-04	0.124	1652	3865.97	5599.21	2280	5139.555	7443.78
	2	2.62E-04	0.156	745	2116.14	3374.97	1090	3029.623	4831.85
	3	8.89E-04	0.091	1637	3010.40	3953.28	2044	3711.871	4874.46
H135A19	1	8.89E-04	0.091	691.01	1262.18	15665.00	852.02	1556.293	20150
	2	6.69E-03	0.130	4677.12	11035.42	16383.00	6303.74	14873.348	22035
	3	6.69E-03	0.130	4677.12	11035.42	16383.00	6303.74	14873.348	22035
H151B19	1	1.36E-03	0.266	789.37	4044.78	8570.00	1457.44	7467.970	15750
	2	2.67E-03	0.207	1743.12	6223.50	11117.00	2810.29	10033.622	17973
	3	2.28E-03	0.211	1476.97	5382.84	9675.00	2399.65	8745.553	15766
H160A09	1	2.78E-04	0.163	825	2178.77	3344.15	1243	3172.456	4869.35
	2	4.38E-04	0.146	1154	2767.40	4061.38	1674	3874.165	5685.64
	3	4.98E-04	0.132	1216	2621.58	3704.42	1666	3550.157	5016.54
H168A09	1	2.32E-03	0.118	4849	11181.15	15861.12	6800	14659.118	20794.81
	2	1.12E-03	0.106	2236	4627.64	6344.25	2964	5908.756	8100.60
	3	1.13E-03	0.124	2505	5919.68	8558.01	3518	7875.755	11385.88

5.3 *Material Comparisons*

The structural properties of the recycled materials are compared to those of typical HMA mixtures in this section. Since there were fewer HMA mixtures than recycled materials and since the HMA mixtures did not vary much in dynamic modulus values, average values of HMA dynamic modulus values are compared to the recycled materials. Figure 5.1 through Figure 5.16 summarize the dynamic modulus properties for all of the recycled materials. The dashed line in each figure represents the corresponding average value for the HMA mixtures. The recycled materials are divided into five categories based on process and stabilizer type. The average and standard deviation values for each property by group are also illustrated in the figures.

Master curve fitting parameters are studied to compare HMA vs. recycled materials. Also dynamic modulus in different reduced frequencies were compared.

- As shown in Figure 5.1, the cold-recycled materials had smaller lower shelf stiffness values than the HMA materials. The cold-recycled materials had average upper shelf value of VALUE ksi vs. VALUE ksi for HMA. Figure 5.2 compares the lower shelf values for the cold-recycled materials by process type.
- As shown in Figure 5.3, the cold-recycled materials had smaller upper shelf stiffness values than the HMA materials. The cold-recycled materials had average upper shelf value of 1980 ksi vs. 3140 ksi for HMA. Figure 5.4 compares the upper shelf values for the cold-recycled materials by process type.
- The beta fitting parameter determines the slope of the master curve in the transition zone. Large beta values (in an absolute value sense) correspond to a

shallow slope while small beta values correspond to a steep slope. The average value of β for the cold-recycled materials was -1.4, which is very similar to the average value of -1.06 for the HMA mixtures as it can be seen in Figure 5.5. Figure 5.6 compares the beta values for the cold-recycled materials by process type. The cold-recycled materials generally had higher magnitudes of beta and thus shallow slopes in the transition region of the master curve. This means that these materials are less sensitive to loading rate than conventional HMA.

- The gamma parameter defines the horizontal location of the center of the transition zone. Recycled materials had smaller magnitude of gamma which indicates that the master curve was less S shaped as it can be interpreted from Figure 5.7. Figure 5.8 compares the gamma values for the cold-recycled materials by process type.
- The Activation Energy (EA) is the fitting parameter in the Arrhenius equation that shows the degree of temperature sensitivity of the material. EA was in a similar range for recycled and HMA mixes as it can be seen from Figure 5.9. The average value for the cold-recycled materials was 196,660 vs. 191,393 for HMA. Figure 5.10 compares the EA values for the cold-recycled materials by process type.

Insights into the stiffness of the materials can also be gained by examining modulus values at discrete reduced frequency values. To serve this purpose, three points were chosen on each DM master curve to represent the different behavior regimes: one at higher reduced frequencies (4ºC and 25 Hz) corresponding to lower temperatures, one in the middle (20ºC and 10 Hz) corresponding to the transition zone, and one at lower reduced frequency (40ºC and 1 Hz) corresponding to higher temperatures.

- As shown in Figure 5.11, at higher reduced frequencies (4ºC and 25 Hz) the HMA mixes had higher modulus values than the cold-recycled materials. The recycled materials moduli were at least 500 psi less and their average modulus was half that of the HMA mixes. Figure 5.12 compares the high reduced frequency modulus values for the cold-recycled materials by process type.
- As shown in Figure 5.13, at medium reduced frequencies (20ºC and 10 Hz) the average modulus value for the cold-recycled materials was approximately half that of the HMA mixtures. Figure 5.14 compares the medium reduced frequency modulus values for the cold-recycled materials by process type.
- As shown in Figure 5.15, at lower reduced frequencies (40ºC and 1 Hz) the average modulus of the cold-recycled materials is in the same range as that for the HMA mixtures. Figure 5.16 compares the lower reduced frequency modulus values for the cold-recycled materials by process type.

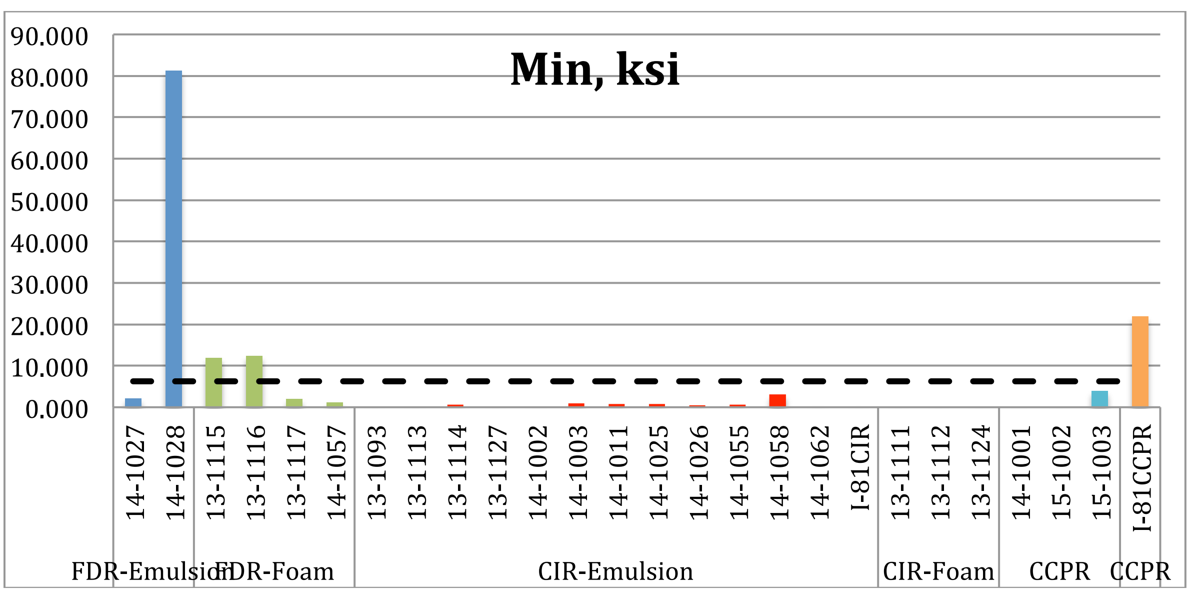

Figure 5.1. Limiting minimum E* parameter of master curve for recycled mixtures (dashed line represent average value for HMA mixtures.)

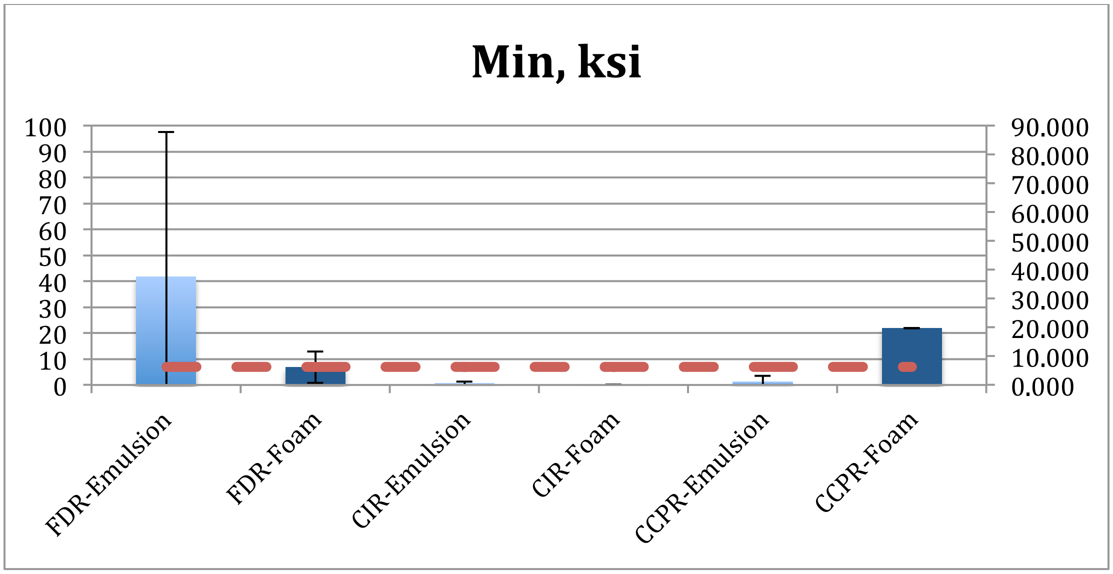

Figure 5.2. Limiting minimum E* parameter of master curve for each group of recycled mixtures (black vertical lines show the standard deviation in each group)

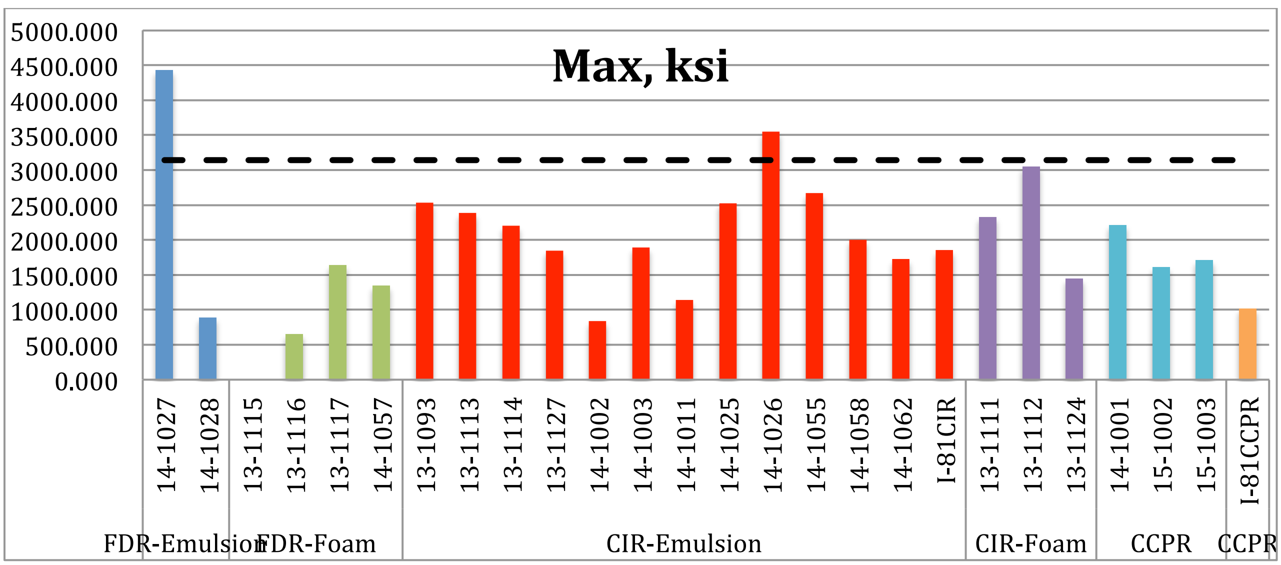

Figure 5.3. Limiting maximum E* parameter of master curve for recycled mixtures (dashed line represent average value for HMA mixtures)

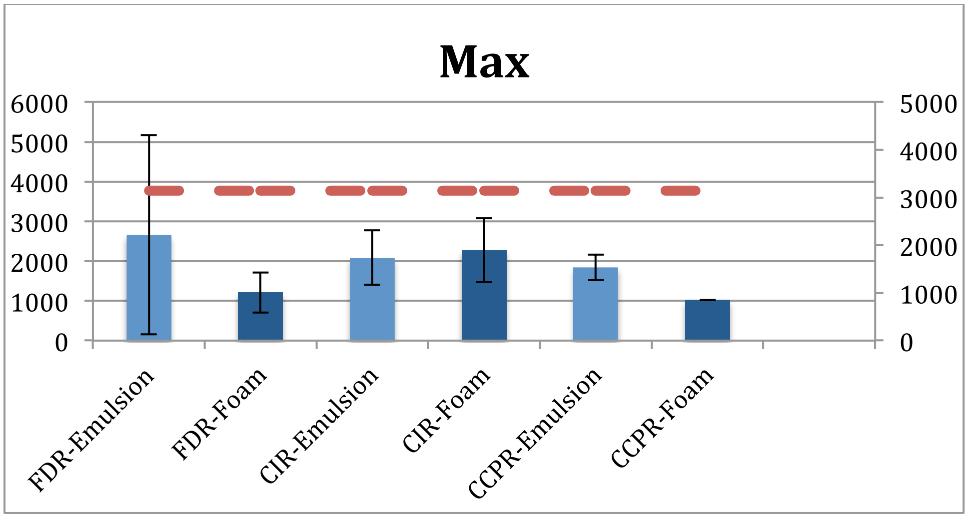

Figure 5.4. Average Limiting minimum E* parameter of master curve for each group of recycled mixtures (black vertical lines show the standard deviation in each group)

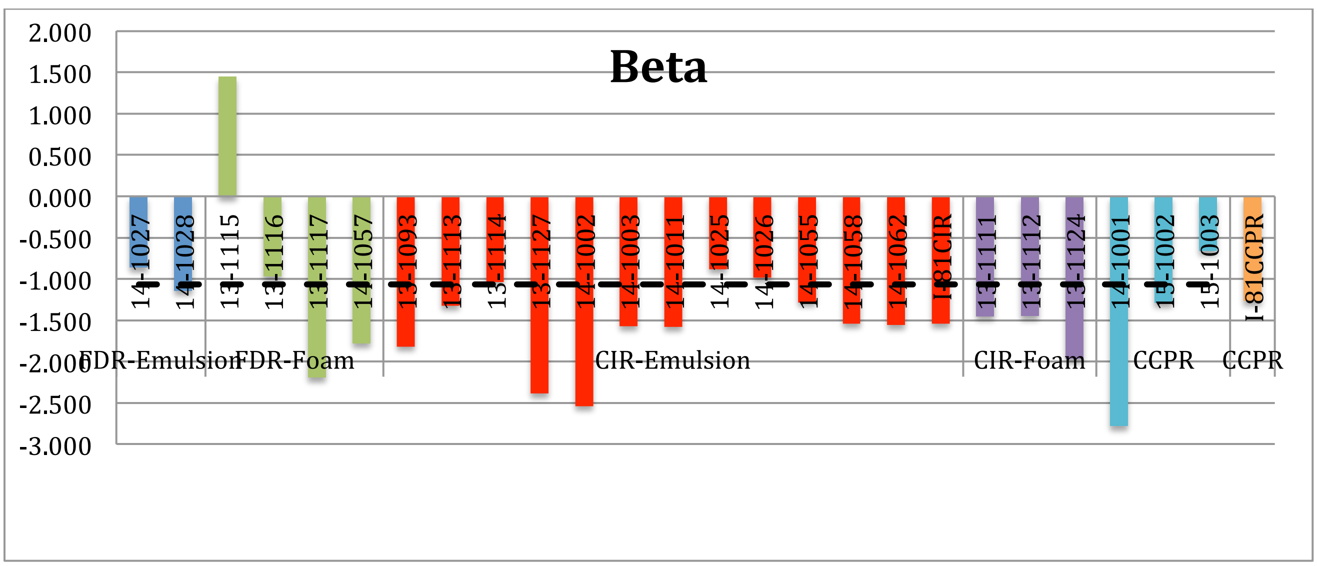

Figure 5.5. Beta parameter of master curve for recycled mixtures (dashed line represent average value for HMA mixtures)

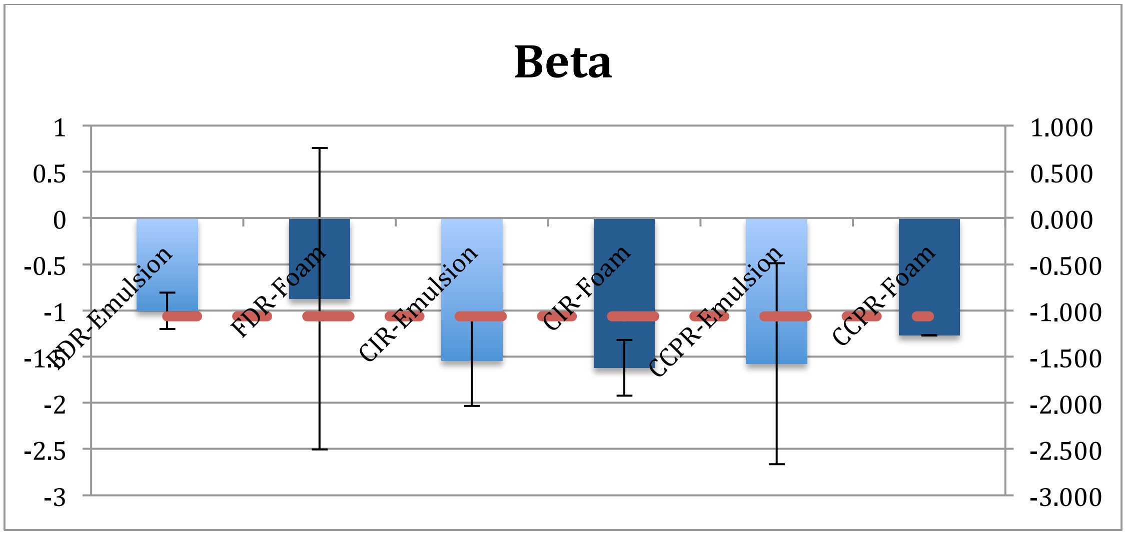

Figure 5.6. Average Beta parameter of master curve for each group of recycled mixtures (black vertical lines show the standard deviation in each group)

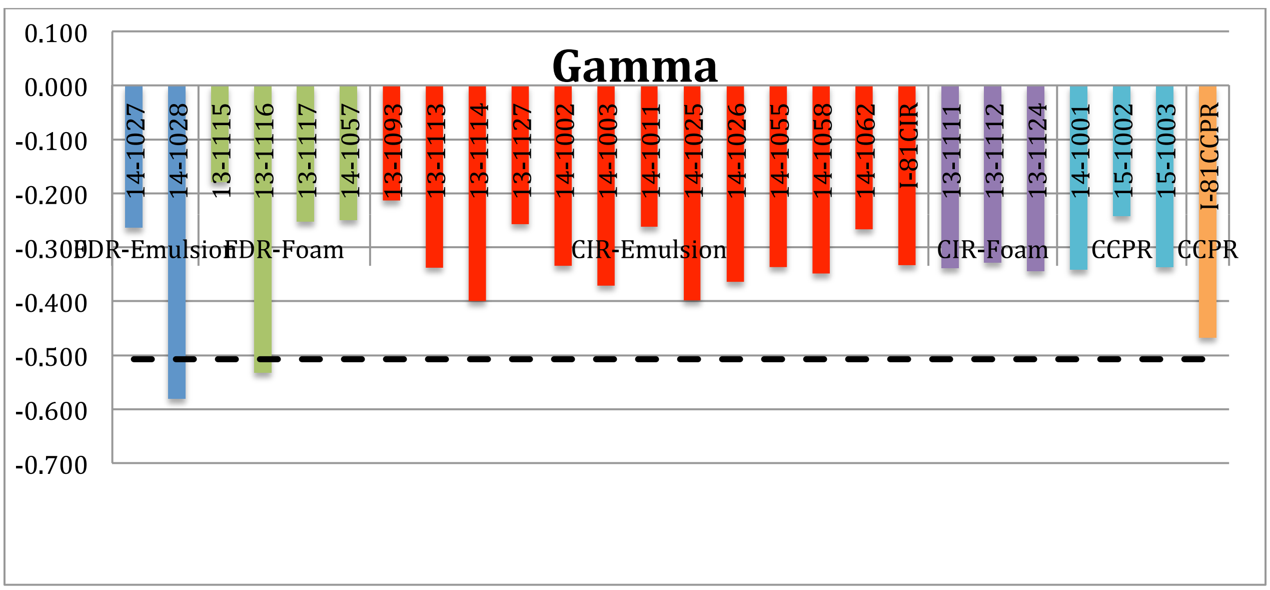

Figure 5.7. Gamma parameter of master curve for recycled mixtures (dashed line represent average value for HMA mixtures)

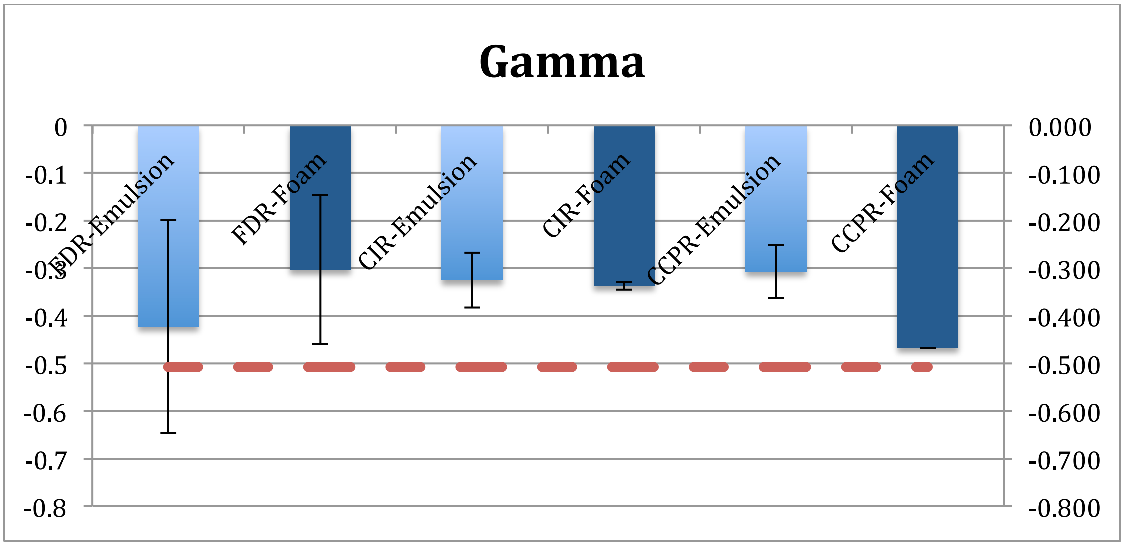

Figure 5.8. Average Gamma parameter of master curve for each group of recycled mixtures (black vertical lines show the standard deviation in each group)

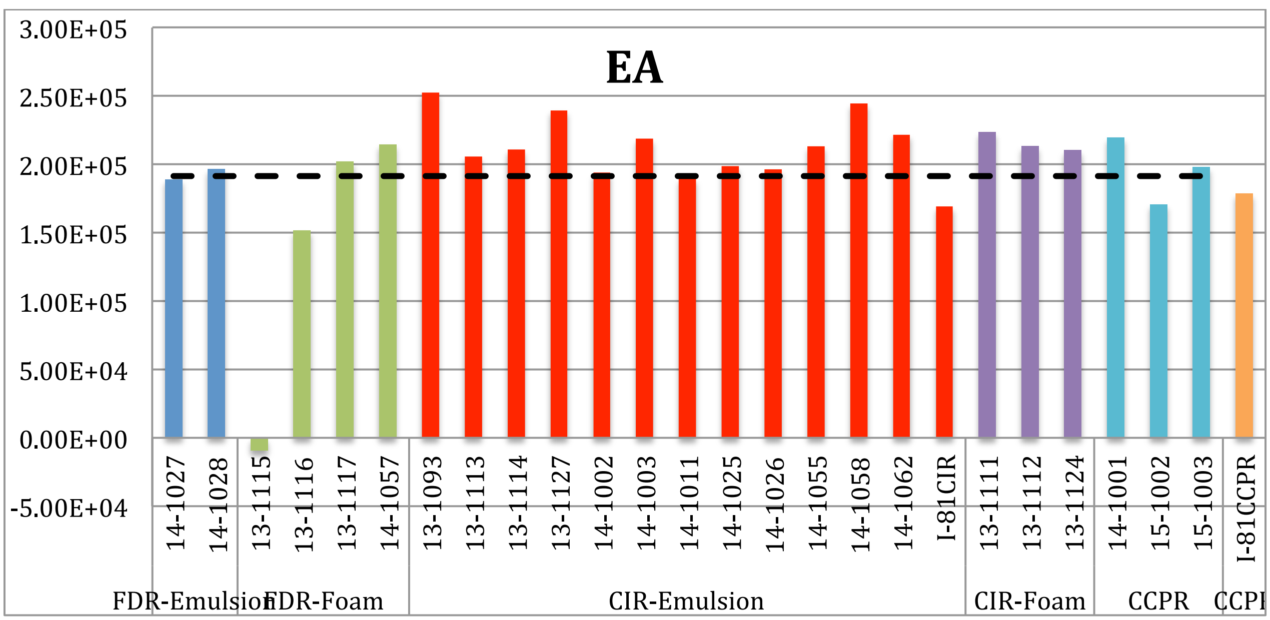

Figure 5.9. EA parameter of master curve for recycled mixtures (dashed line represent average value for HMA mixtures)

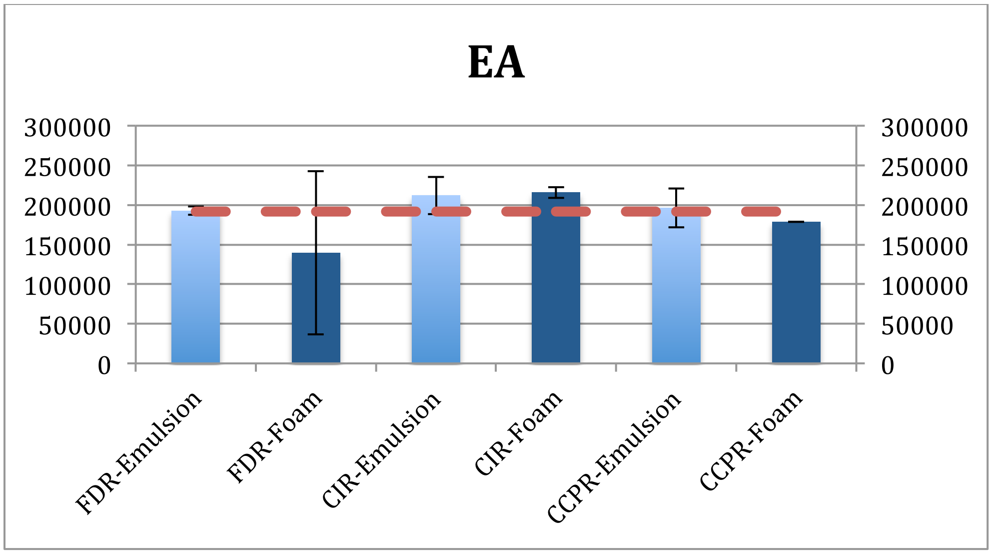

Figure 5.10. Average EA parameter of master curve for each group of recycled mixtures (black vertical lines show the standard deviation in each group)

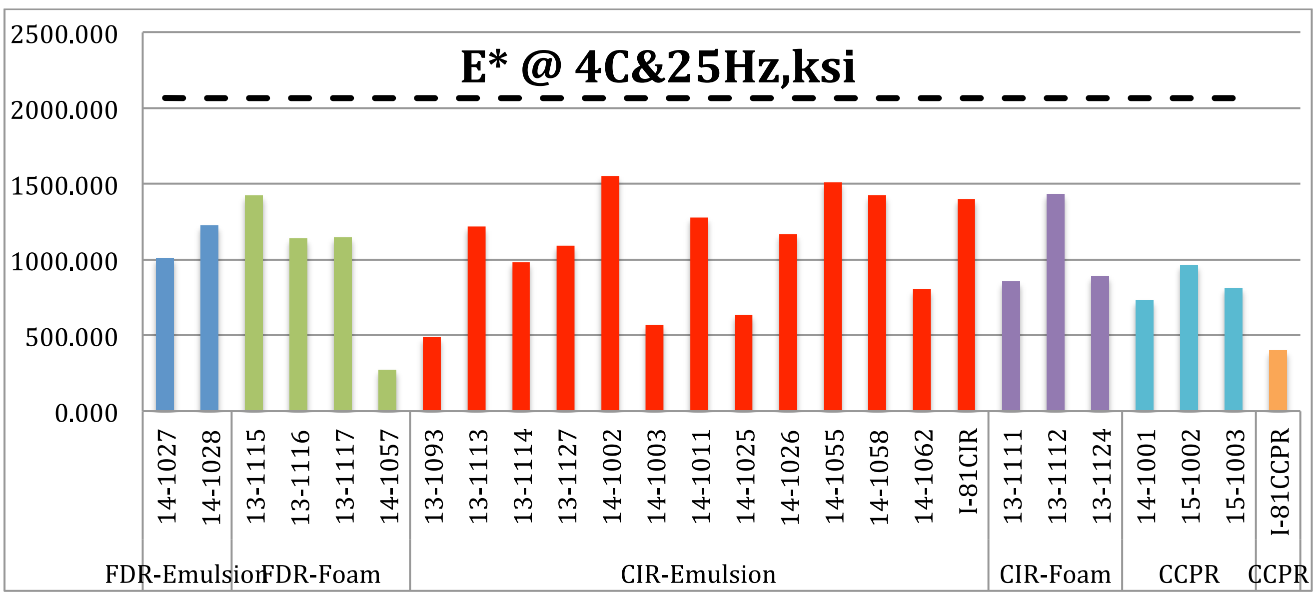

Figure 5.11. E* @ 4 ˚C & 25Hz for recycled mixtures (dashed line represent average value for HMA mixtures)

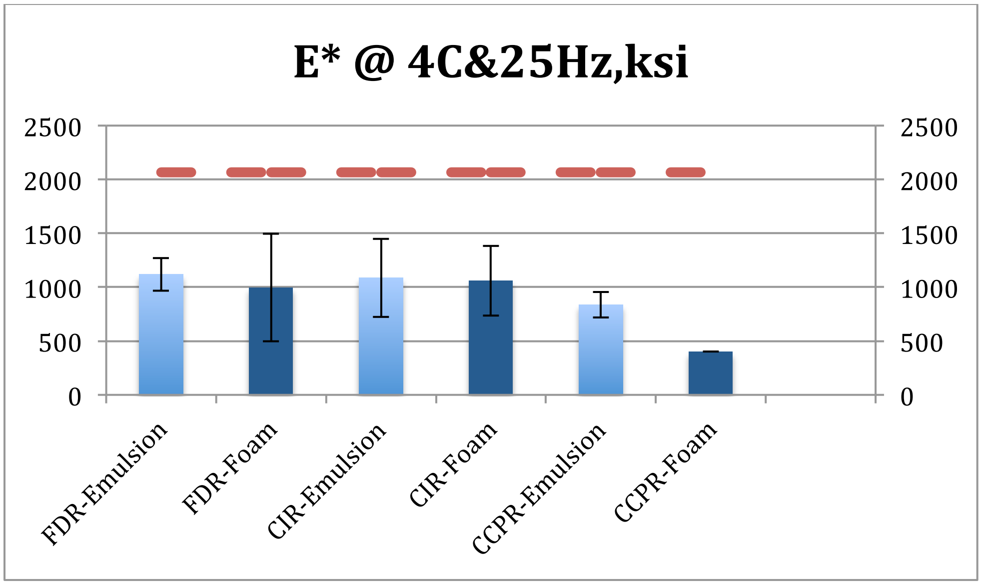

Figure 5.12. E* @ 4 ˚C & 25Hz for each group of recycled mixtures (black vertical lines show the standard deviation in each group)

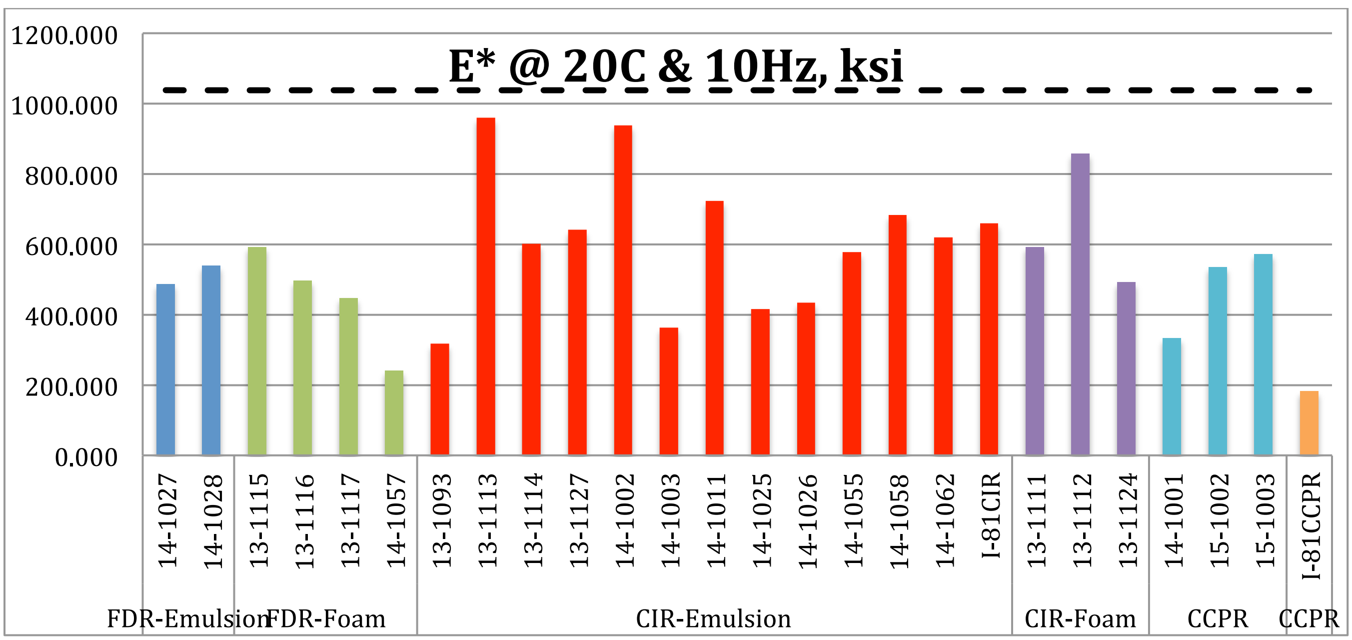

Figure 5.13. E* @ 20˚C & 10Hz for recycled mixtures (dashed line represent average value for HMA mixtures)

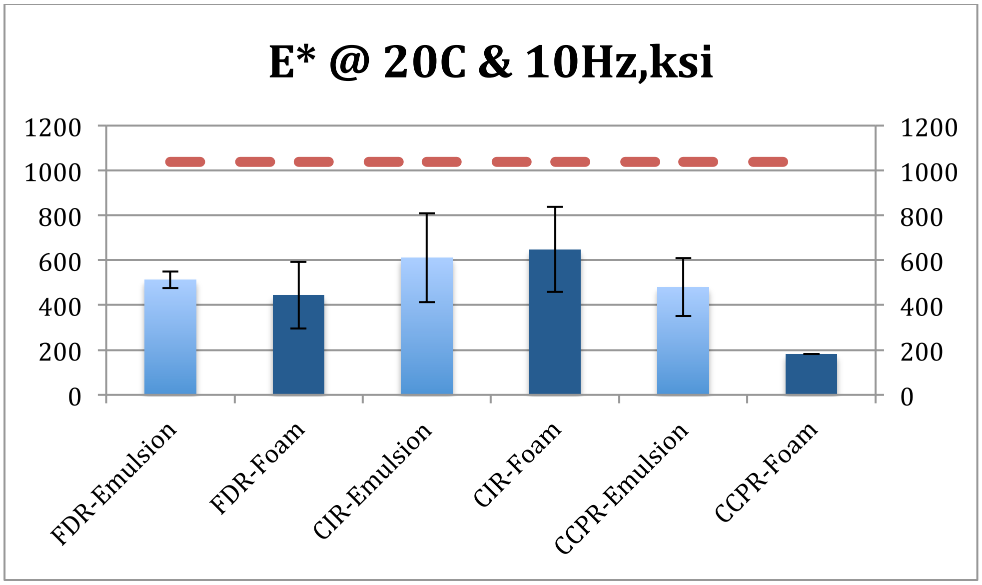

Figure 5.14. E* @ 20 °C & 10Hz for each group of recycled mixtures (black vertical lines show the standard deviation in each group)

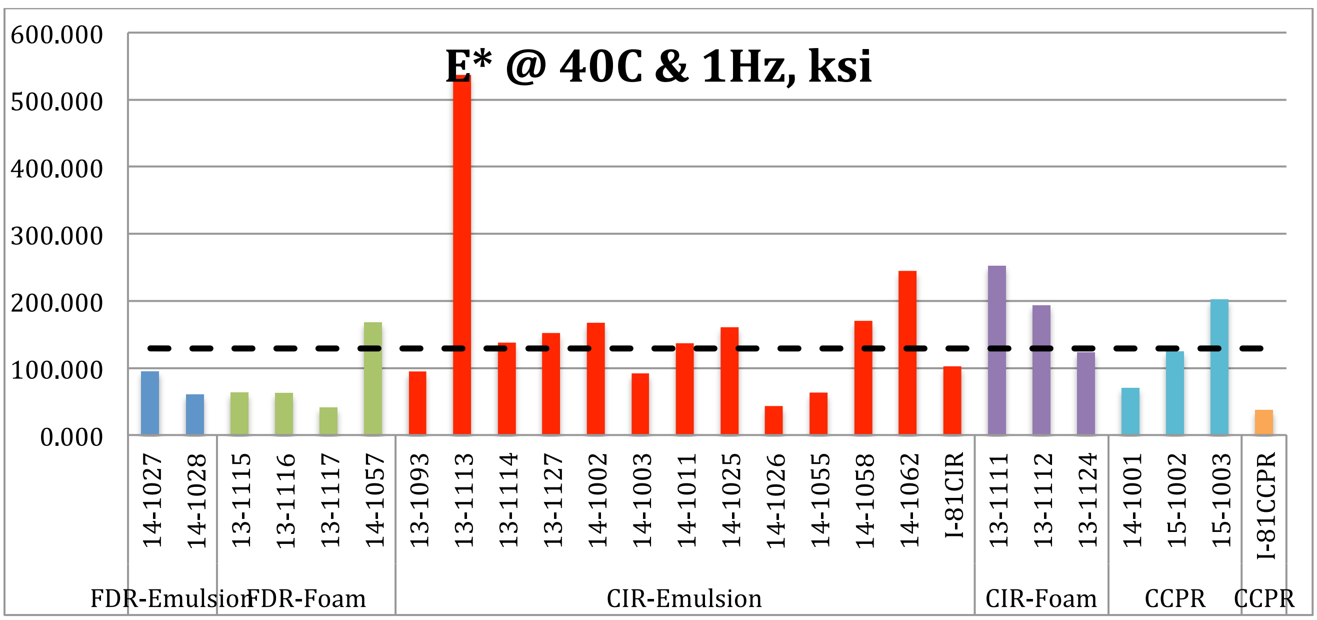

Figure 5.15. E* @ 40°C & 1Hz for recycled mixtures (dashed line represent average value for HMA mixtures)

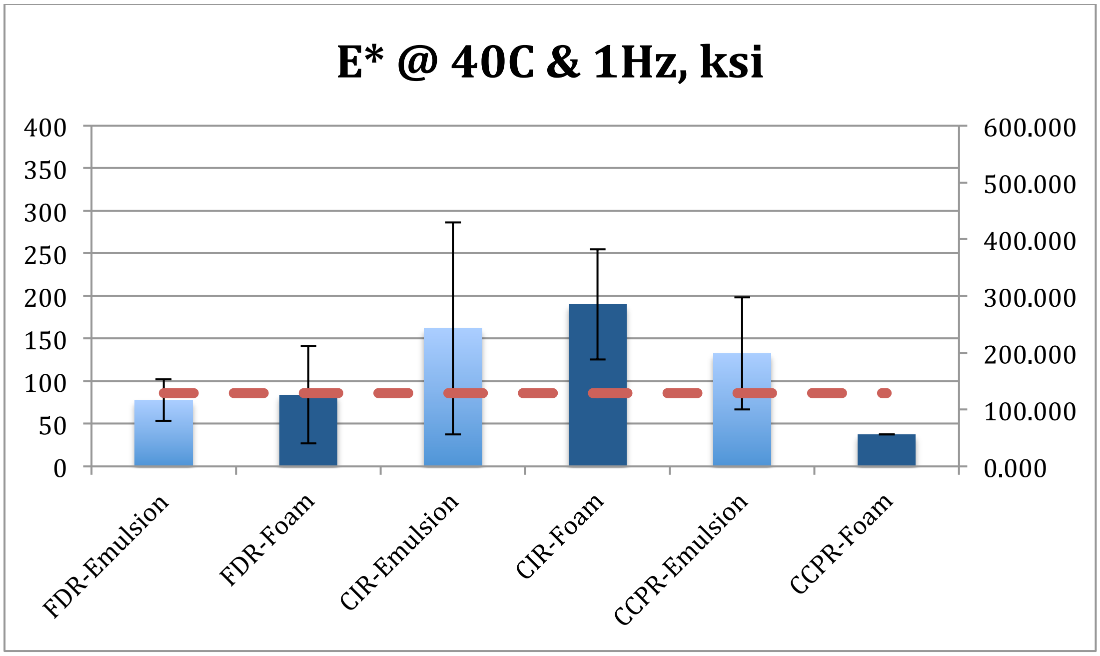

Figure 5.16. E* @ 40 ˚C & 1Hz for each group of recycled mixtures (black vertical lines show the standard deviation in each group)

The RLPD behavior of the materials are summarized in Figures 5.17 through 5.25. The dashed line in these figures again show the average value for the reference HMA mixtures. RLPD testing was not performed on Mixture I-81 (CIR), therefore it does not have a bar in following figures. Overall, there was a wider range of values for the cold-recycled materials both for dynamic modulus and RLPD characteristics.

- The average intercept and slope values for cold-recycled and HMA materials are compared in Figure 5.17 through 5.21. The HMA materials had lower intercept and slope values than did the cold-recycled materials. The mean for slope was 0.14 for the HMA mixtures and 0.25 for CIR. The cold-recycled CIR materials also had a wider range (Figure 5.17).
- The average of intercept for recycled material was 0.003 vs. 0.0014 for HMA materials.

- Measured Microstrains at the 1000th and 10,000th cycles at 45ºC are depicted in Figure 5.22 through Figure 5.25. Overall, the cold-recycled materials exhibited higher permanent deformations than did the HMA mixtures. The CIR materials also tended to exhibit higher permanent deformations than did the other process types.

Lower slopes and intercepts demonstrate less permanent deformation and better rutting performance. Generally, the HMA mixtures had smaller slopes and intercepts than did the cold-recycled materials. Some recycled samples had very high slope and intercepts, which can be expected to lead to large amounts of rutting in the field, but others had similar behavior to the HMA mixtures. The influence of RLPD slope and intercept on rutting performance of pavements will be discussed more thoroughly in Chapter 6.

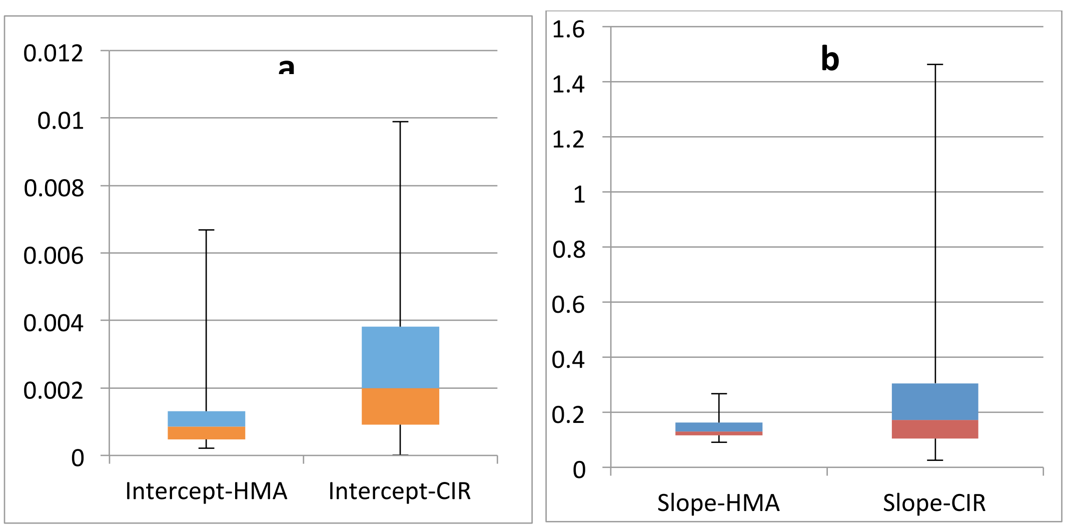

Figure 5.17. (a) Variability of intercept in RLPD curves of HMA vs. CIR, (b) Variability of slope in RLPD curves of HMA vs. CIR

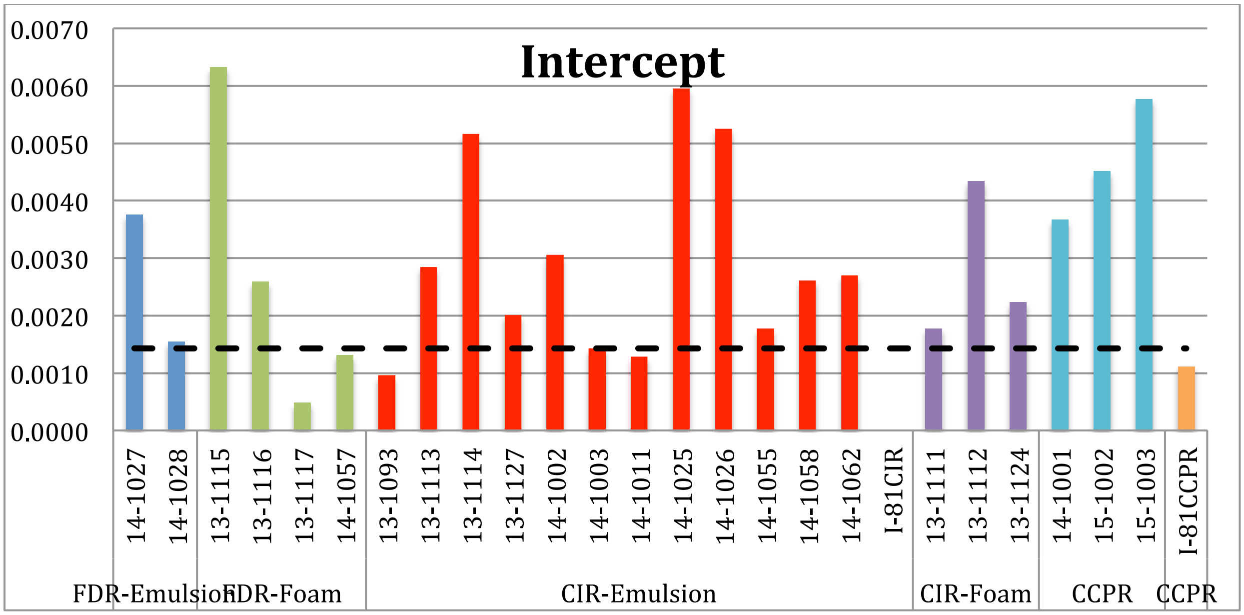

Figure 5.18. Intercept of RLPD graph for recycled mixtures (dashed line represent average value for HMA mixtures)

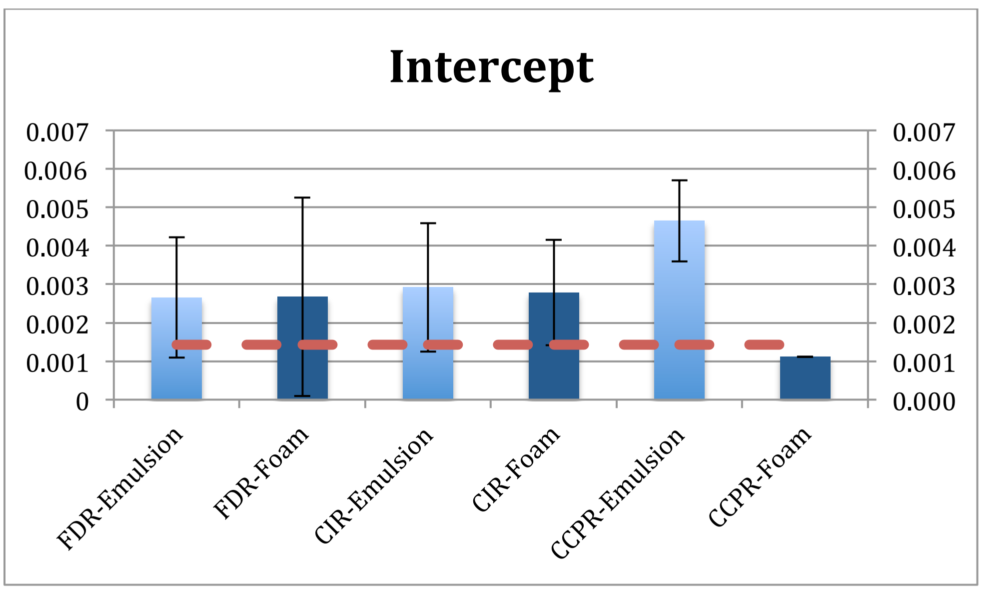

Figure 5.19. Intercept for each group of recycled materials. (black vertical lines show the standard deviation in each group)

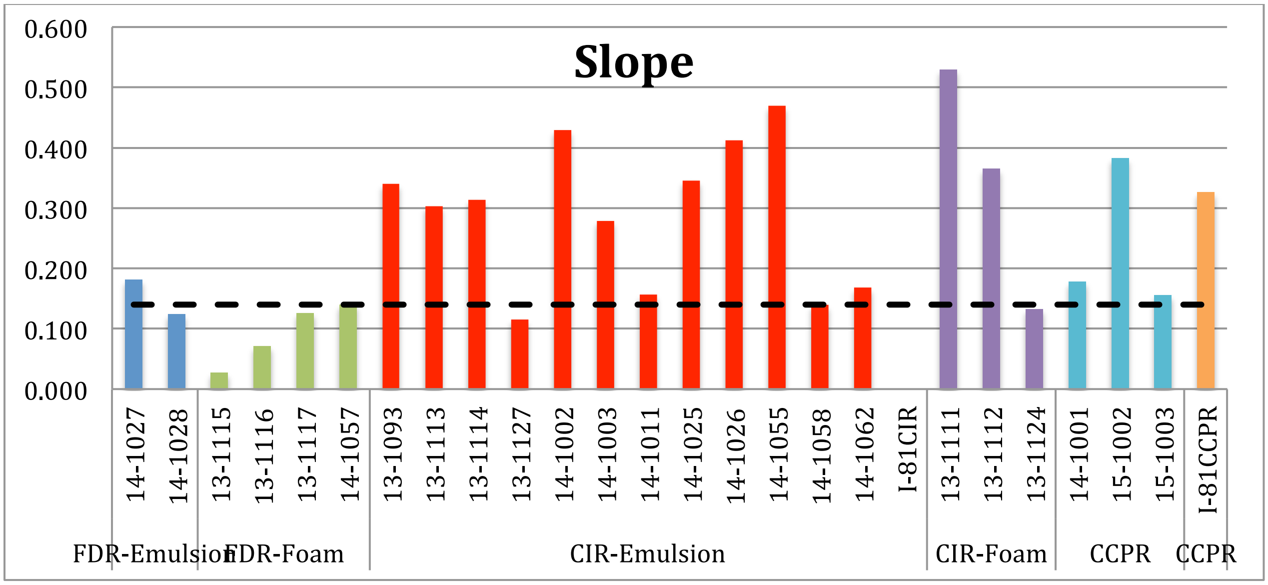

Figure 5.20. Slope for recycled mixtures (dashed line represent average value for HMA mixtures)

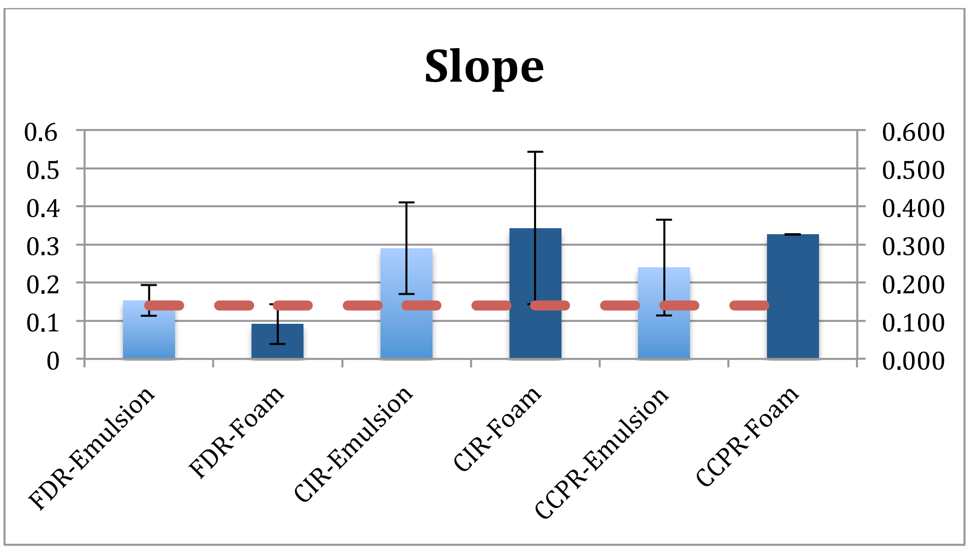

Figure 5.21. Slope for each group of recycled mixtures. (black vertical lines show the standard deviation in each group)

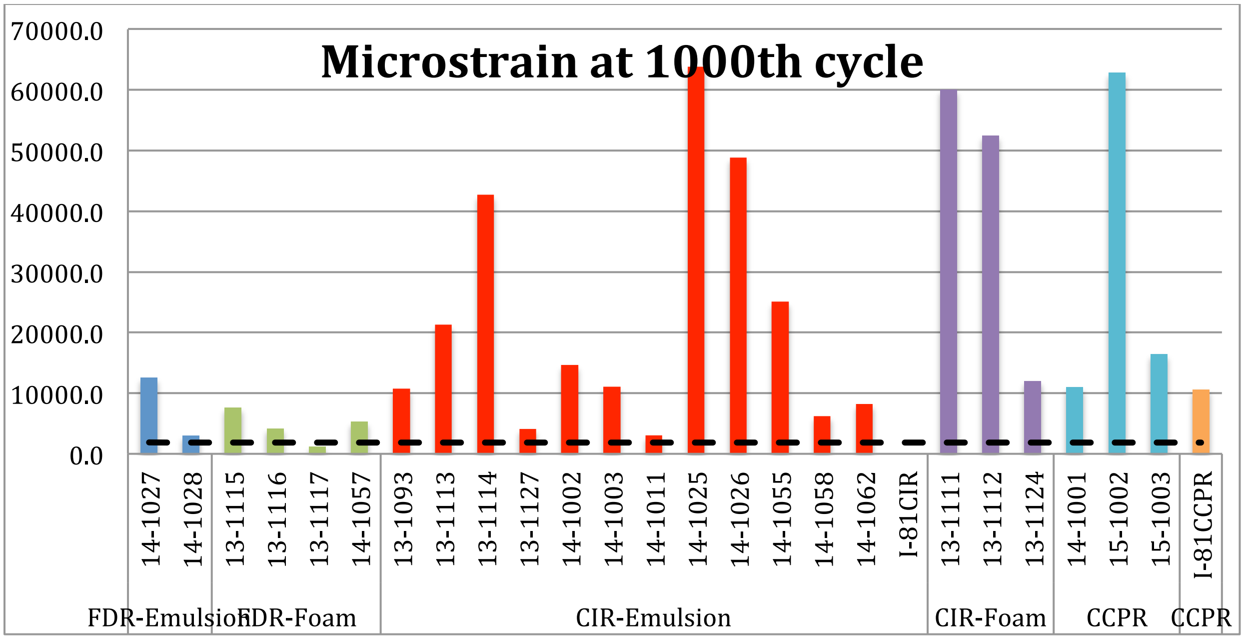

Figure 5.22. Microstrain at 1000th cycle for recycled mixtures.(dashed line represent average value for HMA mixtures)

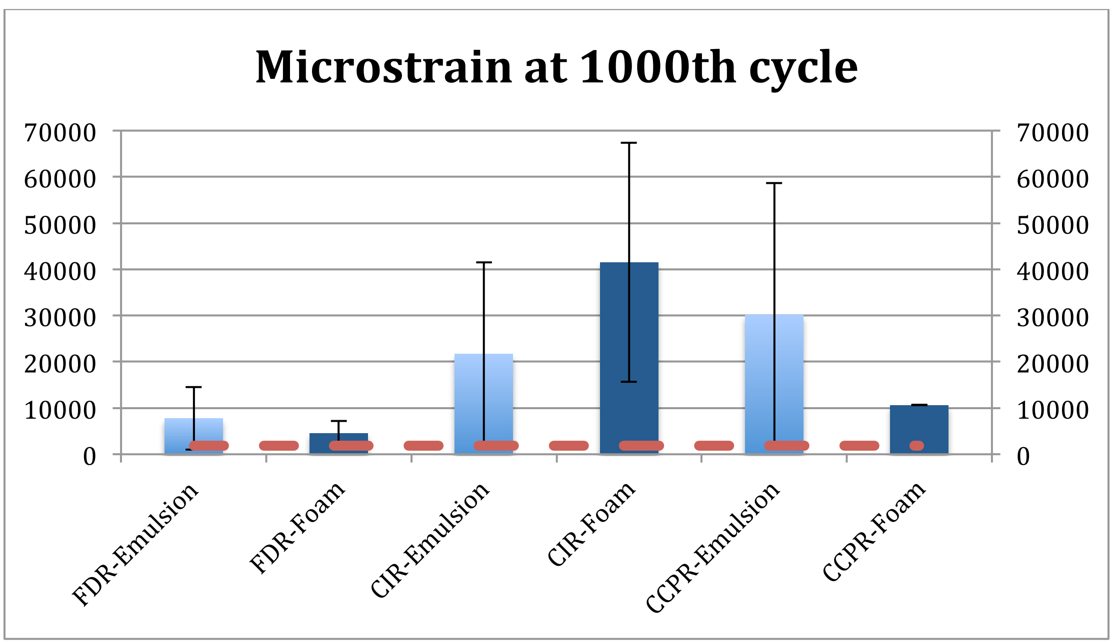

Figure 5.23. Microstrain at 1000th cycle for each group of recycled mixtures (black vertical lines show the standard deviation in each group)

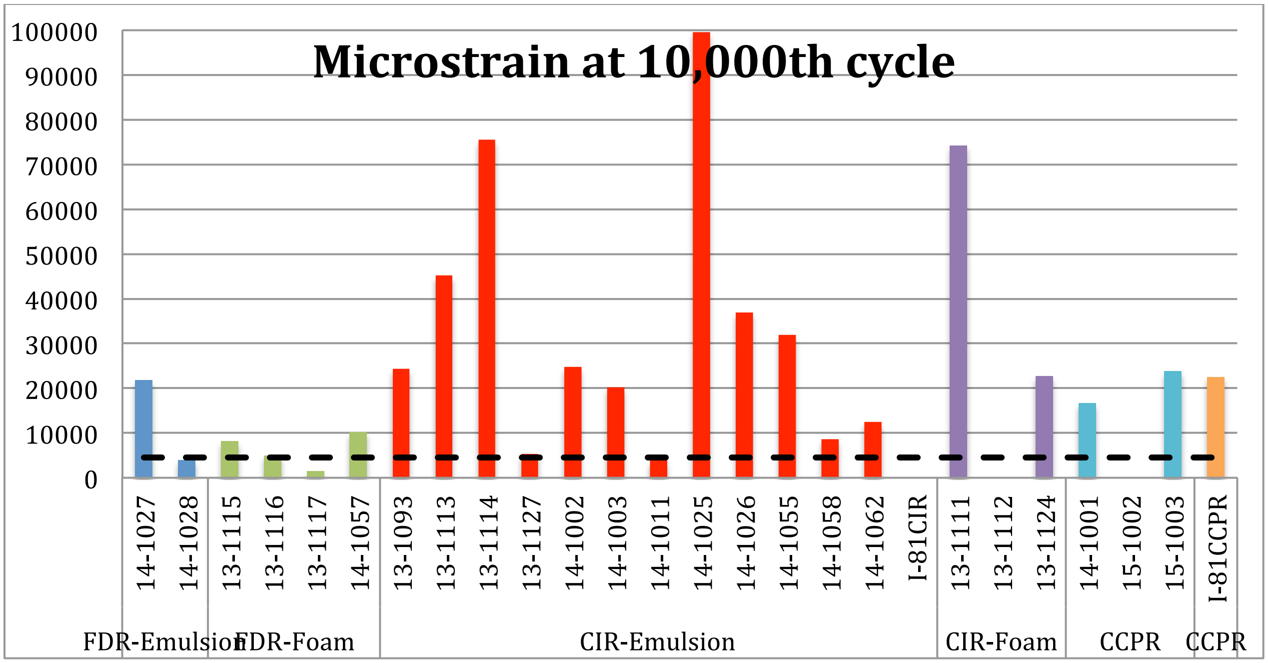

Figure 5.24. Microstrain at 10,000th cycle for recycled mixtures (dashed line represent average value for HMA mixtures) *In this figure, Mix 13-1112 and 15-1002 do not have a bar because they failed before 10,000th cycle

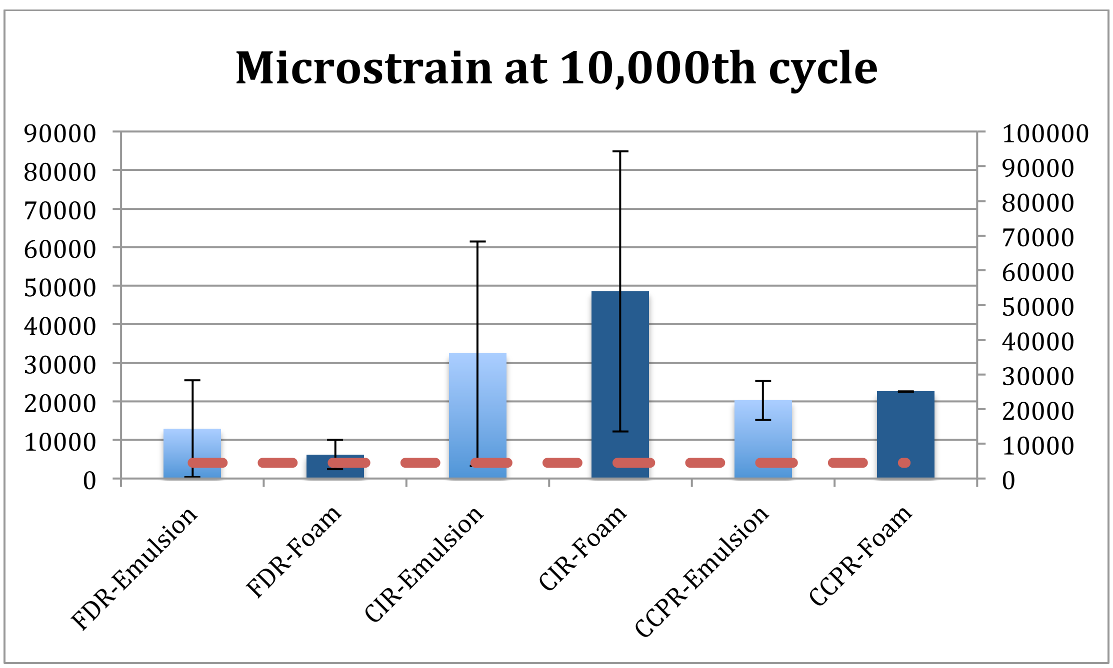

Figure 5.25. Microstrain at 10,000th cycle for each group of recycled mixtures (black vertical lines show the standard deviation in each group)

5.4 OVERALL CONCLUSIONS

- The cold-recycled materials had dynamic modulus values similar to those of HMA at high temperatures/slow loading rates. However, the stiffness of the cold-recycled materials was roughly half that of HMA mixtures at low and medium temperatures/high and medium loading rates.
- The master curves for the cold-recycled materials had a milder slope and a less pronounced S-shape than for the HMA materials.
- EA was in the similar range for HMA and recycled materials.
- There were no systematic differences observed in the stiffness properties of the cold-recycled materials as a function of process or stabilizer type.
- The cold-recycled materials had a wider range of RLPD behavior in comparison to HMA. Both the intercept and slope values are more than approximately two times greater for the cold-recycled materials as compared to the HMA mixtures.
- Overall, the CIR materials exhibited larger permanent strains and thus higher rutting potential than the materials from the other process types. The foam stabilized CIR materials exhibited somewhat greater rutting potential than did the emulsion stabilized CIR.

Chapter 6: Sensitivity Analysis

6.1 Introduction to Mechanistic Empirical Pavement Design Guide (AASHTOWARE™ Pavement ME Design®)

The Mechanistic-Empirical Pavement Design Guide (MEPDG; AASHTO, 2008)) is the current recommended method for the structural design of heavily trafficked pavements in the United States. The MEPDG methodology is implemented in the AASHTOware™ Pavement ME Design® software. This software predicts distresses in various types of pavements (flexible, rigid, semi-rigid/composite) as functions of traffic, climate, material properties, and other design inputs. It evaluates flexible pavement performance based on rutting, fatigue cracking, thermal cracking and International Roughness Index (IRI). ("NCHRP report 704: a performance-related specification for hot-mixed asphalt.")

6.1.1 Inputs

There are three different levels of inputs in the Pavement ME Design® software based on accuracy. Level 1 is the highest level of accuracy. Level 1 data typically are project-specific values measured in the field or in the lab. Level 2 data are typically based on correlations and require less measured data from the field/lab than for Level 1. Level 3, the least accurate data level, uses typical default values for inputs (AASHTO 2008).

The three major categories of inputs are traffic, climate, and material properties. These are each briefly described in the following sections.

6.1.2 Traffic

Primary traffic data are as the following:

1. Average Annual Daily Truck Traffic (AADTT), including growth rate
2. Vehicle type distribution
3. Axle load distributions for each vehicle type

Additional secondary traffic inputs include tire pressure, axle/wheel geometry, and lateral wander.

The software defines the vehicle mix in terms of a Truck Traffic Classification (TTC) group. Which varies by road functional class. Default vehicle mixes for each TTC are based on Long Term Pavement Performance (LTPP) data. Default axle load distributions for the different vehicle classes are also based on LTPP data.

6.1.3 Climate

Required climate data include hourly values of air temperature, precipitation, humidity, percentage sunshine, and wind speed. The Pavement ME Design® software includes a database of weather stations throughout United States. Users can select a station near the project site or interpolate among multiple stations. Additional climate inputs include water table depth, and surface shortwave absorptivity.

6.1.4 Material properties

The MEPDG categorizes pavement materials into 3 groups: asphalt materials, chemically stabilized materials, and unbound materials. The main material characteristics are the thickness and stiffness of each layer. Asphalt material stiffness is defined by the dynamic modulus, which takes into account the time-temperature sensitivity of the material. Stabilized and unbound material stiffnesses are specified by their elastic and resilient moduli, respectively. These and the other material inputs required by the MEPDG are summarized in Table 6.1.

Table 6.1. MEPDG material properties classification

Material type	Input category	Detailed inputs
Asphalt Material	Mixture Volumetric	Unit weight Effective binder content Percentage of air voids Poisson's ratio
	Mechanical Properties	Dynamic modulus E* predictive model Reference temperature Asphalt binder Indirect tensile strength at 14°
	Thermal Characteristics	Thermal conductivity Heat capacity Thermal contraction
Stabilized Material	General	Unit weight Poisson's ratio
	Strength	Elastic/resilient modulus Modulus of rapture
	Thermal	Thermal conductivity Heat capacity
Unbound Material	Modulus Poisson's ratio Coefficient of lateral earth pressure Gradation	

6.1.5 Rehabilitation

For rehabilitation designs, the user must input pavement condition at the time of rehabilitation. Rutting in each layer, percentage of fatigue cracking, and milled thickness are principal inputs. The damaged modulus measured from Non-Destructive Testing (NDT) can also be input.

6.1.6 Outputs

The principal outputs from the Pavement ME Design® software are the predicted distresses, which are then compared to the design criteria. The primary pavement distresses predicted for flexible pavements are the following:

- Rutting or permanent
- Bottom-up fatigue cracking or alligator
- Longitudinal cracking or top-down fatigue
- Thermal cracking

The primary pavement distresses are combined with climate and other data to predict the composite International Roughness Index (IRI).

6.2 Comparison Analyses

A two case rehabilitation scenario with equivalent structural capacity was designed to evaluate HMA vs. cold-recycled material performance using the AASHTOware^{TM} Pavement ME Design® software. The two pavement structures are shown in Figure 6.1. The first is a recycled pavement with a CIR (or CCPR/FDR) overlay (RP-CIR). It consists of, from bottom to top, a A-7-5 subgrade with an input resilient modulus of 5000 psi, 12 inches of A-1-a granular base with an input resilient modulus of 25000 psi, 2 inches of existing HMA, 5.5 inches of CIR, and a variable thickness (1.5, 2, 3, and 4 inches) HMA wearing course. The second section is a recycled pavement with an HMA layer (RP-HMA). The structure similar to the first except for the mid-layer HMA; the 5.5 in. cold-recycled layer in the first section is replaced with a 4 inch HMA layer. This difference in overlay thickness is consistent with the typical ratios of AASHTO 93 structural layer coefficients for these materials—i.e., 0.32 for cold recycled vs. 0.40 for a base HMA. The RP-HMA structure is the standard against which the cold-recycled overlay in RP-CIR structure is compared. Level 1 dynamic modulus (E*) and repeated load permanent deformation (RLPD) characteristics were used for the asphalt mid-layer and wearing course layer. The test results from the present study were used to determine the Level 1 E* and RLPD inputs for the cold-recycled layer. Level 3 properties were used for the existing asphalt. Varying AADT values consistent with the different thicknesses of the HMA wearing course were applied.

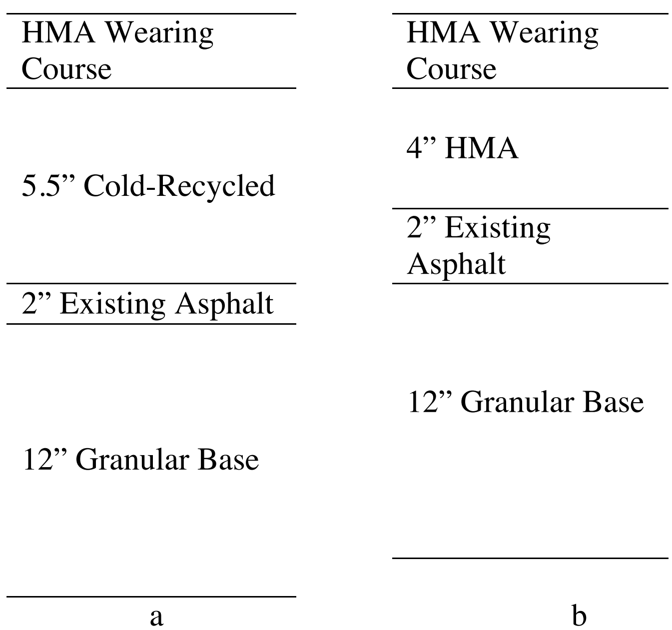

Figure 6.1. Pavement sections: (a) RP-CIR; (b) RP-HMA.

6.2.1 Dynamic Modulus Input

Each pavement sections had three different asphaltic material layers; HMA wearing course, HMA or cold-recycled mid-layer, and existing/old HMA asphalt layer. Level 1 dynamic modulus data for the overlay and mid-layer in both sections were used as input the Pavement ME Design® software. The HMA wearing surface properties for both sections were taken from a typical Maryland State Highway (MDSHA) 9.5 mm surface mix. Several 9.5 mm mixes were tested in the lab with a fairly narrow range of dynamic modulus master curves as depicted in Figure 6.2. The HMA mid-layer properties for the RP-HMA structure corresponds to a typical MDSHA 19 mm mix designated H151B19; the dynamic modulus master curve for this and for a range of other 19 mm mixtures and illustrated in Figure 6.3. For the RP-CIR layer, Level 1 dynamic modulus properties from recycled projects were used. Recycled materials had a wider range of dynamic modulus in comparison to HMA mixtures, which can be seen in Figure 6.4.

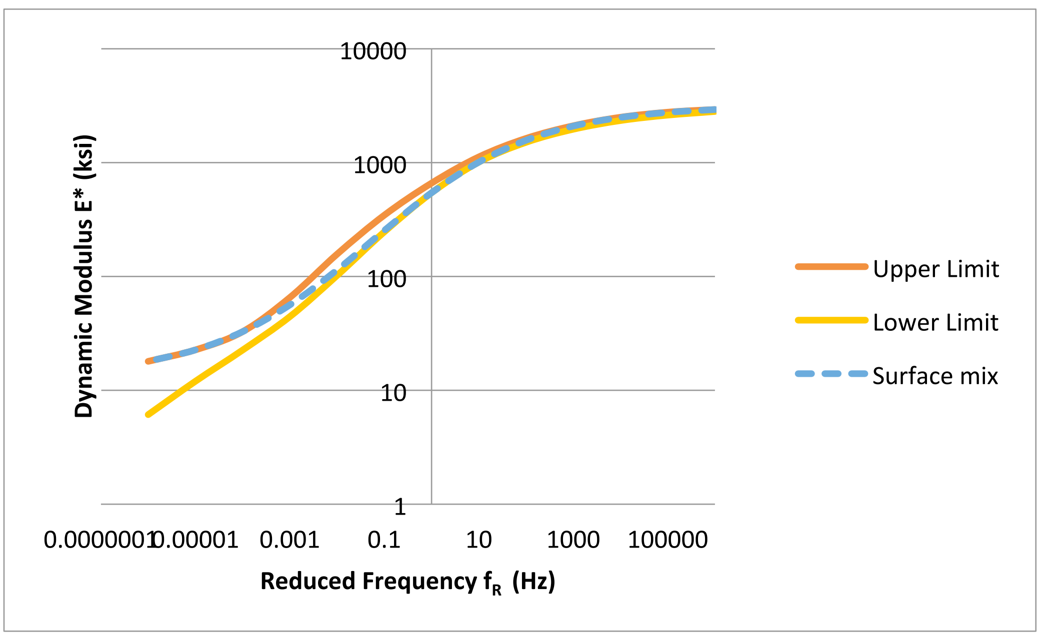

Figure 6.2. Master curve for 9.5 mm HMA surface mixture. Upper and lower bounds for typical MDSHA 9.5 and 12.5 mm mixtures are also shown.

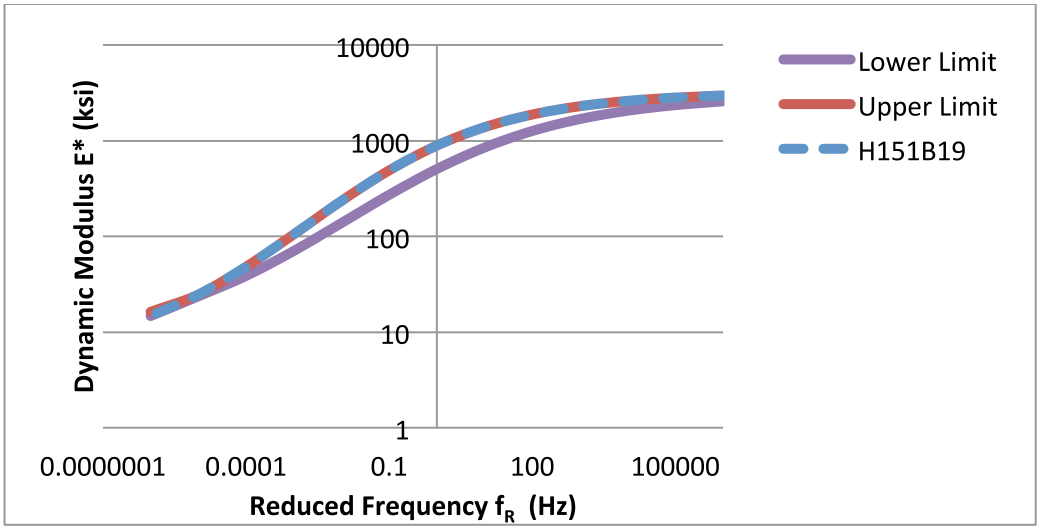

Figure 6.3. Master curve for 19 mm HMA overlay mixture (H151B19). Upper and lower bounds for typical MDSHA 19 mm mixtures are also shown.

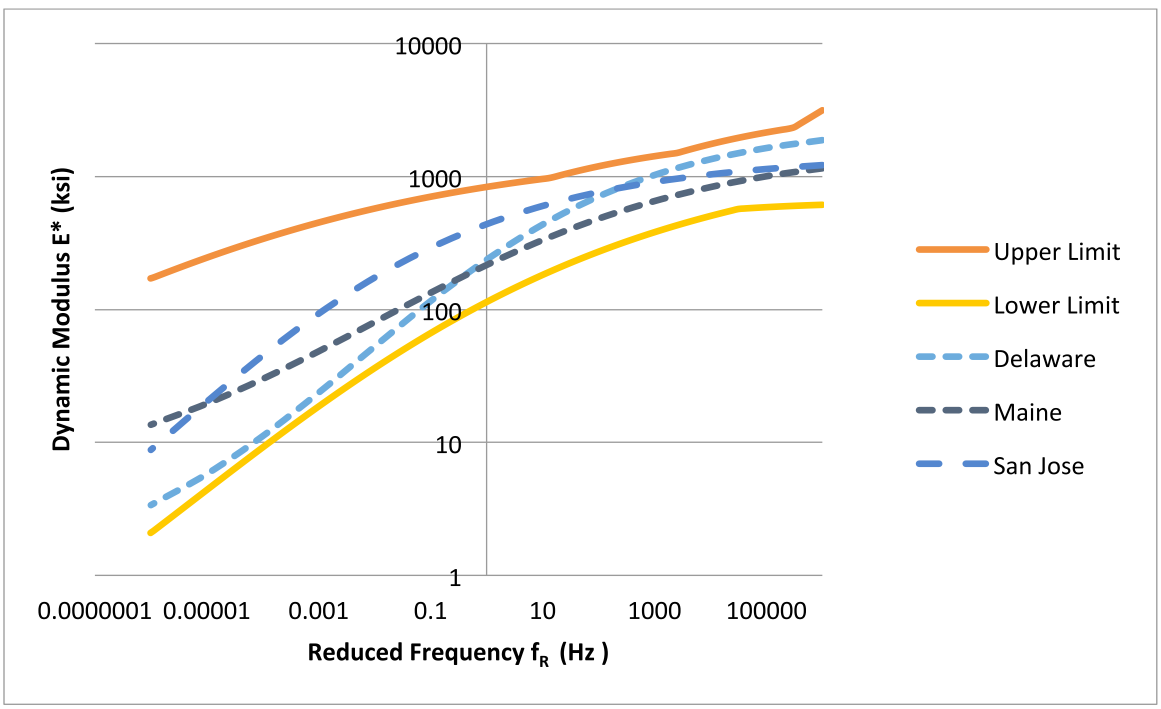

Figure 6.4. Master curves for cold-recycled overlay materials (Delaware/CIR, Maine/CCPR, San Jose/CIR). Upper and lower bounds for the cold-recycled materials in this study are also shown.

6.2.2 RLPD Input

Rutting was the main distress measure evaluated in these comparisons. Therefore, the Level 1 rutting coefficients are needed for input into the Pavement ME Design® software. To derive the rutting calibration coefficients, the MEPDG rutting model was fit to the measured laboratory test results as previously described in 'Processed Data' section. The calibration coefficients obtained from fitting the model to lab data were used as direct RLPD input (K_1, K_2, and K_3). During the fitting procedure for some mixes, negative values were obtained for the temperature coefficient, which suggests that resilient strains are more sensitive to temperature than permanent strains. It should be noted that this does not imply lower rutting at higher temperatures; the strain ratio decreases but plastic strains keep increasing with increasing temperature. **Error! Reference source not found.** shows the rates of change for plastic strains and resilient strains at the 10,000th cycle. Each group of strains is normalized by its respective strain at 20°C; in other words, the plastic strains at each temperature are divided by the plastic strain at 20°C and the resilient strains are divided by the resilient strain at 20°C. These negative coefficients were due to the fact that Dynamic modulus tests on samples were performed in unconfined conditions that lead to lower stiffness at higher temperature. As discussed in previous chapters, confined modulus curves were produced to estimate appropriate resilient strains values. After calculation of true resilient strain values all Br_2 values were positive.

6.2.3 Traffic Input

Different traffic loads were applied for the different HMA wearing course thicknesses. Appropriate AADT values were determined based on the 1993 AASHTO flexible pavement design standard. The 1993 AASHTO procedure predicted 10, 15, 27, and 46 million ESALs over 20-year design life for the 1.5”, 2”, 3”, and 4” HMA wearing courses, respectively. For the Pavement ME Design® inputs, the vehicle mix consisted of a 100% distribution of Class 5 vehicles. Class 5 includes 2-axle vehicles with dual rear tires such as single-unit trucks, mini school bus, camping vehicles, etc. To simplify the traffic loading, the load for all rear axles was set at 18 kips (i.e., one ESAL) and the load for all front axles was set at zero. The traffic distribution was assumed to be constant in all months with zero growth rate.

6.2.4 Climate Input

Three weather station having different climatic characteristics were chosen for this study: MD as temperate, AZ as hot, and MN as cold weather conditions.

6.2.5 MEPDG Analyses

All recycled materials tested in NCHRP Project 9-51 were analyzed and input into the MEPDG software to compare levels of rutting against rutting for the reference HMA overlay case.

As an initial analysis, three different projects having recycled materials with different levels of RLPD behavior were analyzed for the MD weather conditions to evaluate the influence of a range of recycled material behavior on predicted rutting. Delaware (14-1025), a CIR emulsion project, exhibited high laboratory-measured permanent strains in comparison to the other materials; Maine (15-1003), a CCPR emulsion project, had moderate measured permanent strains, and San Jose (13-1124), a CIR foam project, had the smallest measured permanent strains. All three projects also had acceptable R^2 values for the multiple-regression fits of the laboratory RLPD data. Goodness of fit was also a criterion for choosing HMA mixtures for the wearing course and overlay layer in the pavements. The range of behavior for the HMA mixtures was much narrower in comparison to the cold recycled materials. The range of RLPD behaviors of both HMA and cold recycled materials are shown in **Error! Reference source not found.** through **Error! Reference source not found.**. As it can be seen from these figures, the Delaware project has the highest permanent deformations all three temperatures while San Jose has the lowest and Maine is in between.

The Level 1 dynamic modulus for each mixture was input into the Pavement ME Design® software for the HMA/cold-recycled overlay layer and the HMA wearing course. The corresponding Level 1 calibrated coefficients for the RLPD behavior for these layers were also input. These initial analyses are designed to give insight into how the laboratory measured Level 1 RLPD behavior affects the rutting performance of the rehabilitated asphalt pavements.

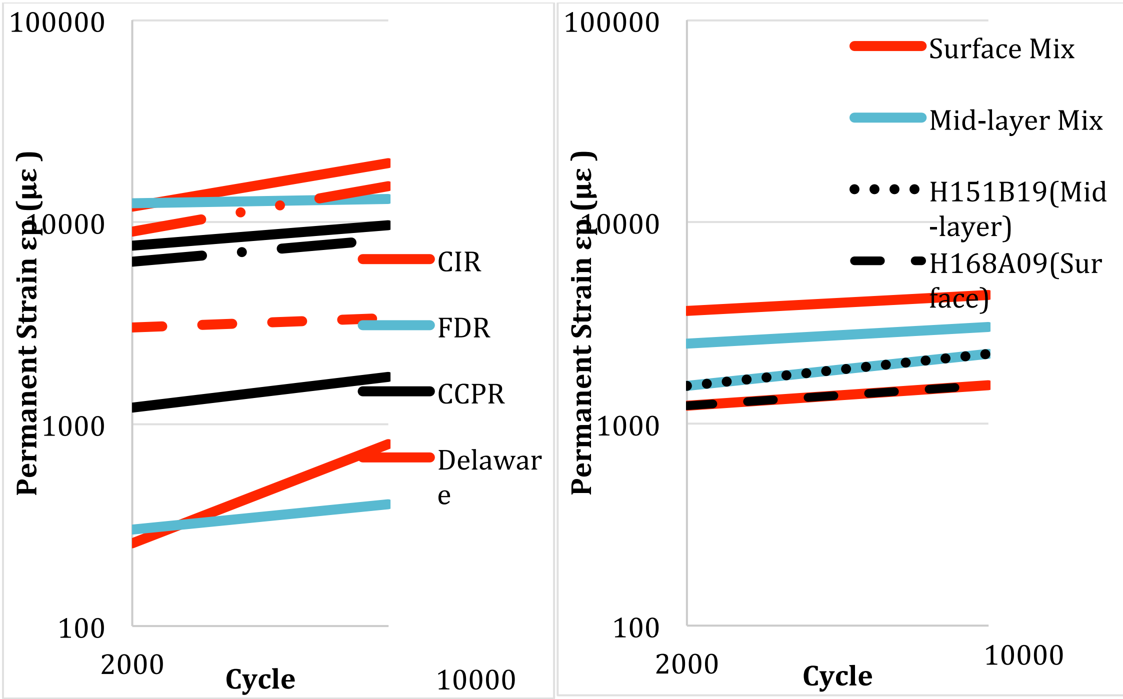

Figure 6.5. Measured permanent strains at 20°C: (a) cold recycled materials; (b) HMA mixtures. Dashed lines depict individual mixtures while colored areas show the range for each type of rehabilitation.

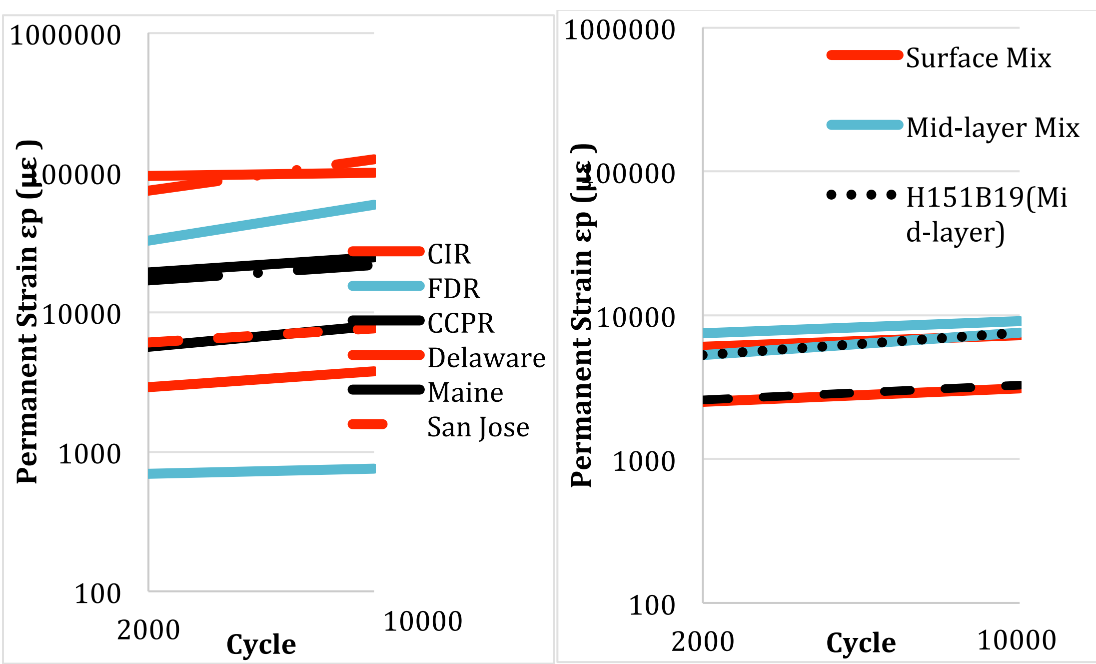

Figure 6.6. Measured permanent strains at 45°C: (a) cold recycled materials; (b) HMA mixtures.

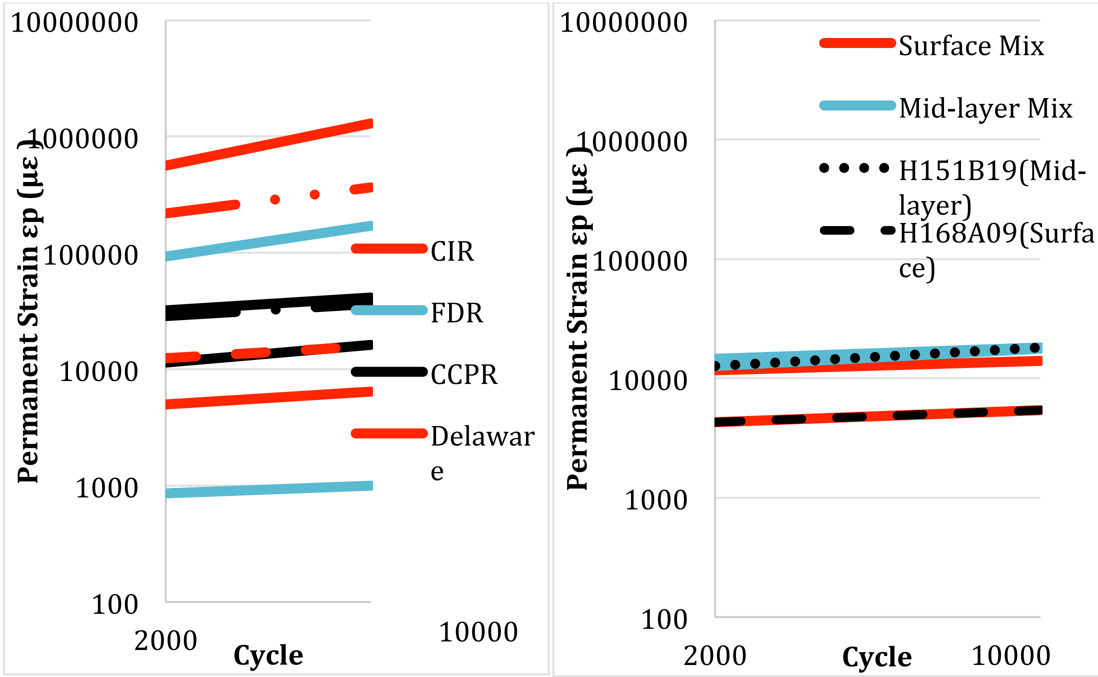

Figure 6.7. Measured permanent strains at 58°C: (a) cold recycled materials (b) HMA mixtures.

6.3 MEPDG Output

6.3.1 Initial Analyses

The MEPDG results for Asphalt Concrete (AC) rutting are shown in Figure 6.8 through Figure 6.10. AC rutting includes the contributions from all bituminous materials—the HMA surface course, the HMA/cold-recycled structural overlay, and the underlying existing HMA material. The numeric suffix for each category indicates the thickness of the HMA wearing course. The RP-CIR overlay sections using the Maine CCPR properties (Figure 6.9) exhibited better performance than the reference RP-HMA sections for 3" and 4" wearing surfaces and only 0.07" more plastic strain for the 1.5" wearing surfaces. The RP-CIR overlay sections using the San Jose CIR properties (Figure 6.10) exhibited better performance than the reference RP-HMA sections for all wearing course thicknesses. Only the Delaware CIR material (Figure 6.8) showed consistently inferior performance as compared to the RP-HMA reference, and as expected this poor performance is worst for the thin HMA wearing course case. This is due to the higher rutting susceptibility of the Delaware material, which can be observed in **Error! Reference source not found.** through **Error! Reference source not found.** where the Delaware material is at upper range of plastic strains at all three temperatures. The predicted rutting results overall are consistent with the measured RLPD behavior of each of the materials in the lab.

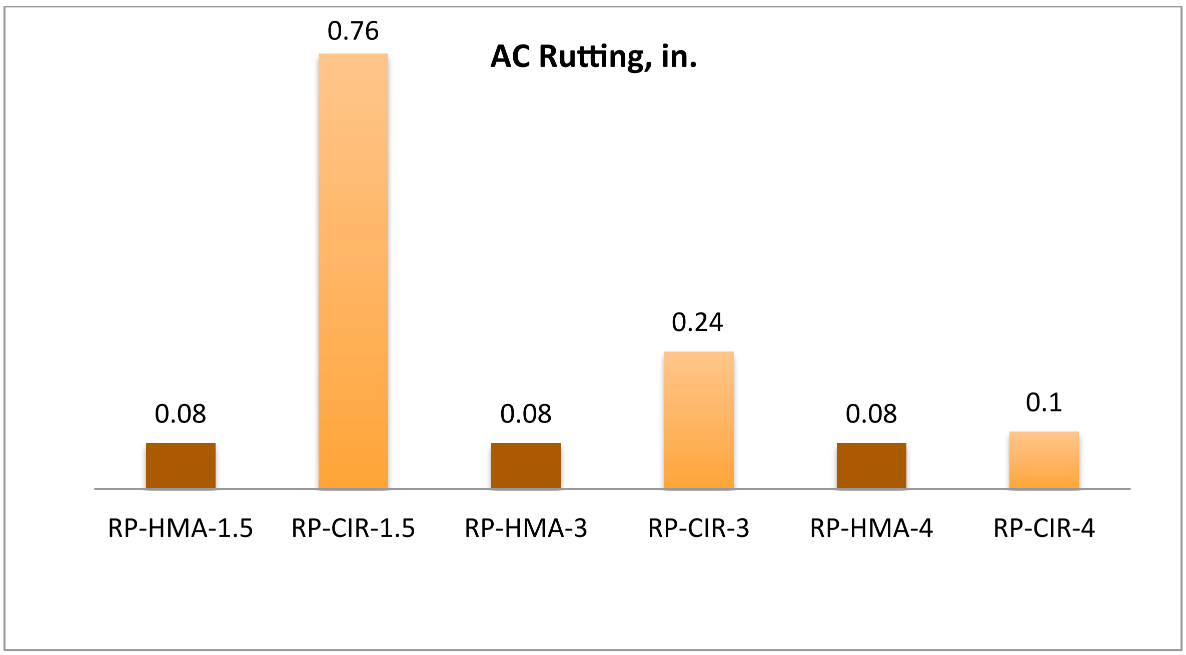

Figure 6.8. Asphalt rutting for Delaware CIR overlay in comparison to HMA overlay.

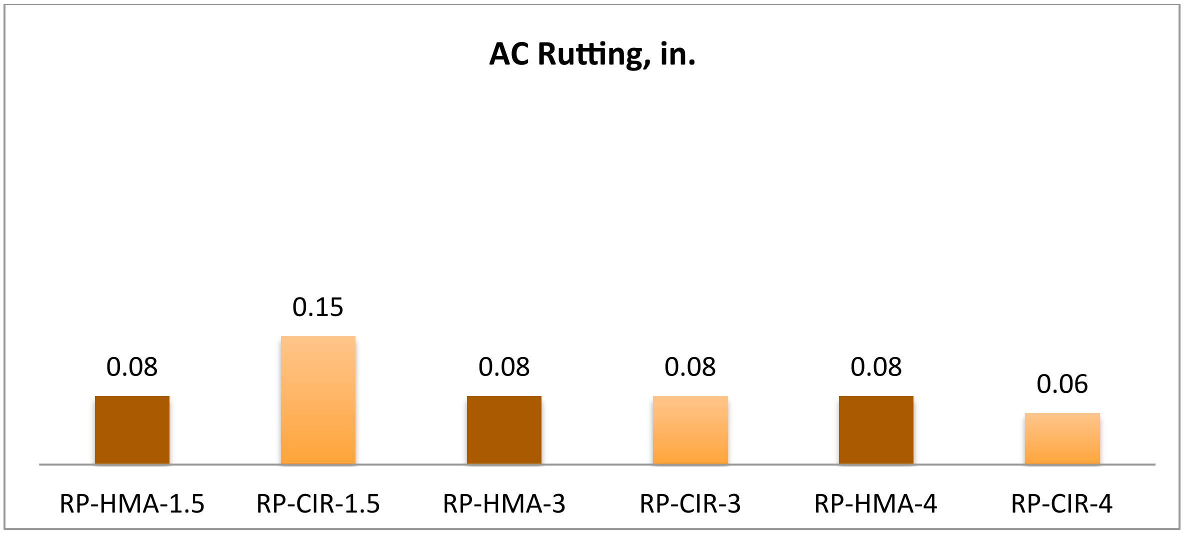

Figure 6.9. Asphalt rutting for Maine CCPR overlay in comparison to HMA overlay.

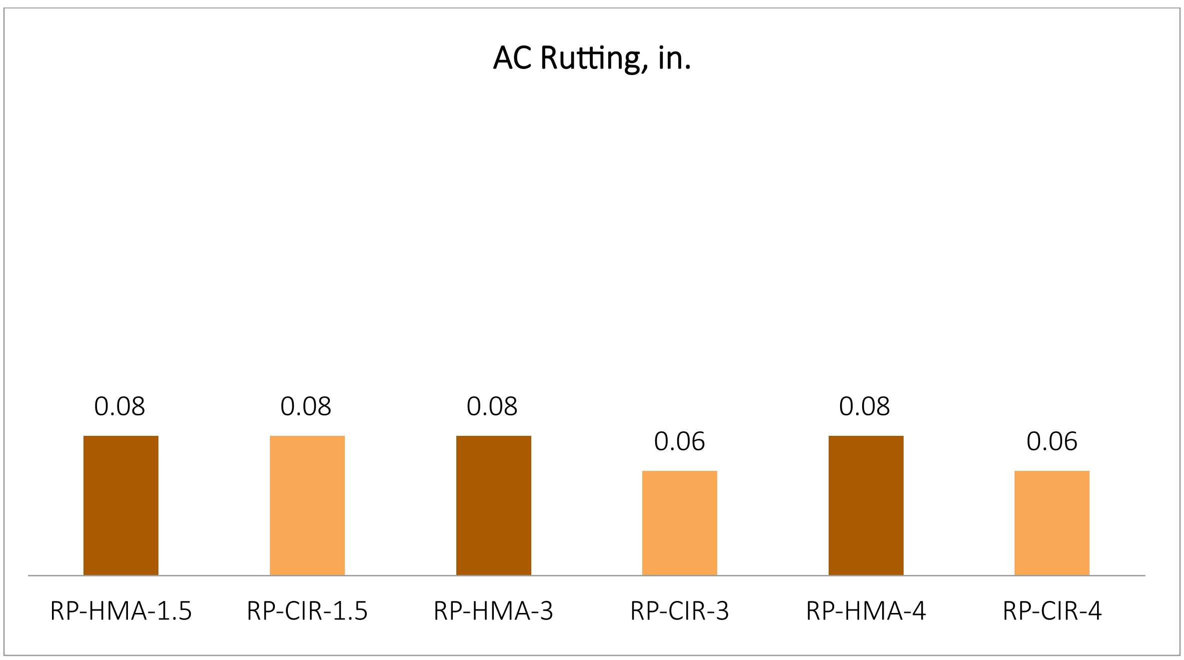

Figure 6.10. Asphalt rutting for San Jose CIR overlay in comparison to HMA overlay.

6.4 Complete Analyses

In addition to the initial three projects selected to represent the range of material qualities, all recycled projects accumulated for this study were analyzed for rutting performance.

Different climatic conditions were also added to the study to observe the effect of temperature on rutting performance.

Each project was analyzed with 4 different sections (1.5”, 2”, 3”, and 4” HMA wearing courses) in three different weather conditions. Results are represented in Figure 6.11 through Figure 6.13. Rutting values are also represented in Table 6.2.

Note that in the following graphs some projects do not have a column, This is due to the failure of the MEPDG software to run for these projects. Specifically, the software was unable to fit a master curve to the input laboratory-measured dynamic modulus data for these projects, so no predicted rutting is shown for these projects. This occurred for projects 13-1093, 13-1115, 13-1117, 13-1127, 14-1001, 14-1002, 14-1057, 15-1002. In addition, the RLPD test was not performed on the I-81CIR project, so rutting was not predicted for this project as well.

It can be observed in Figure 6.11 through Figure 6.13 that five of the seventeen analyzed projects had very high rutting values. These large rutting values are highly correlated with the RLPD calibrated coefficients input into MEPDG. The coefficients on temperature and traffic load play an important role in the predictions of rutting values. Analysis of the five projects with the highest ruttings (14-1025, 14-1026, 14-1055, 13-1111, and 13-1112) showed that these projects had higher permanent deformation in the laboratory tests (RLPD graphs of these materials are included in Appendix II. In the following paragraphs each of these projects is analysed to determine the reason for high rutting values.

Project 13-1111, a CIR Foam material, had very steep slope for its RLPD data. The slope value (exponent on N) was 0.52, which is double the average slope of 0.23 for all recycled materials in this study. Another issue with this project is its temperature susceptibility. At the highest test temperature of 58° C, the accumulated permant strains exceeded 10^6 microstrain at the end of 10,000 cycles, which is a very high value in comparison to rest of recycled materials.

Project 13-1112, also a CIR Foam material, also had a steep slope for its RLPD data. The slope was 0.36, which is significantly higher than the average value of 0.23 for all recycled materials. The plastic deformation at highest temperature was also close to 10^6 microstrains and the range of final permanent deformations among the three tested temperatures was high, indicating high temperature susceptibility.

Project 14-1055, a CIR Emulsion material, had a steep RLPD slope of 0.47 with final permanent deformations of more than 10^5 microstrains. This project also had more samples and more variability among the different temperatures, which produced high coefficients for the temperature term. The cases were similar for projects 14-1025 (CIR Emulsion) and 14-1026 (CIR Emulsion).

The rest of the projects with low predicted rutting had laboratory RLPD data with much lower final permanent deformations at high temperatures. For example, project 14-1058 (CIR Emulsion) had around 10^4 microstrains at the end of 10,000 cycles and its RLPD slope was 0.15, which is very close to average slope of the HMA mixtures (0.14). As a result, this project exhibited very small predicted rutting.

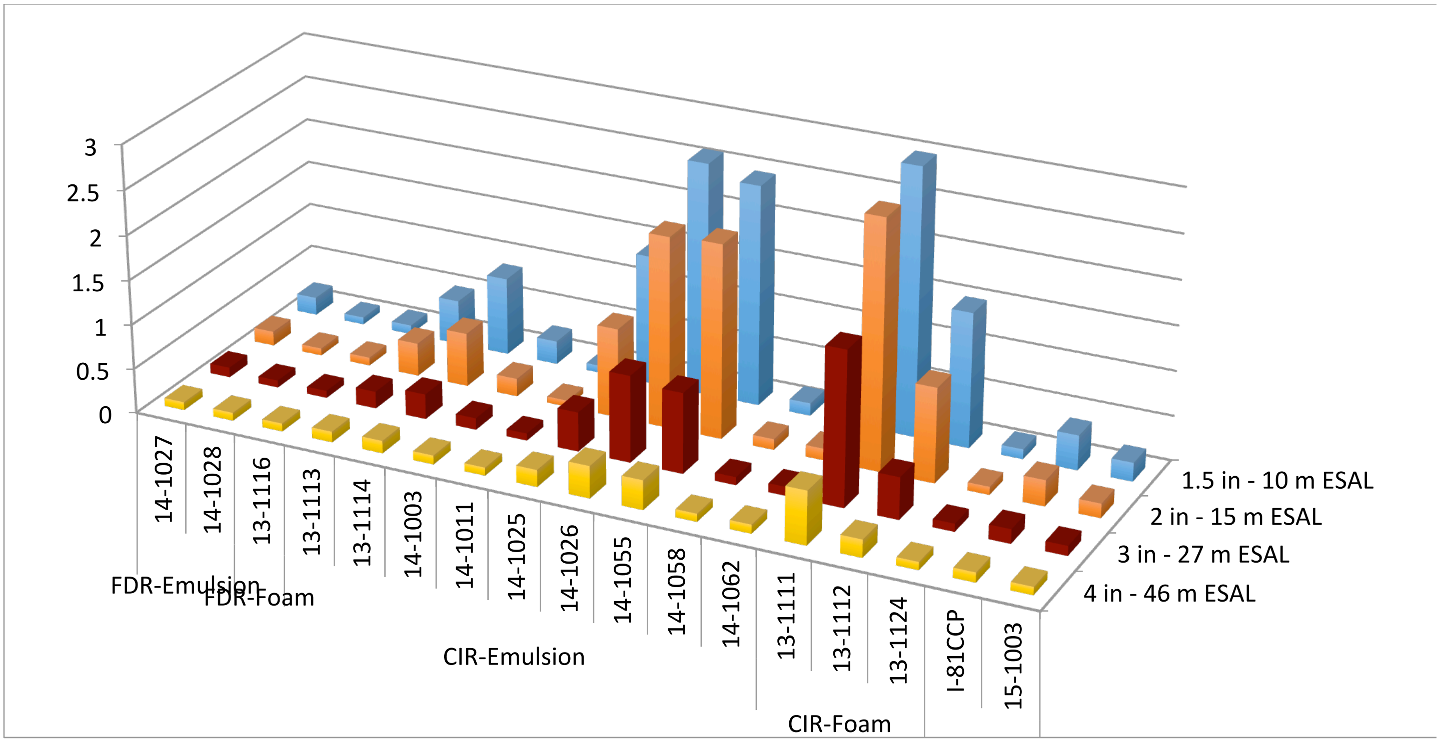

Figure 6.11. Rutting performance of all projects: 4 different sections in AZ weather.

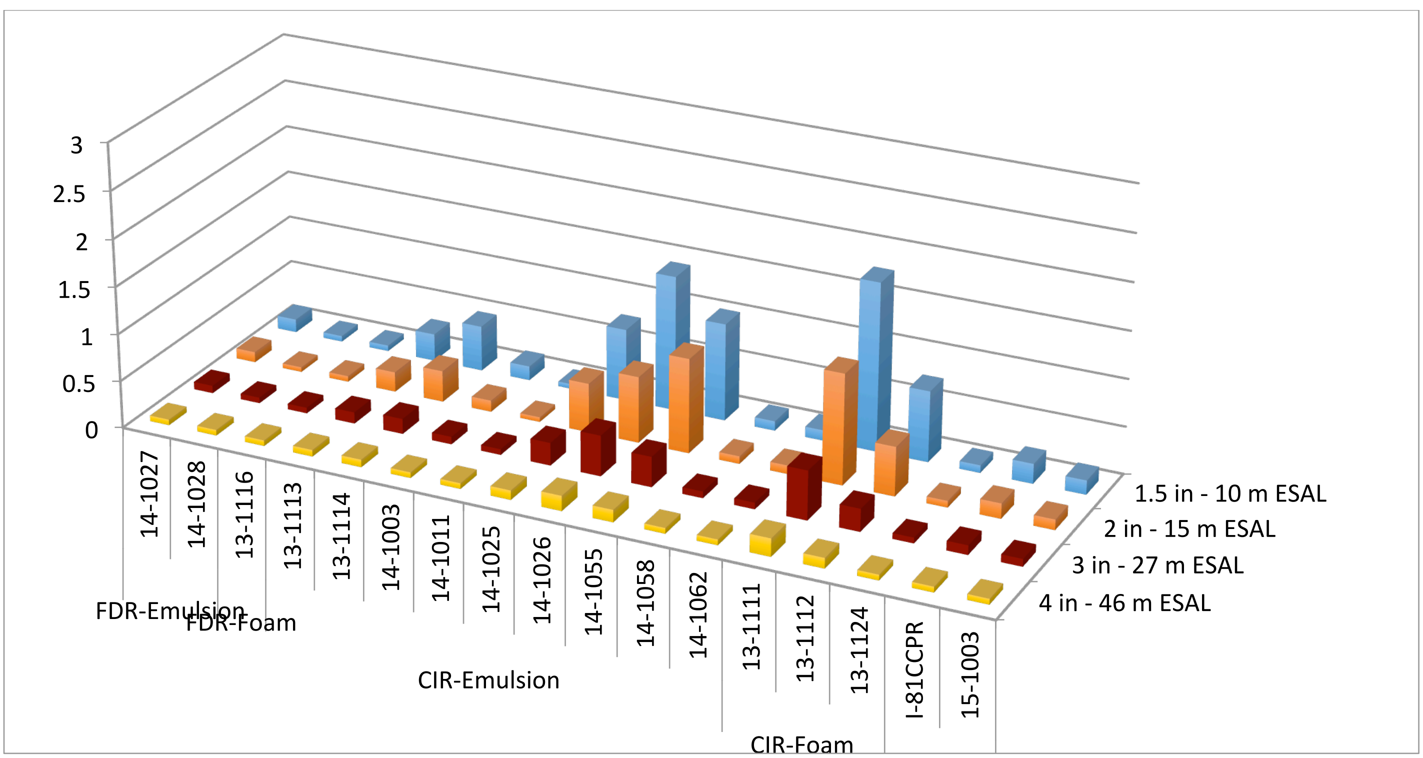

Figure 6.12. Rutting performances of all projects: 4 different sections in MD weather.

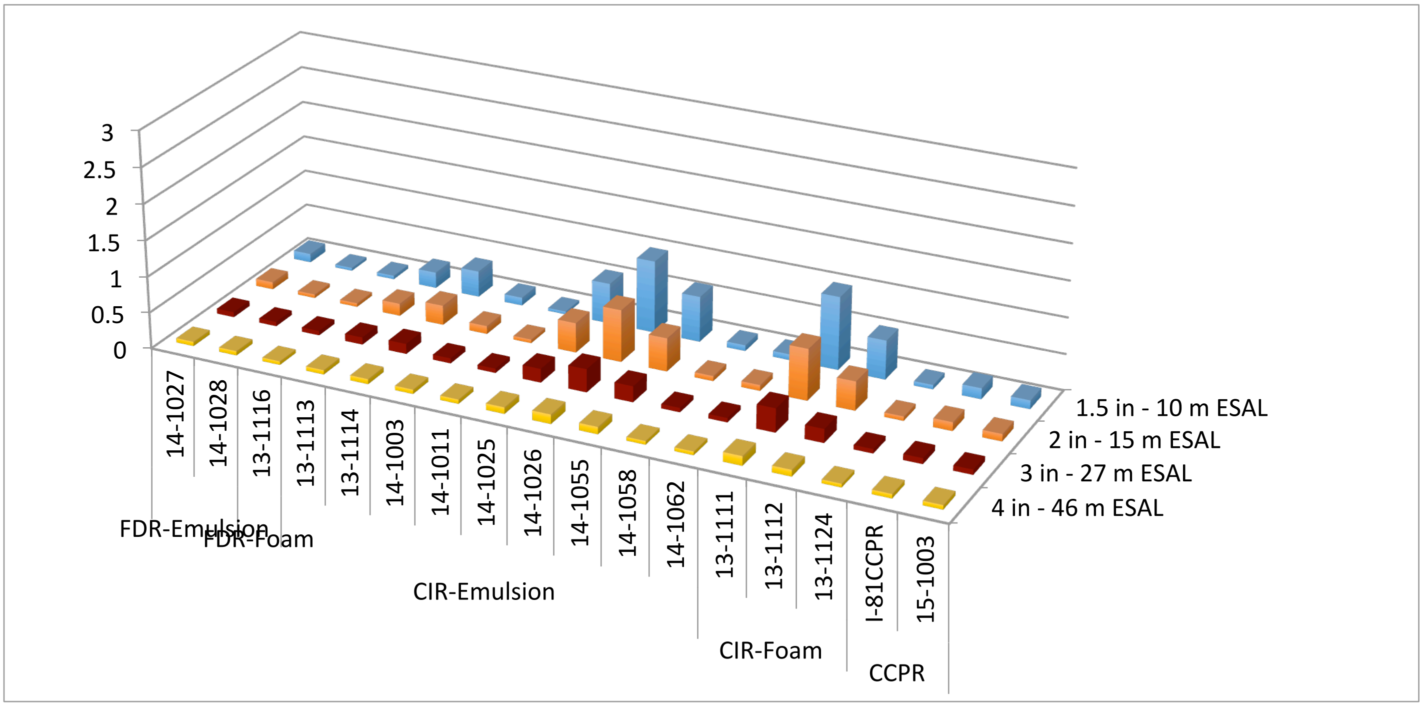

Figure 6.13. Rutting performance of all projects: 4 different sections in MN weather.

Table 6.2. Predicted rutting for all projects: 1.5" and 2" HMA wearing courses.

	1.5"			2"		
PROJECT	**AZ**	**MD**	**MN**	**AZ**	**MD**	**MN**
14-1027	0.2	0.14	0.12	0.16	0.11	0.1
14-1028	0.08	0.06	0.04	0.08	0.05	0.05
13-1116	0.1	0.06	0.05	0.09	0.06	0.05
13-1113	0.5	0.29	0.22	0.37	0.21	0.17
13-1114	0.87	0.48	0.36	0.6	0.33	0.27
14-1003	0.26	0.15	0.11	0.2	0.12	0.11
14-1011	0.08	0.05	0.04	0.07	0.05	0.05
14-1025	1.45	0.76	0.56	1	0.52	0.41
14-1026	2.61	1.43	1	2.14	0.7	0.72
14-1055	2.47	1.03	0.63	2.17	1	0.46
14-1058	0.14	0.1	0.08	0.12	0.08	0.07
14-1062	0.16	0.11	0.08	0.13	0.09	0.08
13-1111	3.21	1.78	1.01	2.79	1.17	0.71
13-1112	1.51	0.75	0.54	1.06	0.52	0.4
13-1124	0.11	0.08	0.06	0.09	0.07	0.06
I-81CCPR	0.39	0.21	0.15	0.29	0.16	0.12
15-1003	0.21	0.15	0.12	0.16	0.11	0.1

PROJECT	3"			4"		
	AZ	MD	MN	AZ	MD	MN
14-1027	0.11	0.08	0.07	0.09	0.06	0.06
14-1028	0.08	0.06	0.06	0.09	0.06	0.06
13-1116	0.08	0.06	0.06	0.09	0.06	0.05
13-1113	0.19	0.12	0.1	0.12	0.07	0.06
13-1114	0.28	0.16	0.14	0.14	0.08	0.07
14-1003	0.13	0.08	0.07	0.1	0.06	0.06
14-1011	0.08	0.06	0.06	0.09	0.06	0.06
14-1025	0.44	0.24	0.19	0.19	0.1	0.09
14-1026	0.97	0.43	0.32	0.36	0.16	0.13
14-1055	0.9	0.32	0.22	0.33	0.13	0.1
14-1058	0.09	0.07	0.06	0.09	0.06	0.05
14-1062	0.1	0.07	0.06	0.1	0.06	0.05
13-1111	1.73	0.52	0.33	0.6	0.19	0.13
13-1112	0.47	0.24	0.19	0.2	0.11	0.09
13-1124	0.09	0.06	0.06	0.09	0.06	0.05
I-81CCPR	0.16	0.1	0.08	0.11	0.06	0.06
15-1003	0.11	0.08	0.07	0.09	0.06	0.06

The range of predicted rutting for the cold-recycled projects (RP-CIR) is compared with the predicted rutting of conventional HMA overlays (RP-HMA) in Figure 6.14 through Figure 6.16. In these box and whisker plots, each dot represents a single project and project types are differentiated by color (CIR/FDR/CCPR). The blue lines in the graphs represent the predicted rutting for the RP-HMA sections at each wearing course thickness. The CIR projects exhibited a greater range of values in part because there were more of them. Only two CCPR and three FDR projects were analyzed using the MEPDG.

The trends in Figure 6.14 through Figure 6.16 clearly show that wearing course thickness is an important factor for predicted rutting. The 3” and 4” wearing course sections in all three weather conditions had predicted rutting values in a narrow range with a mean value very close to their RP-HMA counterparts. Rutting decreased as the wearing course increased despite the increase in traffic with increased wearing course thickness. Thus it can be concluded that as long as HMA wearing course thickness is above some threshold—2” to 3” based on Figure 6.14 through Figure 6.16—the cold-recycled rehabilitated sections exhibit predicted performance comparable to that for conventional HMA rehabilitated sections.

It can also be observed from Figure 6.14 through Figure 6.16 that the range and mean values of predicted rutting for the cold-recycled sections decreases with decreasing temperature. The mean predicted rutting in all three weather conditions is also acceptable for design, except perhaps for the thinnest wearing course (1.5 inches). The average values of rutting for the temperate MD weather conditions for the 1.5”, the average predicted rutting for the 2”, 3”, and 4” wearing course thicknesses were 0.44”, 0.31”, 0.16”, and 0.084” respectively. The last two values are well below the default design limit of 0.25”. For the thinner 1.5” and 2” wearing courses, the rutting performance can still be considered reasonably good considering that the traffic applied to these sections was quite high. CIR rehabilitation had historically been most commonly used on low volume roads. The results from the present analyses clearly show that with a wearing course thickness of more than 2” these cold-recycled materials can be used successfully in higher traffic roads. As discussed previously, the 5 projects with poor rutting performances also had substandard laboratory RLPD behavior. Good quality cold-recycled materials that exhibit satisfactory laboratory RLPD behavior exhibit satisfactory predicted rutting performance similar to that for conventional HMA mixes.

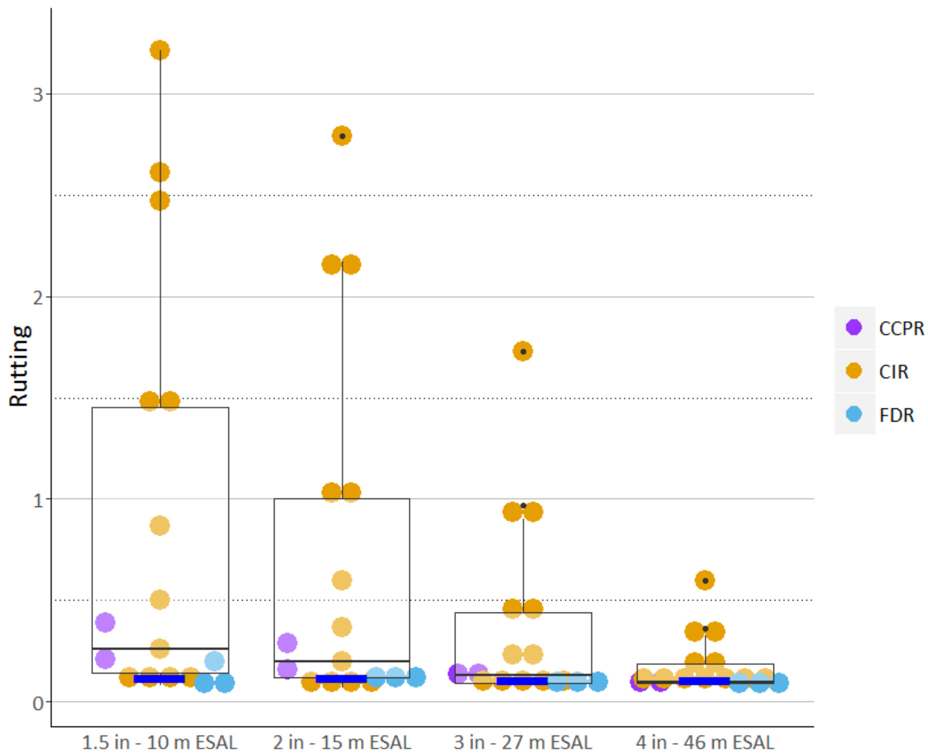

Figure 6.14. Predicted rutting: AZ weather.

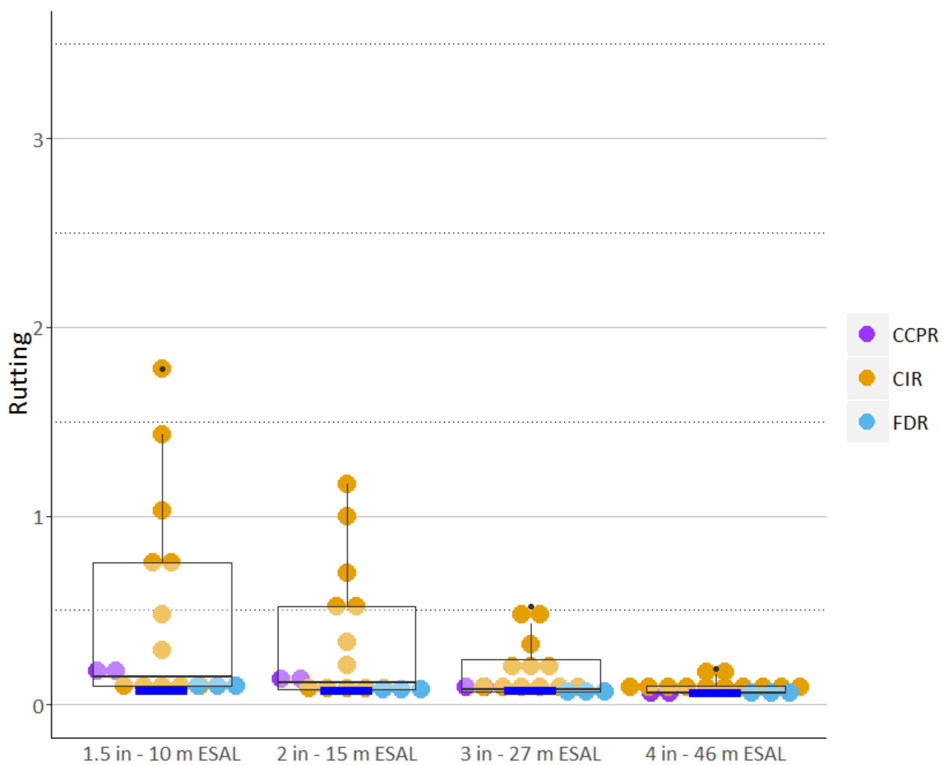

Figure 6.15. Predicted rutting: MD weather.

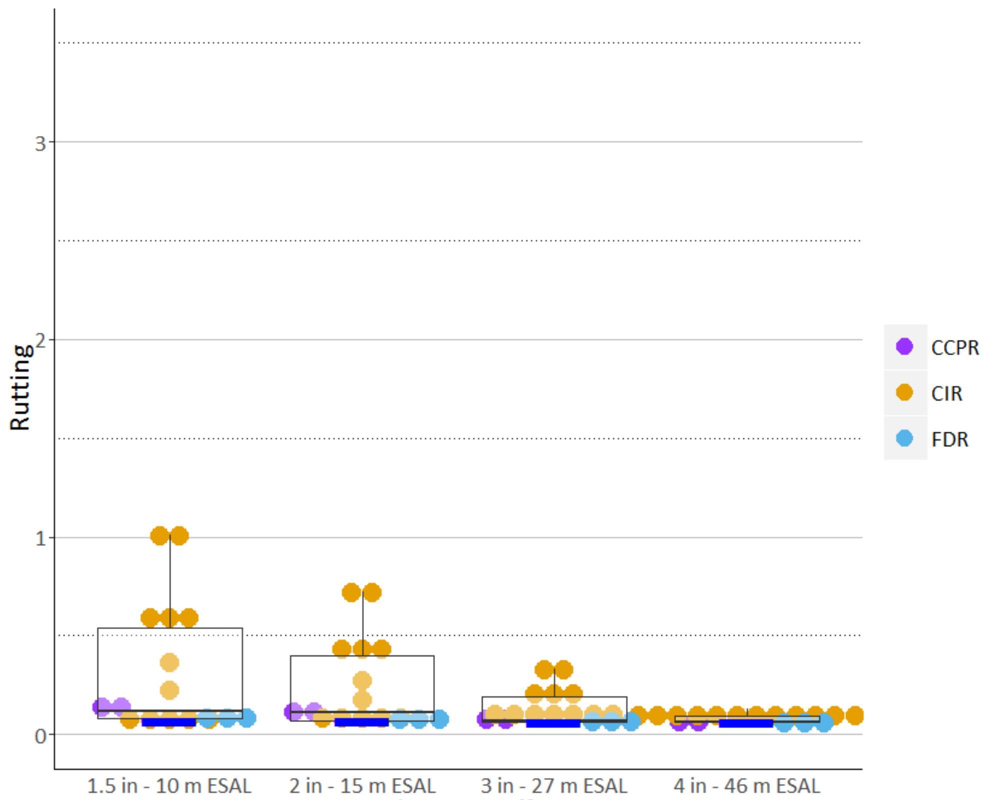

Figure 6.16. Predicted rutting: MN weather.

6.5 *Overall Conclusions*

The overall conclusions from the MEPDG rutting predictions are as follows:

- The temperature and traffic exponents in the RLPD model have a crucial role to determine amount of rutting. These characteristics are calculated based on the laboratory measured RLPD curves. The slope of the RLPD graph and amount of measured plastic deformation at three temperatures define these two exponents.
- Predicted rutting for the cold-recycled overlay scenarios decreases as HMA wearing course thickness increases. As the CIR layer is pushed deeper into the pavement structure, it acts more like the RP-HMA reference.
- The RP-CIR sections performed very well. Only 30% of them had a poor rutting performance, and these were all in sections with thin HMA wearing courses. As

the wearing course thickness increased to 3” and 4”, rutting was reduced substantially. Cold-recycled materials that exhibit poor laboratory RLPD behavior (e.g., high traffic exponent, high temperature susceptibility) also exhibit poor predicted rutting performance.

- Rehabilitated pavement sections having good quality cold-recycled materials and a moderately thick HMA wearing course (e.g., 2” thick or greater) exhibit predicted pavement performance comparable to that for conventional HMA rehabilitated sections.

Chapter 7: Neural Network Modeling

7.1 Correlation Analyses

One of the goals of this study was to develop a procedure for predicting the field-cured structural material characteristics for cold-recycled materials as a function of mix design and construction variables. In order to accomplish this the information gathered from the projects was divided into two main groups: design properties and performance properties. Design properties include the mix design characteristics and information collected at time of construction like construction equipment, weather conditions, compaction, etc. Performance properties are the dynamic modulus and repeated load permanent deformation data from laboratory testing of field-cured cores.

A bivariate correlation was performed between the design and performance properties. Correlation coefficients between these two groups are summarized in Table 7.1. A few strong correlation was observed in the data that were higher than 0.3. There was a good correlation between modulus at 4 and 20C and bulk density, a good correlation between lower shelf and dry additive and good correlation of modulus at 40C and depth of recycling and C_z. The intercorrelations for each group are also presented in Table 7.2 and

Table 7.3. As expected modulus values had high inter-correlation among themselves (E*@ 4C,25hz,- E*@20C,10Hz- E*@40C,1Hz), as shown in in Table 7.2. Gradation parameters (P200, Cu,Cz) also had high intercorrelation, as can be seen in

Table 7.3.

Table 7.1. Correlation Coefficients of Design vs. Performance parameters

	Stabilizer Content	P200	Cu	Cz	OL thickness	Curing time	Dry additive	Depth of recycling	Bulk density
MaxE*	0.09	0.037	0.06	0.135	0.061	0.023	-0.029	0.044	-0.091
MinE*	-0.043	0.218	0.004	0.212	0.089	0.035	0.32	0.225	-0.074
Beta	0.092	0.073	0.128	0.205	-0.071	0.116	0.142	0.072	0.061
Gamma	0.016	-0.211	-0.156	-0.069	-0.18	0.084	-0.056	-0.174	0.254
EA	-0.141	-0.144	-0.247	0.013	-0.084	0.011	0.107	-0.123	0.169
E*@ 4C,25hz	-0.022	-0.239	-0.276	-0.17	-0.268	-0.064	-0.165	-0.141	0.766
E*@20C,10Hz	-0.055	-0.059	-0.208	0.113	0.123	-0.092	0.097	0.159	0.382
E*@40C,1Hz	-0.033	0.117	-0.129	0.459	0.391	-0.027	0.428	0.536	-0.112

Table 7.2- Intercorrelation of performance parameters

	MaxE	MinE	Beta	Gamma	EA	E4c25hz	E20C10Hz	E40C1Hz
MaxE*	1	0.085	0.518	-0.016	-0.688	-0.178	-0.152	-0.031
MinE*		1	0.243	-0.488	0.052	0.017	0.221	0.298
Beta			1	-0.162	-0.318	-0.159	-0.265	-0.117
Gamma				1	0.37	0.309	0.123	0.052
EA					1	0.413	0.344	0.152
E*@ 4C,25hz						1	0.811	0.286
E*@20C,10Hz							1	0.717
E*@40C,1Hz								

Table 7.3- Inter-correlation of design parameters

	Bulk density	Stabilizer Content	P200	Cu	Cz	OL thickness	Curing time	Dry additive	Depth of recycling
Bulk density	1	0.069	-0.181	-0.151	-0.412	-0.49	0.013	-0.391	-0.478
Stabilizer Content		1	0.455	0.681	0.463	-0.221	0.595	-0.083	-0.495
P200			1	0.479	0.248	-0.225	0.165	0.287	0.139
Cu				1	0.237	0.097	0.004	0.055	0.067
Cz					1	0.359	0.386	0.638	0.617
OL thickness						1	-0.288	0.51	0.381
Curing time							1	0.114	-0.335
Dry additive								1	0.721
Depth of recycling									

The next step was to develop a neural network model for predicting the performance properties. The main measured performance properties were dynamic modulus and permanent. Dynamic moduli at specified temperatures and frequencies-- E* at 4°C & 25Hz ,20°C & 10Hz, 40°C & 1Hz—were specified as one set of modeling targets. Inputs for the model were selected based on the correlation analysis. The design parameters with higher correlation coefficient and lower level of significance were selected as the inputs to the neural network.

7.2 Neural Networks

Artificial Neural Network (ANN) is a modeling procedure inspired by the neural system of the human brain. ANNs are generally applied in estimation, interpolation, and classification problems. An ANN predicts an output based on complicated non-linear relations embedded in the network. The ANN structure has multiple layers and sets of nodes. Multiple neurons with weighted coefficients enter a node. Then an activation function is applied on the summation of entries and result is multiplied by specific weight coefficient before being sent to other nodes. Activation functions are usually nonlinear. A very popular activation function is the sigmoid function (Equation 7.1). Other activation functions include Gaussian, sine, hyperbolic tangent, etc.

$$\sigma(x) = \frac{1}{1+e^{-x}} \qquad \text{Equation 7.1}$$

7.2.1 Back-propagation Network

There are different methods to "train" or iteratively adjust the connection weights and activation thresholds in ANNs. Back-propagation is a reliable training methods that is used widely among researchers. After a feed-forward pass that calculates the outputs from inputs in a forward motion, the predicted outputs are compared to actual outputs for the training data. Then a backward pass improves the network by adjusting the connection weights and activation thresholds to reduce the error (Koehn, 1994). The error is calculated according to Equation 7.2:

$$. \ r = \frac{1}{2} \sum_{population} |Output_{predicted} - output_{measured}|^2 \qquad \text{Equation 7.2}$$

In each training step, weights are modified based on the maximum decrease in error summation (Equation 7.2).

7.3 ANN in Pavement Studies

ANN has become a reliable prediction tool in pavement field. Ceylan et al (2008) showed that E* prediction with neural network enhanced the accuracy of prediction and yielded less bias than for regression-based techniques. It demonstrated better E* predictions at extreme temperatures as well. Meier and Rix (1994) used a back-propagation ANN for backcalculation of moduli in a multi-layer flexible pavement. ANN proved to be three orders of magnitude faster than the conventional method for modulus estimation and provided accurate layer moduli values. ANNs have also been used or prediction of flow number in asphalt mixtures. Mirzahosseini et al (2015) developed a model that predicts flow number based on mixture gradation information, percentage air void, and bitumen content.

7.4 Genetic Algorithms

Genetic algorithms based on natural selection and biological evolution can be used in optimization problems. This approach was introduced by John Holand at Michigan University in 1972 and is described in his 1975 book entitled "Adaptation in Neural and Artificial Systems". Genetic algorithms are applicable to complicated optimization problems with discontinuous, non-differentiable, stochastic, or highly nonlinear objective functions. Genetic Algorithm and Neural Networks

Combining of neural networks and genetic algorithm was introduced in the a980's. Genetic algorithms as a search method is an effective approach for optimizing neural networks. Genetic algorithms can be used to optimize number of layers, neurons, and weight coefficients in the network.

7.5 ANN Implementation

Neural network models were designed for predicting dynamic modulus at three temperature and frequencies (40°C & 1Hz, 20°C & 10Hz, 4C & 25 Hz). Inputs are chosen base on high correlation with performance criteria: bulk density, percentage passing sieve #200, C_z (curvature coefficient), dry additive, and depth of recycling. The optimum ANN structure for all of the models had 1 hidden layer. After numerous evaluations a hyperbolic tangent was selected as the transfer function, as it had better performance than the commonly used sigmoid function. The network was trained for 200 generations on XX training data sets. The results are demonstrated in Figure 7.1. The red line in these figures shows the line of equality. Predicted vs. measured are graphed along with the goodness-of-fit R-values. Several different network structures were tested; however, none of them was able to make good predictions. This is due primarily to the lack of sufficient training data.

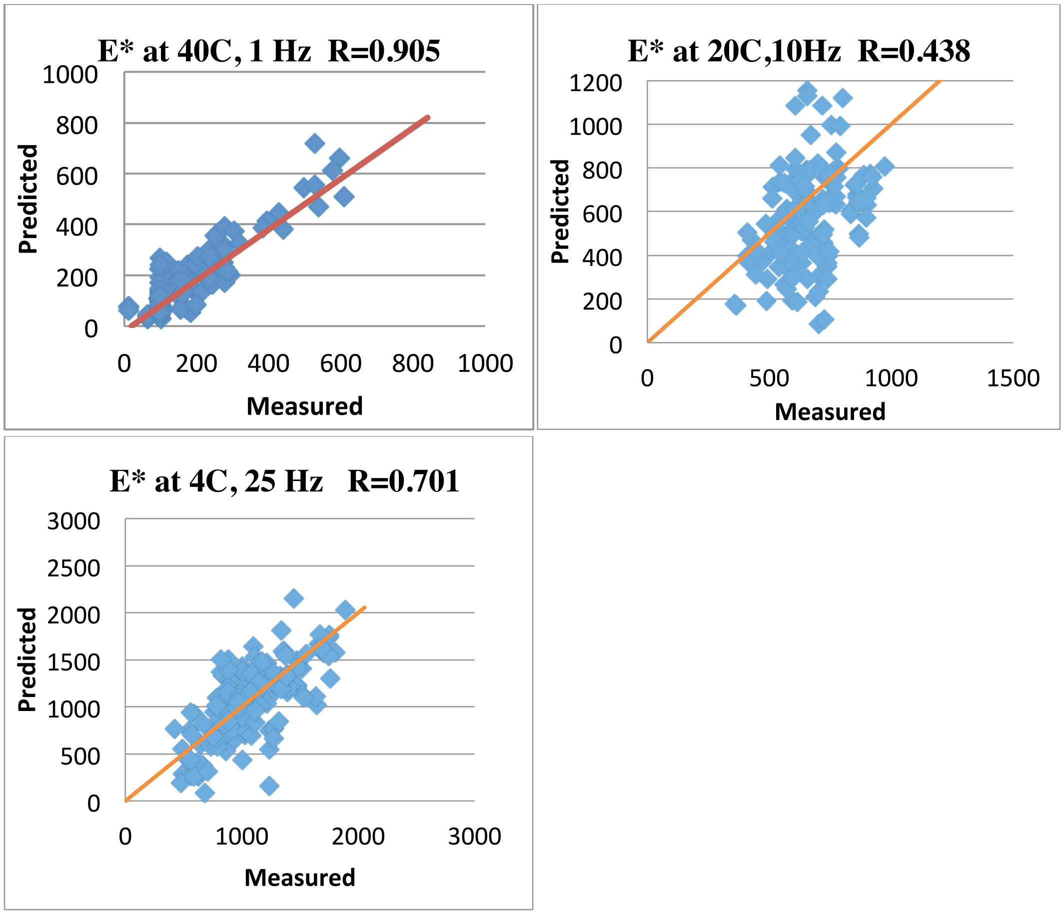

Figure 7.1. ANN implementation on E*

Chapter 8: Summary and Conclusions

Cold in-place recycling (CIR) and cold central plant recycling (CCPR) of asphalt concrete (AC) and/or full-depth reclamation (FDR) of AC and aggregate base are viable, faster, and less costly rehabilitation alternatives to conventional partial- and full-depth reconstruction for structurally distressed pavements. Lack of knowledge in several areas has hampered the acceptance of these cold-recycling techniques.

This study, which is part of the larger National Cooperative Highway Research Program (NCHRP) Project 9-51, investigated the structural properties of asphalt stabilized cold-recycled materials in pavement structures. The structural properties of interest are the dynamic modulus and repeated load permanent deformation characteristics, which are required as inputs to the Mechanistic-Empirical Pavement Design Guide (MEDPG) pavement structural design methodology. Comparisons of these properties for cold-recycled vs. conventional hot mix asphalt (HMA) materials was a major focus of the study.

Dynamic modulus and repeated load permanent deformation characteristics for the cold-recycled materials were determined from laboratory testing of small-scale specimens extracted from the field cores. All laboratory testing of the cold-recycled materials was conducted by others at the Virginia Center for Transportation Research (VTRC). Companion laboratory testing comparison HMA mixtures was performed by others at the Maryland State Highway Administration. All HMA testing was performed on conventional-scale laboratory-prepared test specimens following the relevant AASHTO test protocols. Testing of the cold-recycled materials was performed on small-scale specimens extracted from field cured cores. All testing was performed on Asphalt Material Performance Test (AMPT) devices manufactured by Industrial Pneumatic Controls (IPC) of Australia.

Key findings from the laboratory testing are as follows:

- The dynamic modulus master curves for the cold-recycled materials tended to have a flatter S-shape with a transition slope that was 35% less than for HMA materials on average. This indicates that the cold-recycled materials are less loading rate and/or temperature sensitive than HMA.
- Typical modulus values at low, medium, and high temperatures showed that the cold-recycled materials had stiffness similar to HMA at high temperatures but about half the stiffness of HMA at medium and cold. However, the cold-recycled materials typically are used in the intermediate or deeper layers of the pavement where temperature and stress effects are reduced.
- The cold-recycled materials had a wider range of RLPD behavior than for HMA. The average slope of the secondary region of the RLPD curve for recycled materials was twice that of HMA. The intercept for the cold-recycled materials was also more than twice that of HMA.
- MORE

A rutting sensitivity analysis was performed on two rehabilitation scenarios with recycled and conventional HMA structural overlays in different climatic conditions using the Mechanistic Empirical Pavement Design (MEPDG) methodology. Level 1 dynamic modulus and repeated load permanent deformation inputs were used for the cold-recycled and conventional HMA overlay layers and for the HMA wearing course. Findings from the MEPDG performance predictions are as follows:

- The cold-recycled materials had different quality levels for their structural characteristics. Approximately 30% of the cold-recycled materials showed lower quality and did not have good rutting performance. These materials had steep RLPD curves with high measured plastic deformation and high temperature and traffic coefficients in the MEDPG rutting model. The rutting predicted in the MEPDG analyses was consequently very high, especially for cases with thin HMA wearing courses at the surface. Increasing the wearing course thickness reduced the predicted rutting.
- As the wearing course thickness increased, the predicted rutting decreased in all cold-recycled sections. As the cold-recycled layer is pushed lower in the pavement structure, the difference in the performance of the cold-recycled rehabilitated pavement approached that of the section with a conventional HMA overlay. Generally, no significant difference in predicted rutting for the cold-recycled vs. conventional HMA rehabilitated section was observed for wearing course thicknesses of 3 inches or greater. Under these conditions CIR, FDR, and CCPR are viable and reliable alternatives for conventional pavement construction.
- The MEPDG analyses showed that good-quality cold-recycled materials performed as well as conventional HMA sections even with thin wearing course thicknesses.

- Analysis of pavement sections in three different climatic conditions showed that all of the asphalt materials performed better in cold weather as expected. Since the material is temperature sensitive, it is generally stiffer and has better rutting performance in cold climatic zones.

An attempt was made to design a model to predict the dynamic modulus and repeated permanent deformation structural properties from mix design and field construction characteristics. This would enable pavement engineers to determine the mix design required for a specific traffic load, life cycle, and other criteria. Statistical correlation analyses and artificial neural network (ANN) techniques were employed to construct this model. The statistical correlation results were used to determine the ANN inputs likely to have the strongest influence on the ANN outputs.

The ANN modeling approach was evaluated for the prediction of dynamic modulus. The ANN models failed to provide reasonable predictions for dynamic modulus due to limited number of available projects. There were only 3 CCPR projects and 6 FDR projects; this is insufficient to provide a basis for a good model. In addition, lack of data from the remaining old asphalt layer introduces other uncertainties.

8.1 Suggestions for Future Work

Suggestions for building on and improving the work in this study include:

(1) Collect data from more projects and materials so that more robust statistical and/of ANN models can be developed to relate field-cured structural properties to mix design and construction variables.

(2) Using the field-cured structural properties as targets, develop a laboratory curing procedure that achieves these targets without having to wait 6 to 12 months in the field.

Appendix I: Dynamic Modulus master curve of NCHRP 9-51 projects

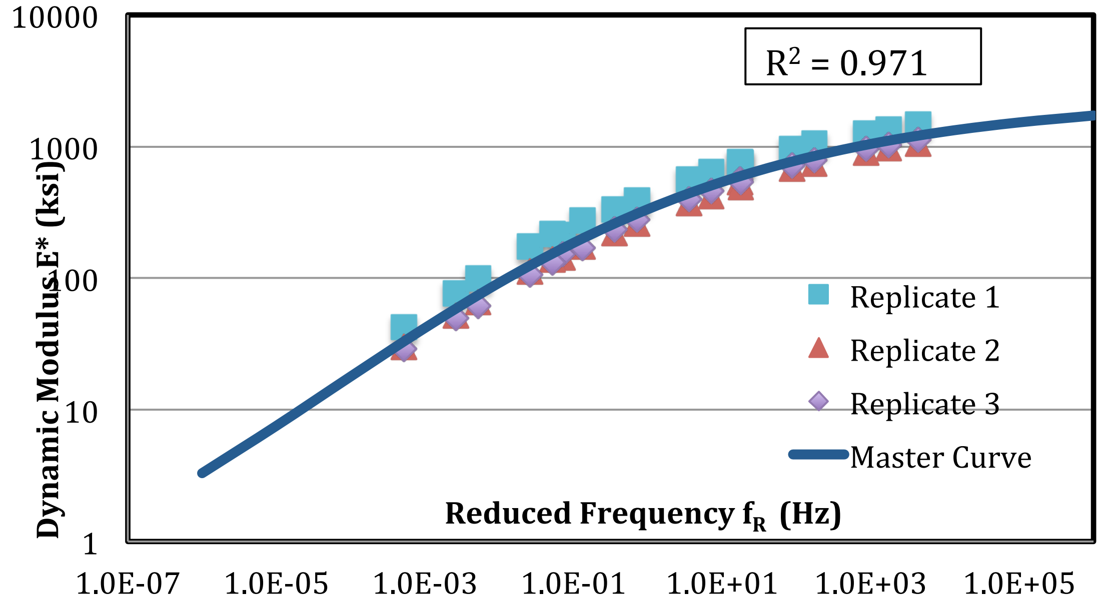

Figure A.I. 1. 13-111 mastercurve

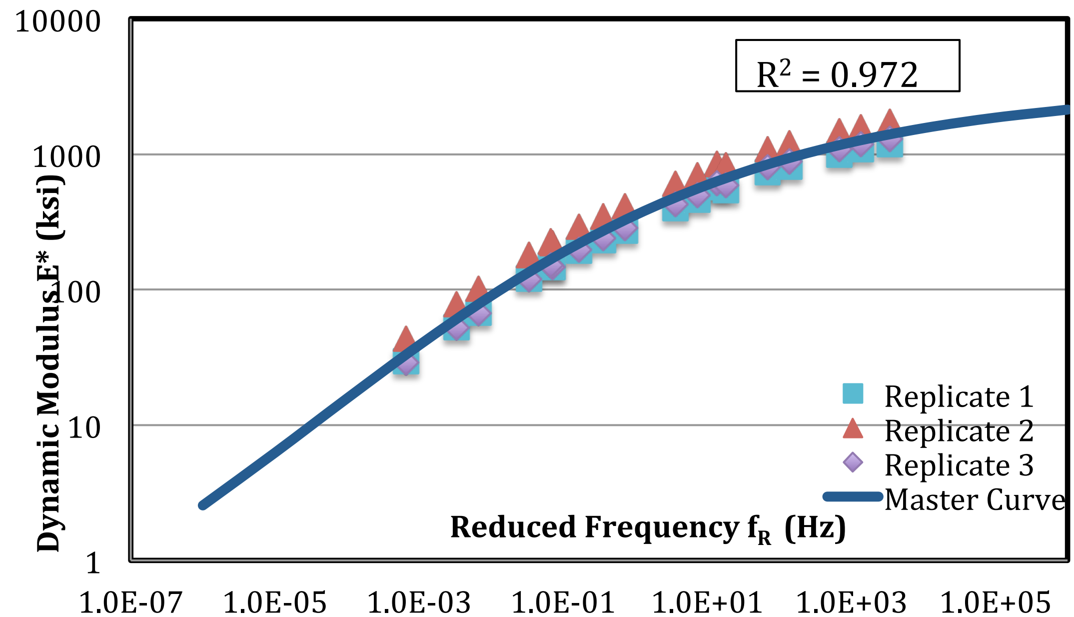

Figure A.I. 2. 13-1112 mastercurve

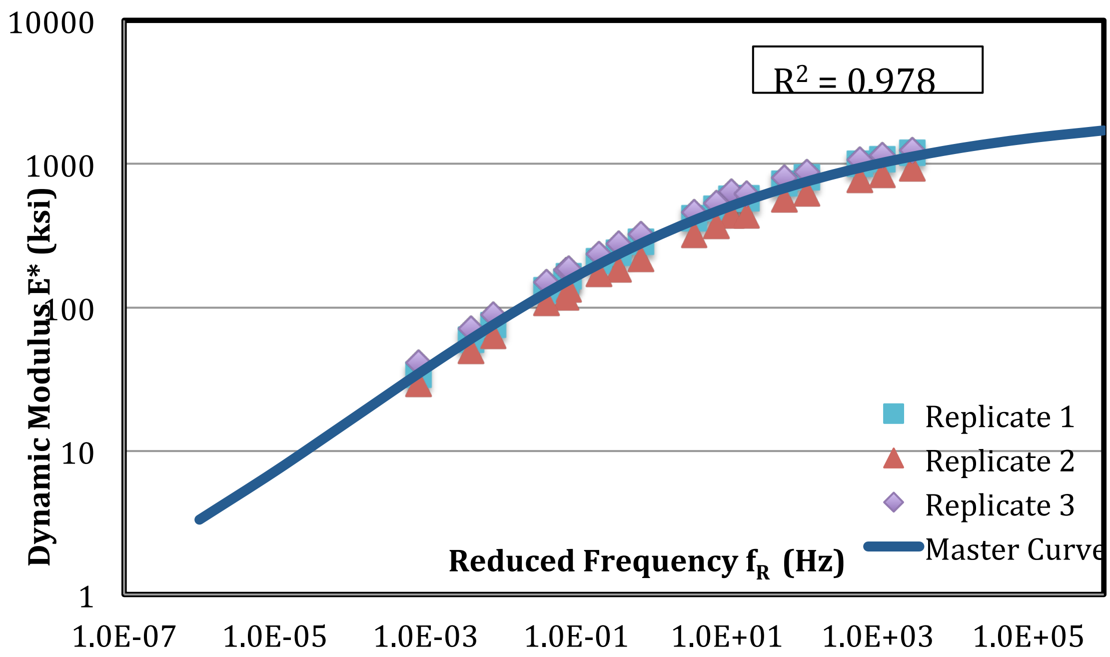

Figure A.I. 3. 13-1113 mastercurve

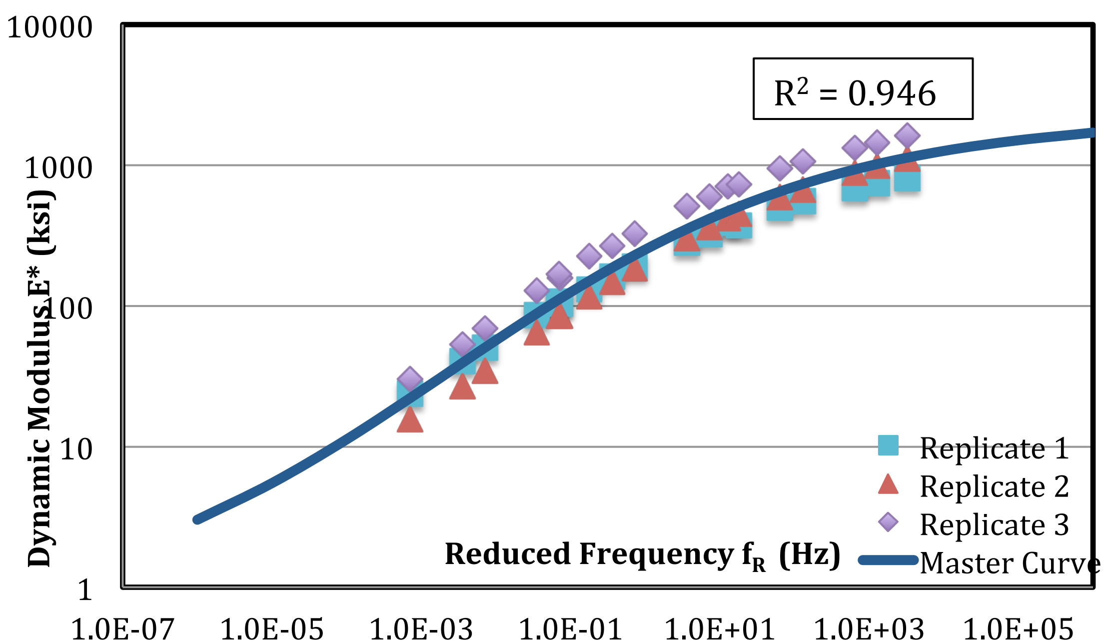

Figure A.I. 4. 13-1114 mastercurve

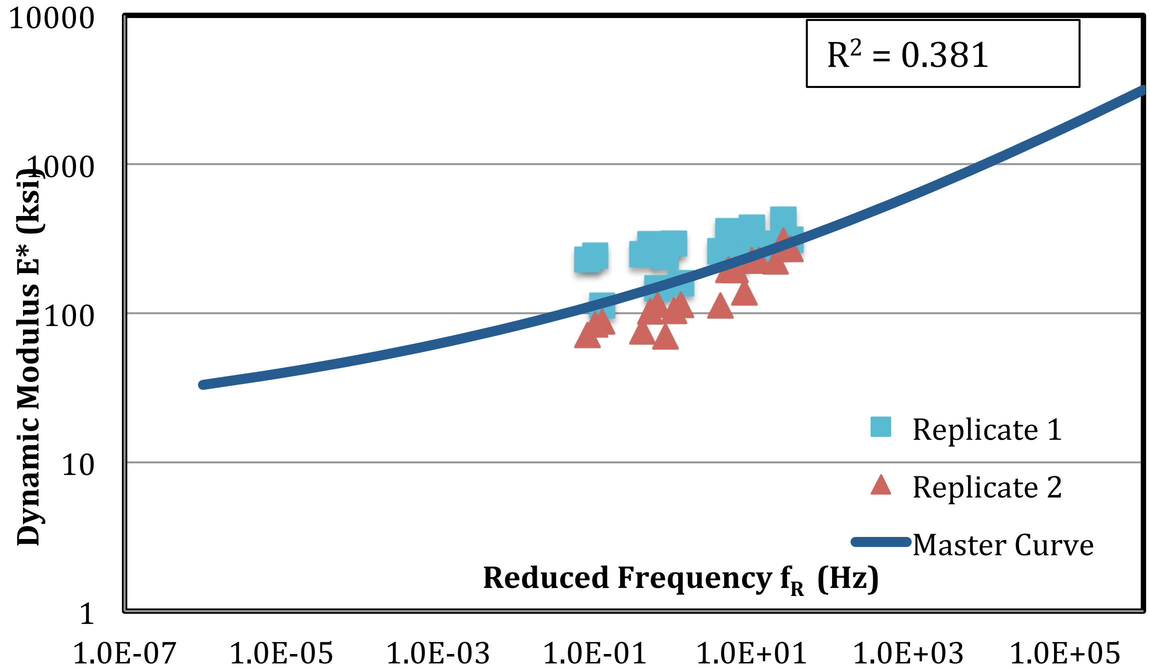

Figure A.I. 5. 13-1115 mastercurve

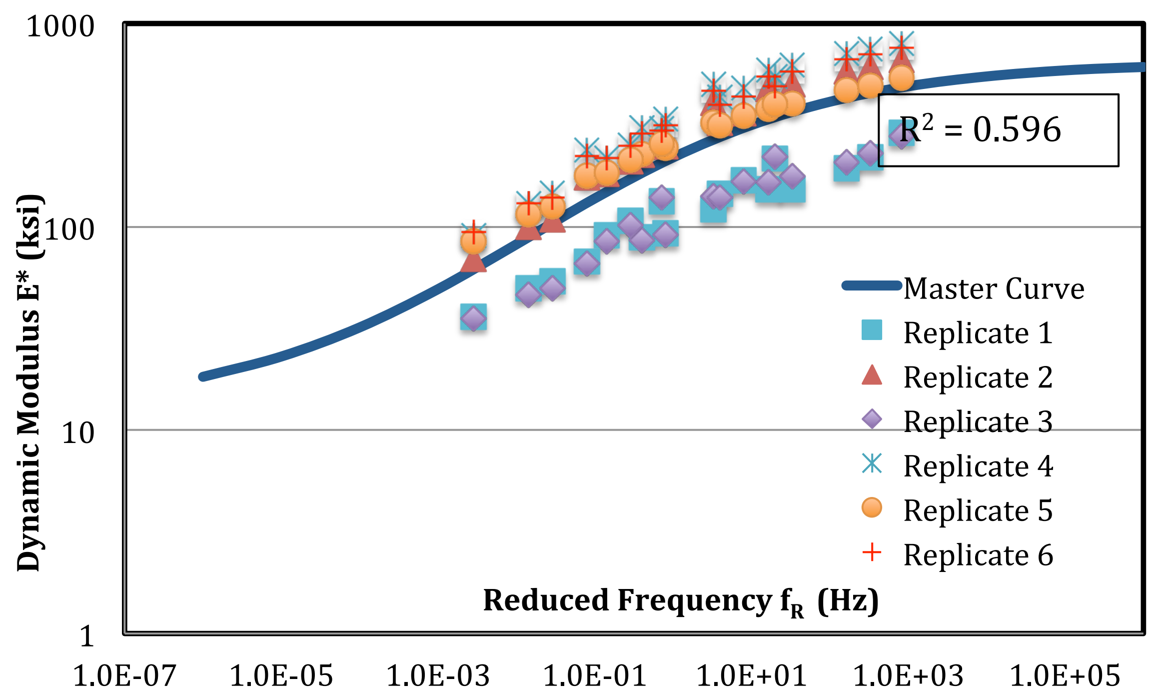

Figure A.I. 6. 13-1116 mastercurve

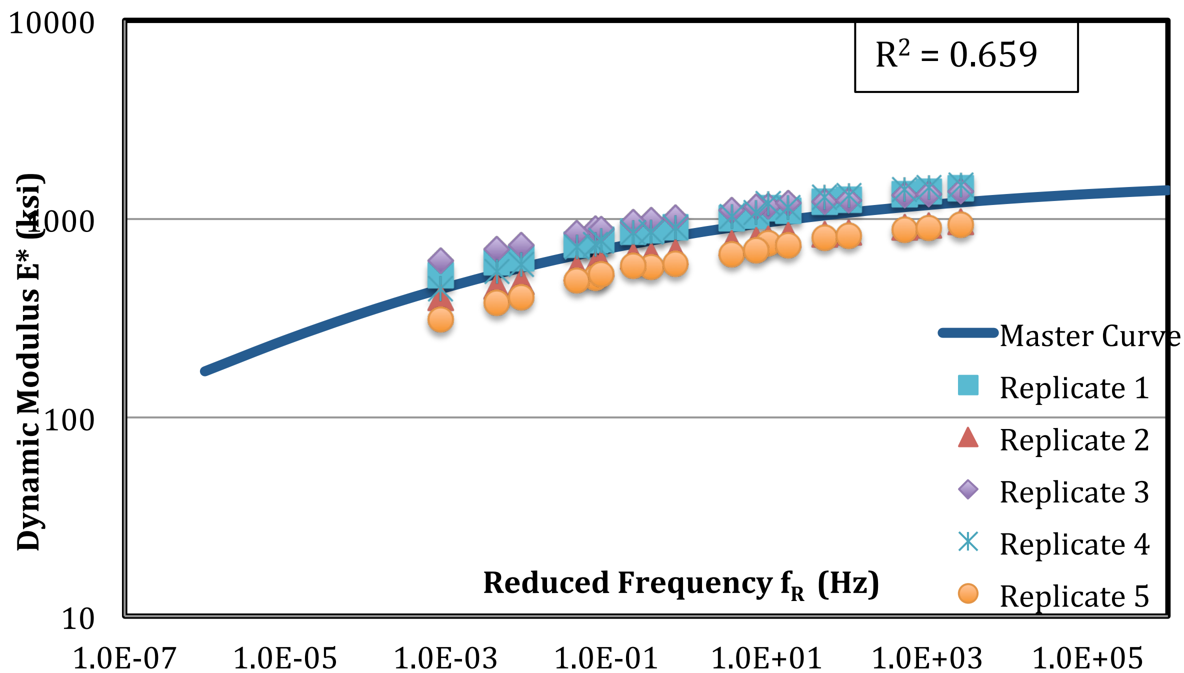

Figure A.I. 7. 13-1117 mastercurve

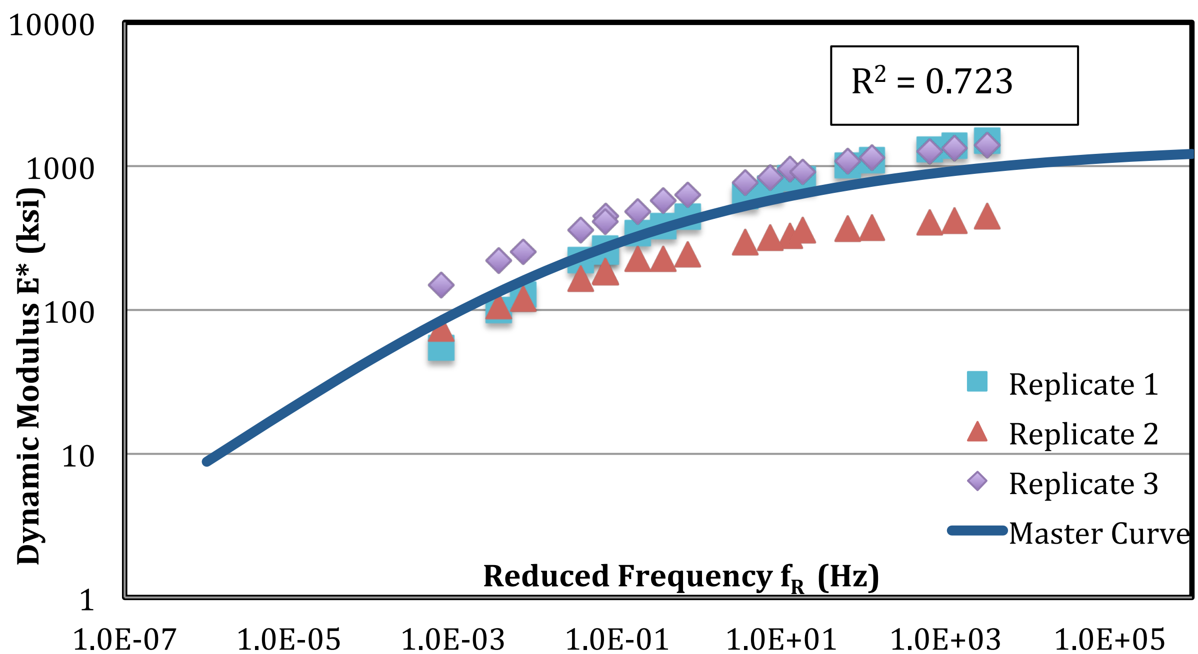

Figure A.I. 8. 13-1124 mastercurve

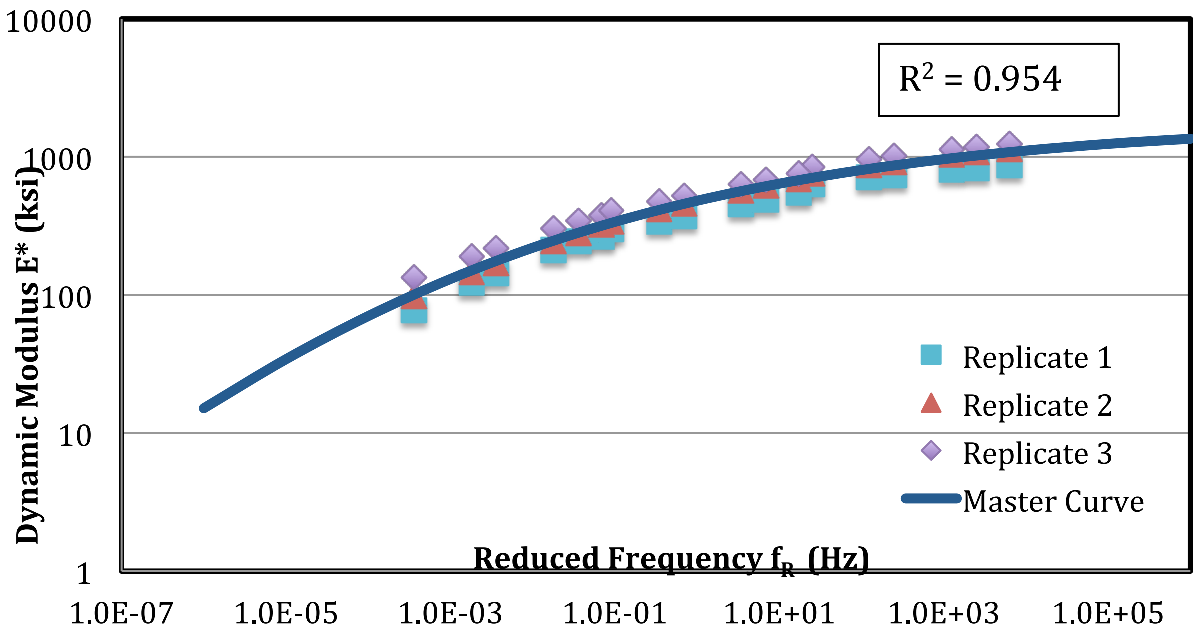

Figure A.I. 9. 13-1127 mastercurve

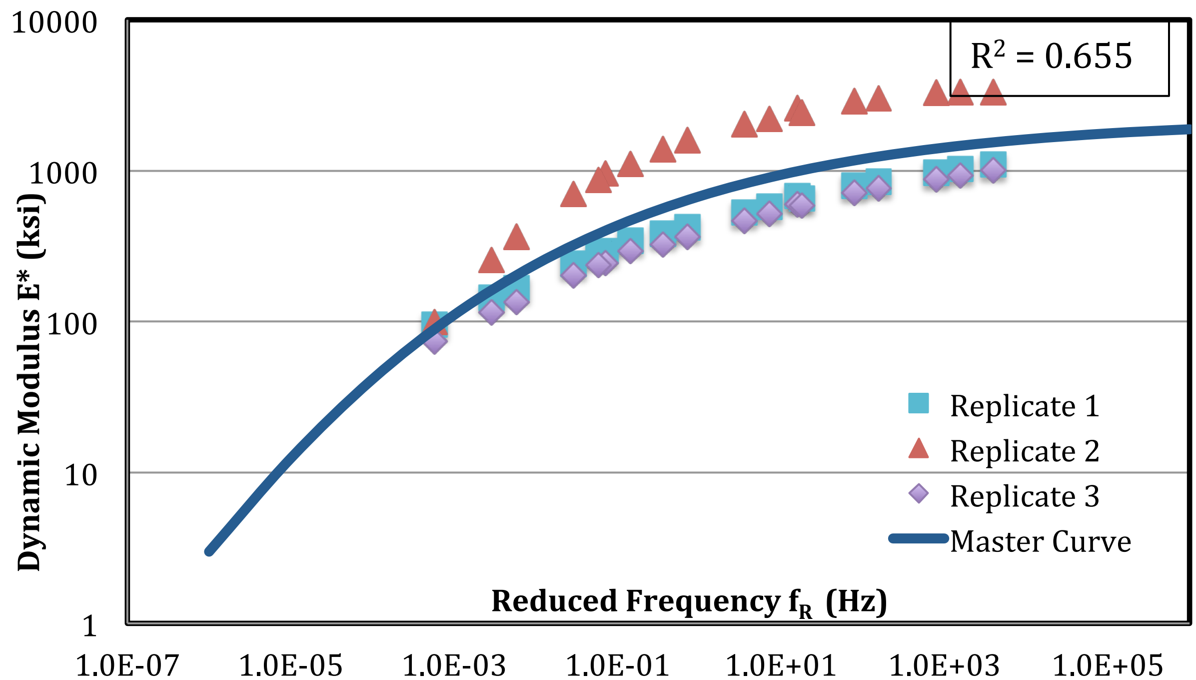

Figure A.I. 10. 14-1001 mastercurve

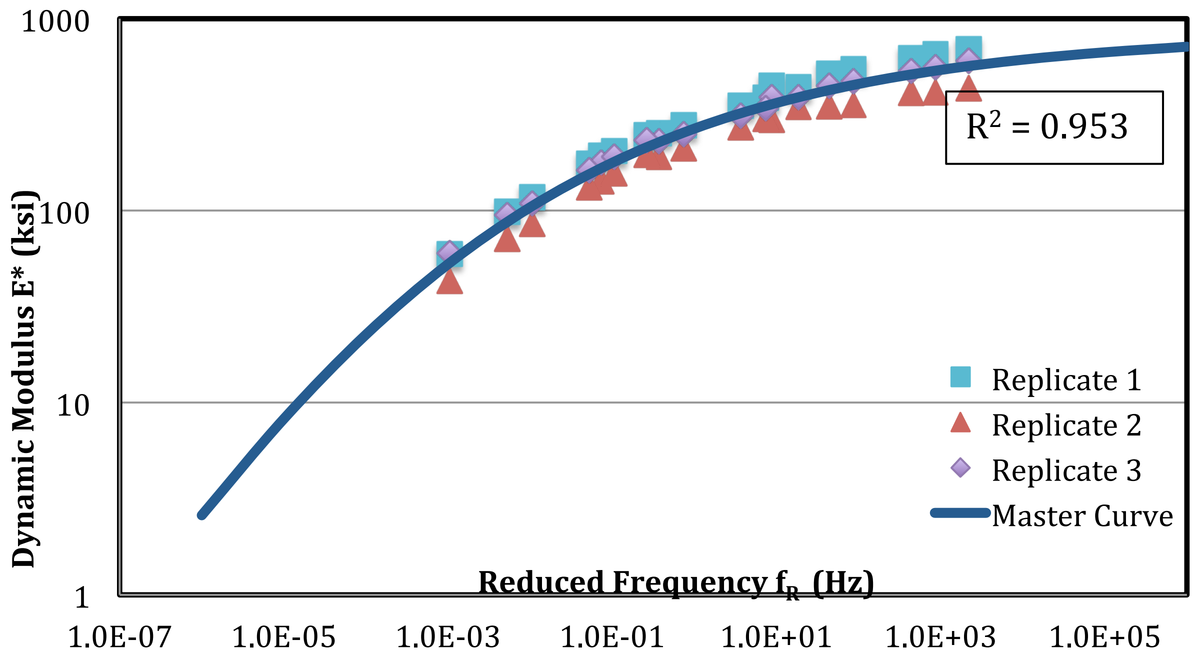

Figure A.I. 11. 14-1002 mastercurve

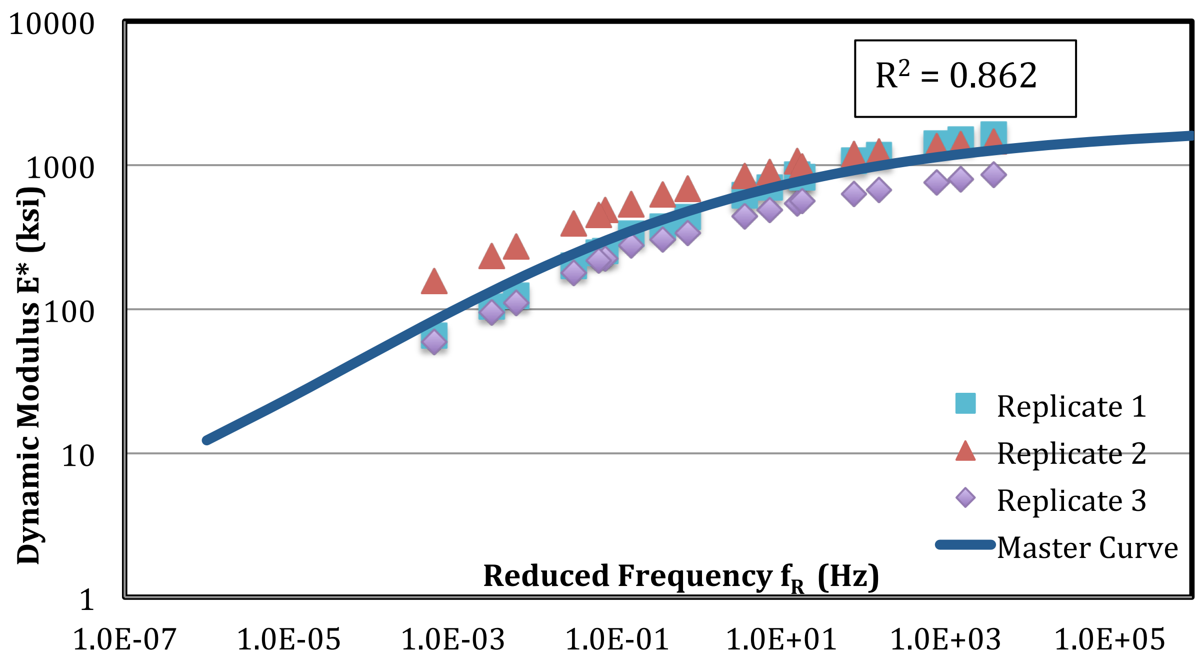

Figure A.I. 12. 14-1003 mastercurve

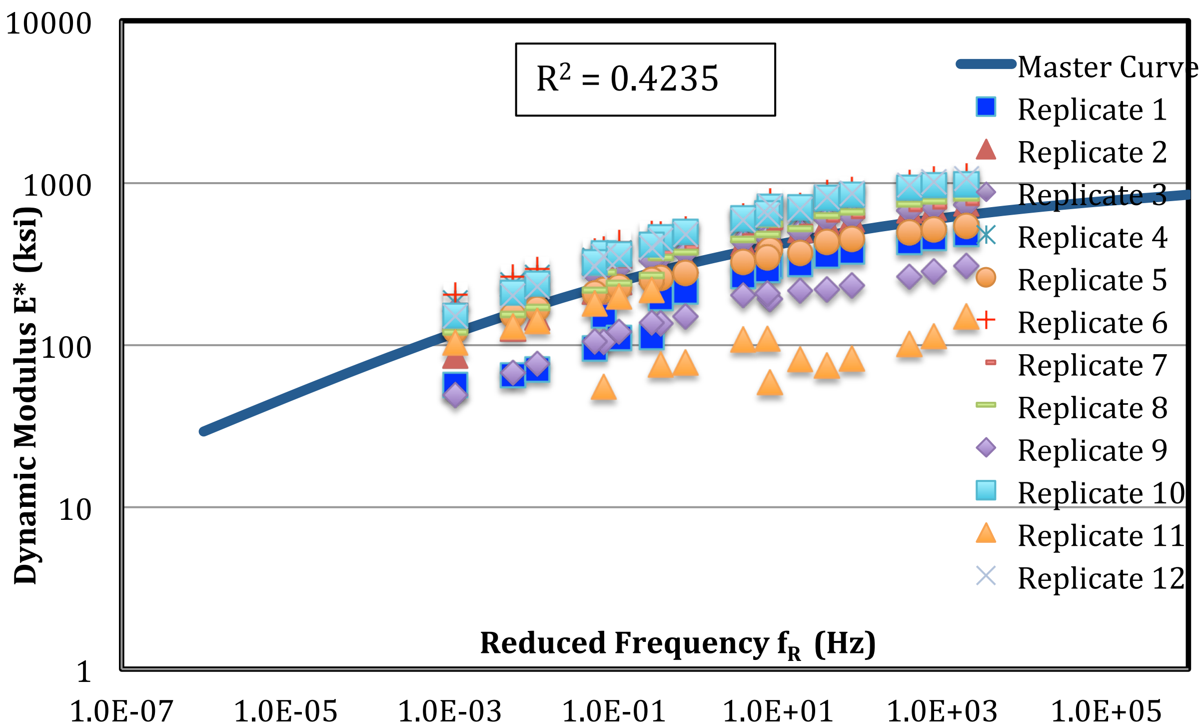

Figure A.I. 13. 14-1011 mastercurve

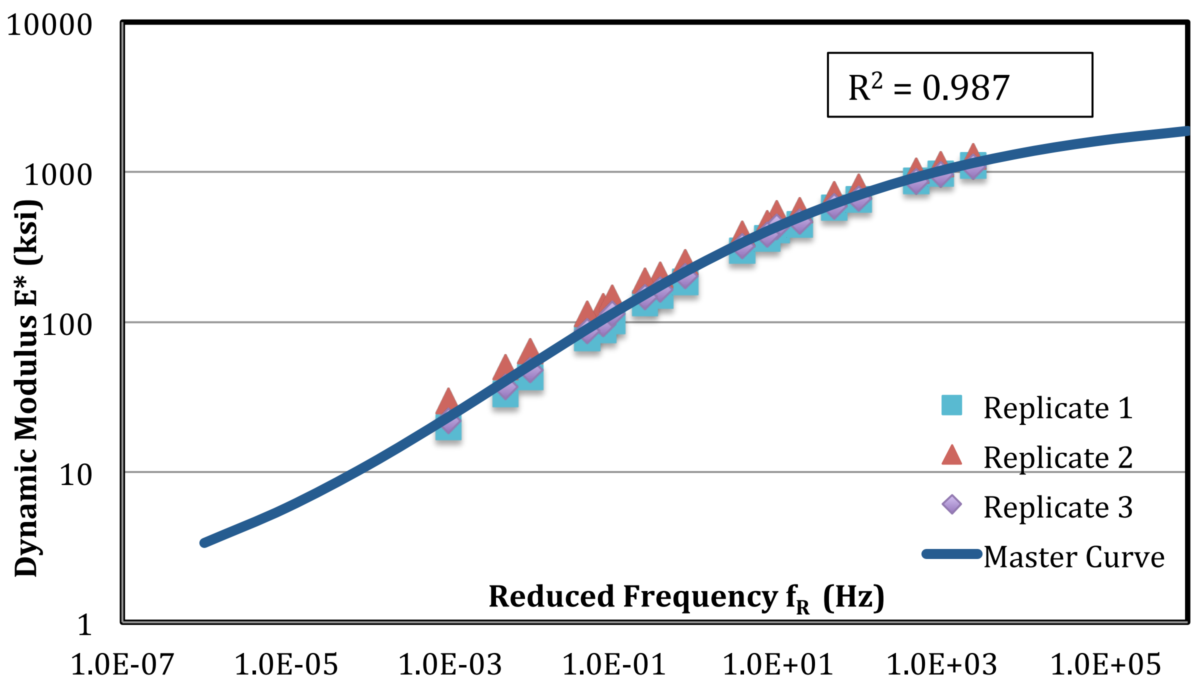

Figure A.I. 14. 14-1025 mastercurve

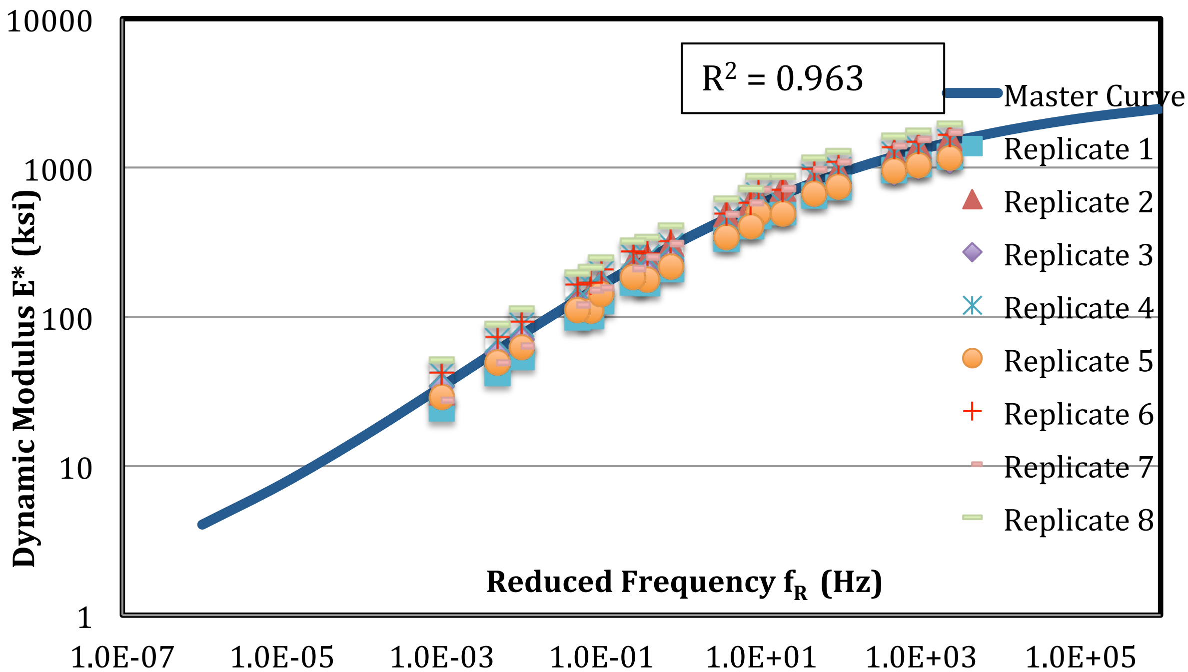

Figure A.I. 15. 14-1026 mastercurve

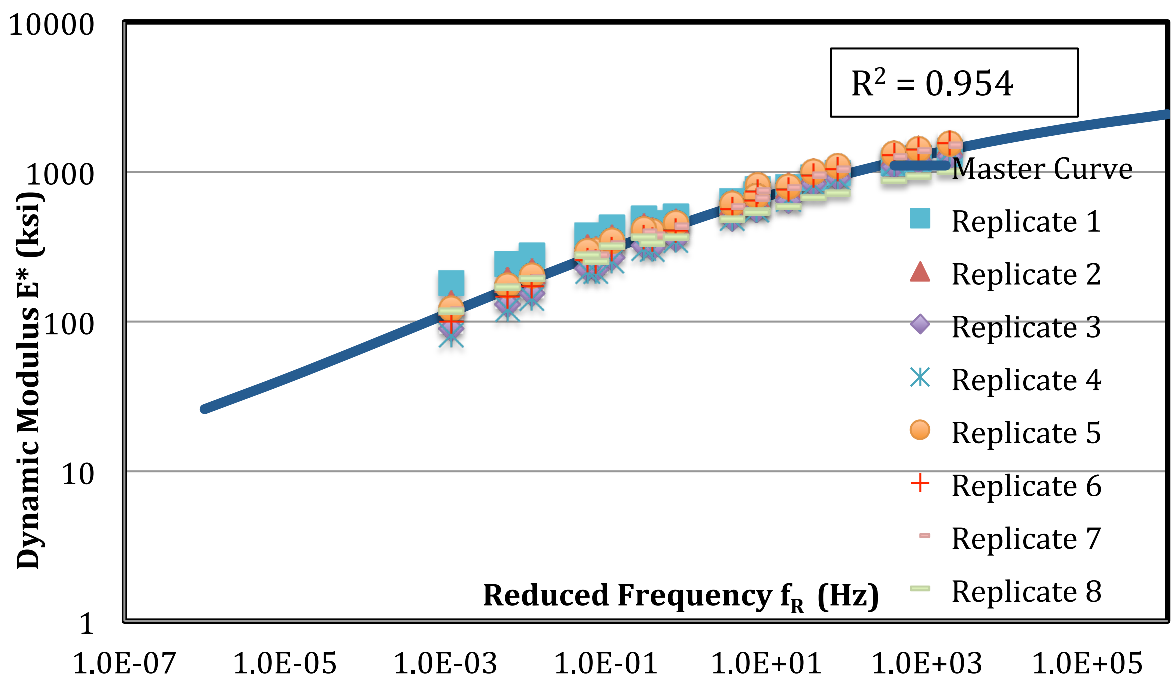

Figure A.I. 16. 14-1027 mastercurve

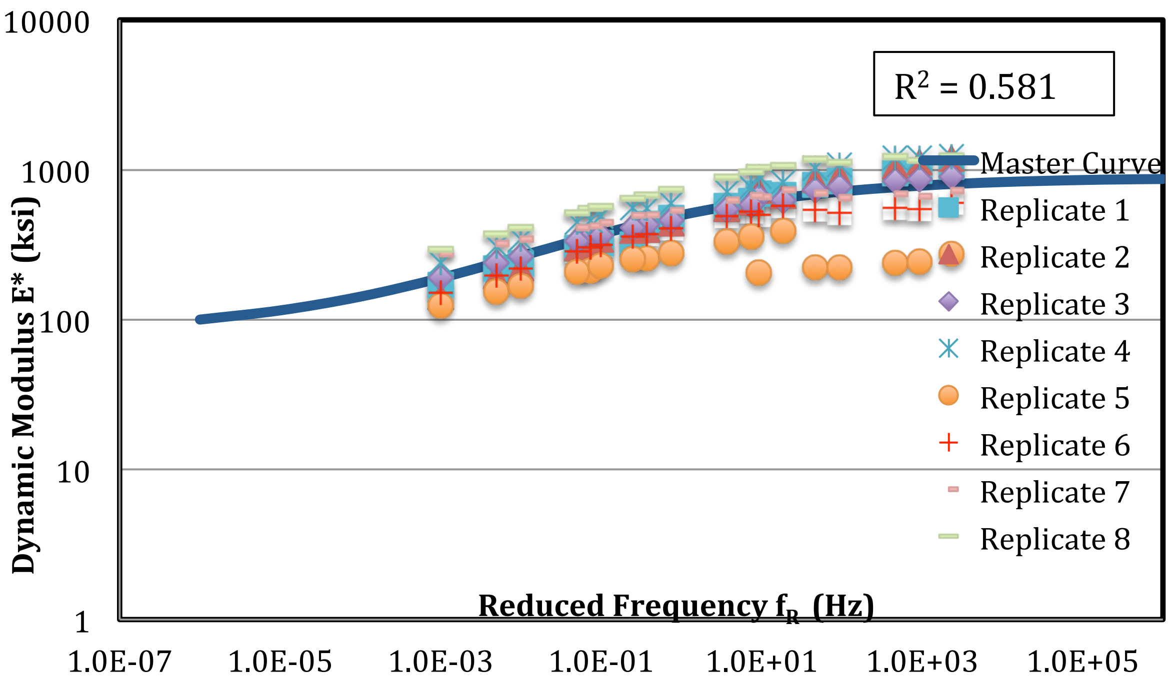

Figure A.I. 17. 14-1028 mastercurve

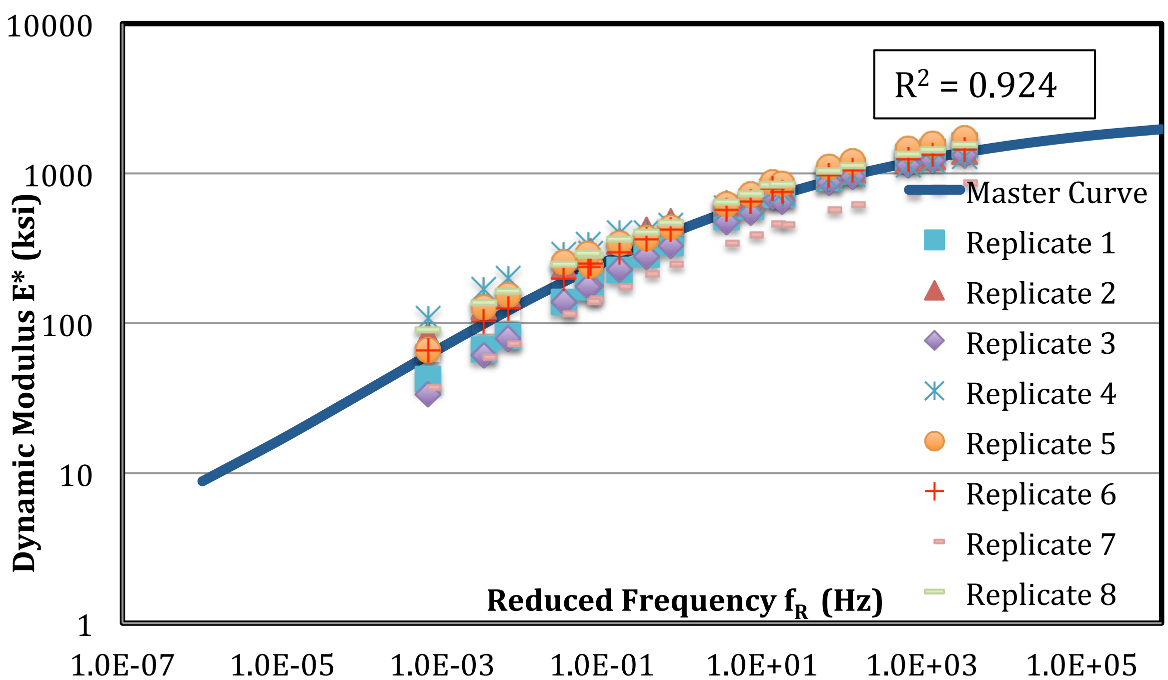

Figure A.I. 18. 14-1055 mastercurve

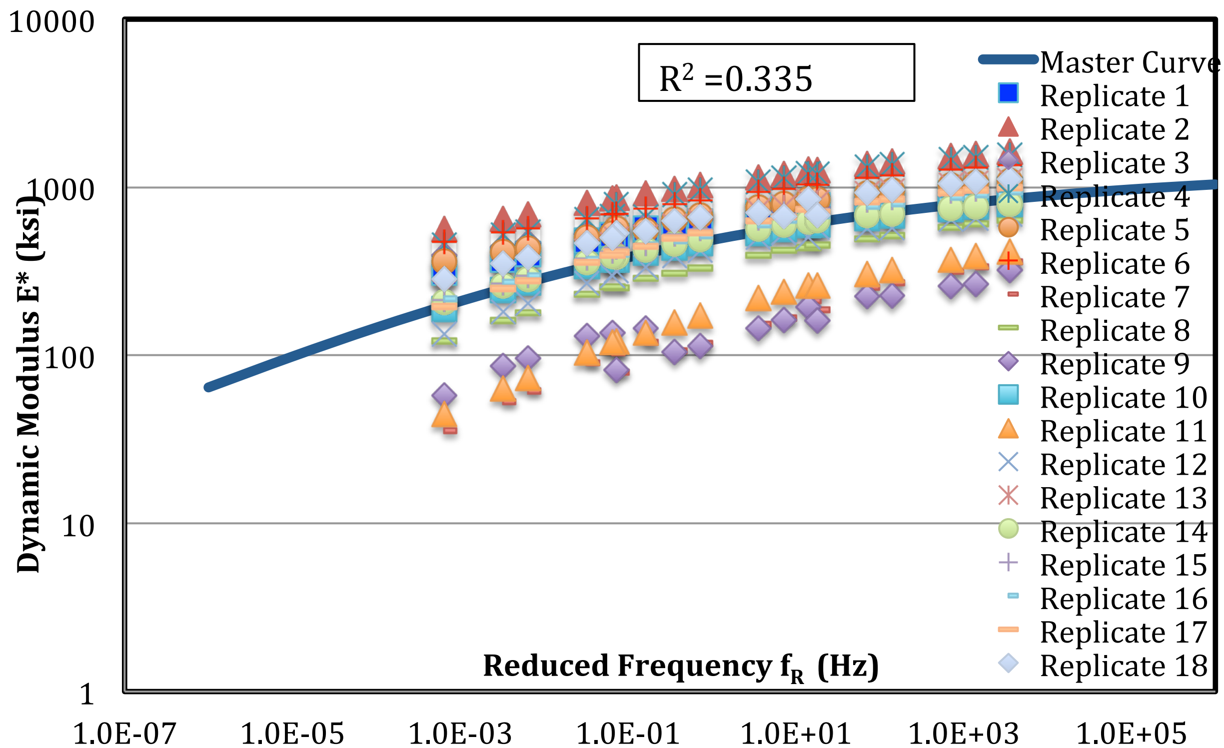

Figure A.I. 19. 14-1057 mastercurve

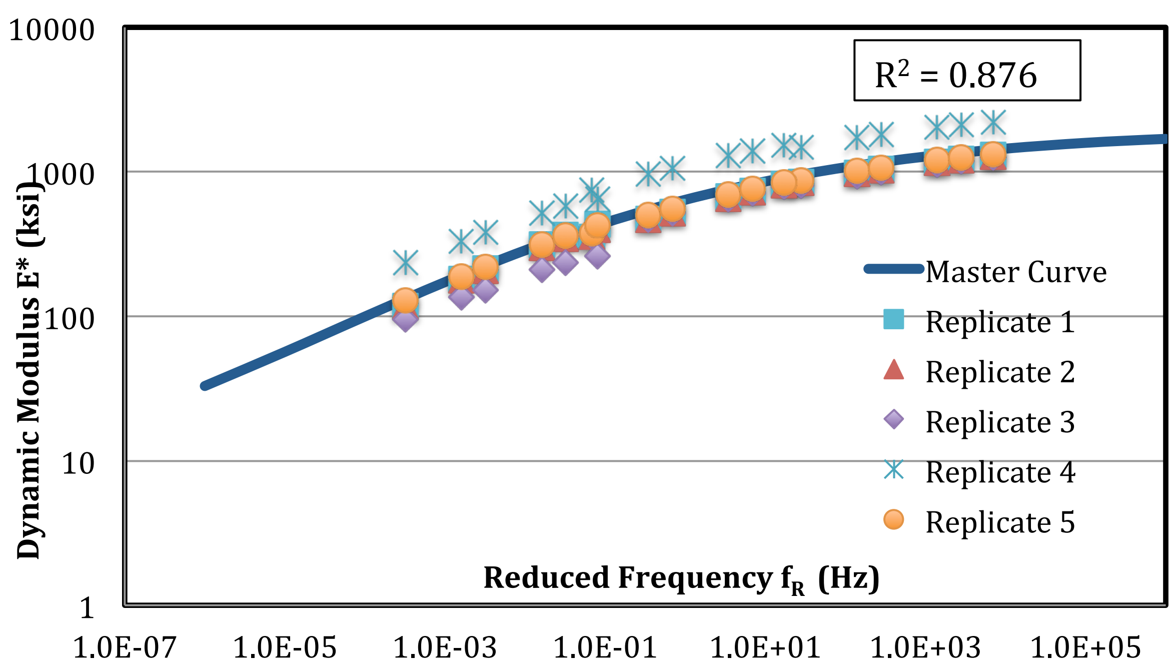

Figure A.I. 20. s14-1058 mastercurve

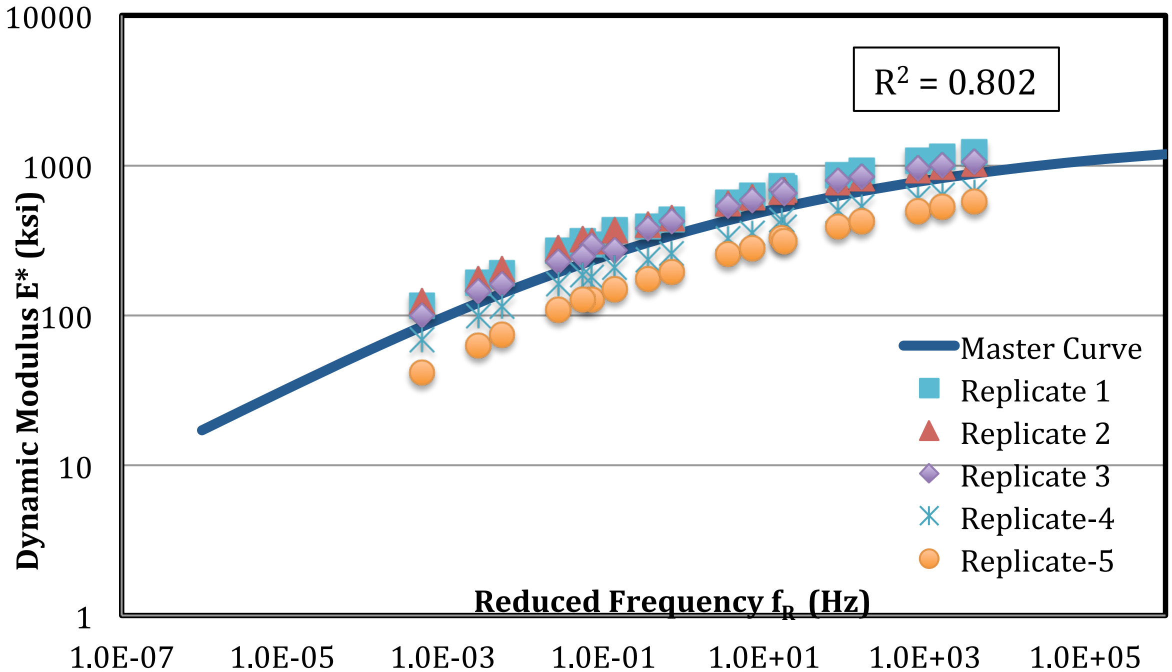

Figure A.I. 21. 14-1062 mastercurve

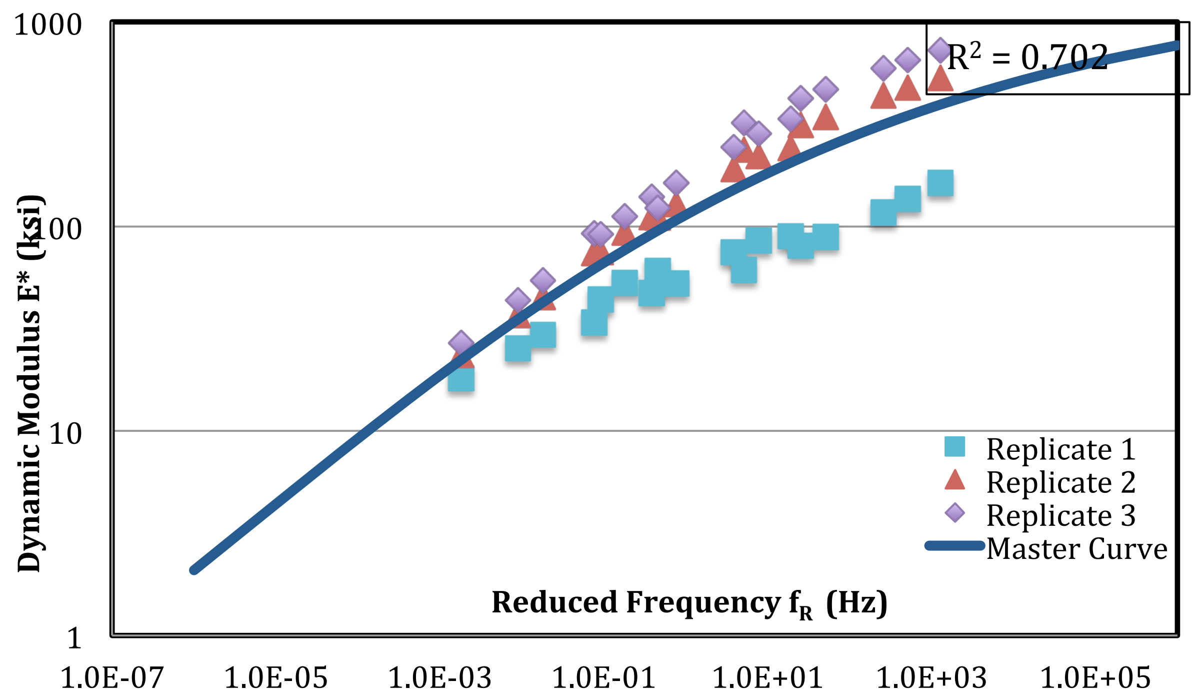

Figure A.I. 22. 15-1002 mastercurve

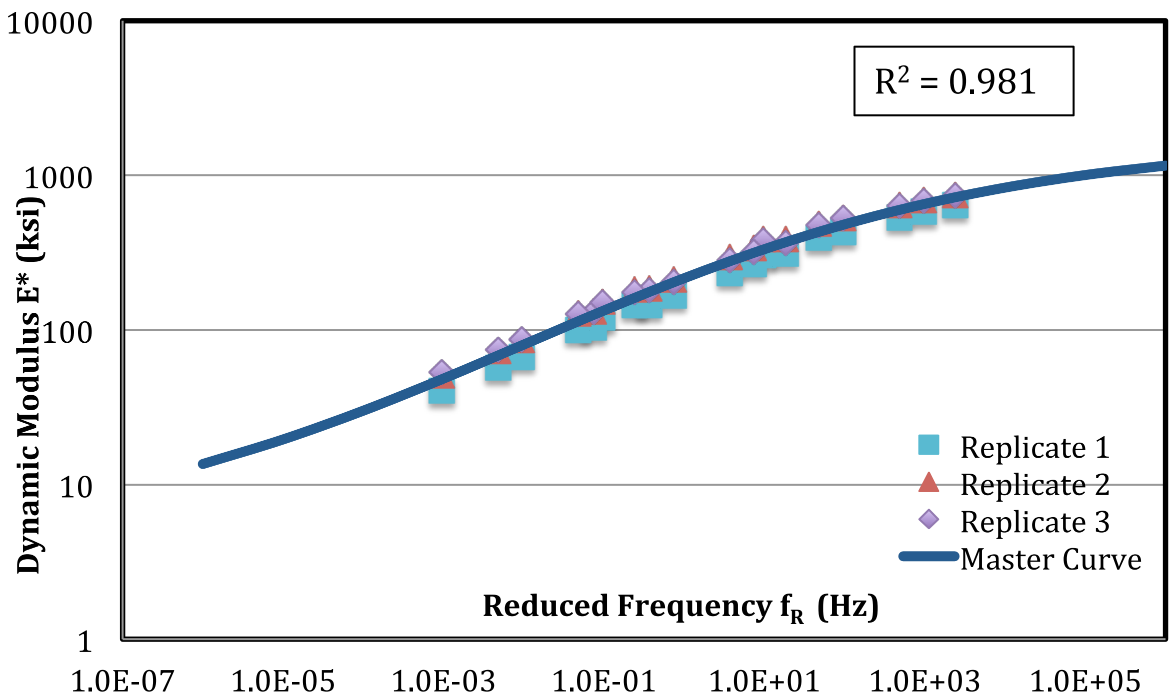

Figure A.I. 23. 15-1003 mastercurve

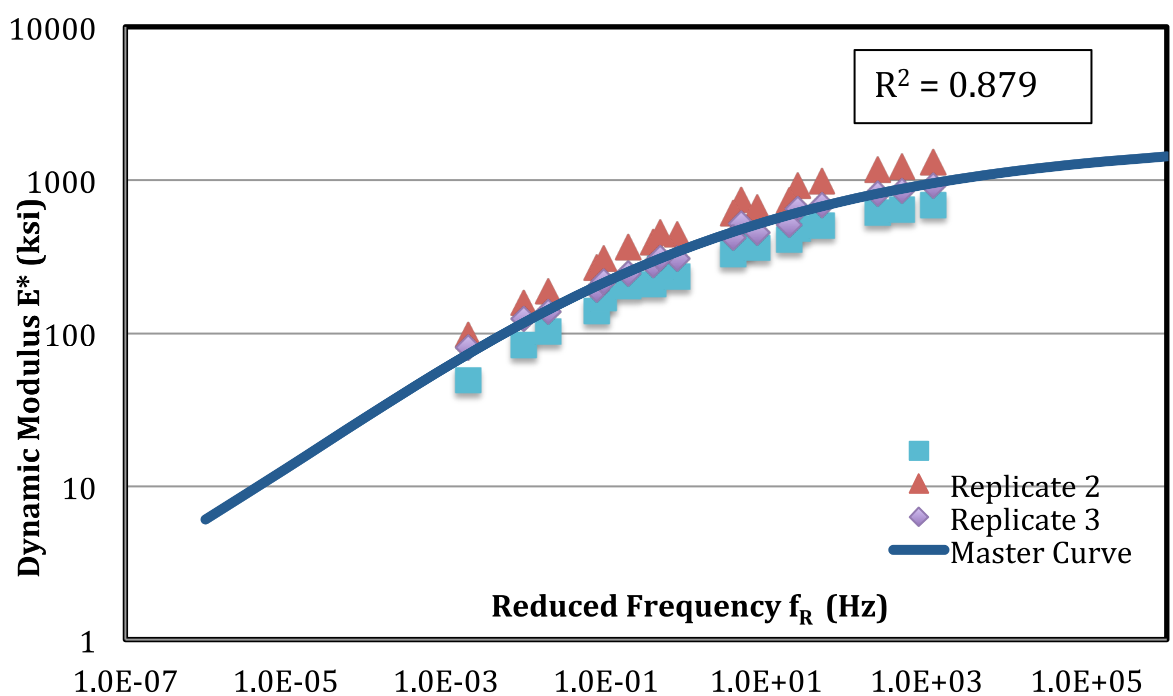

Figure A.I. 24. I-81CIR mastercurve

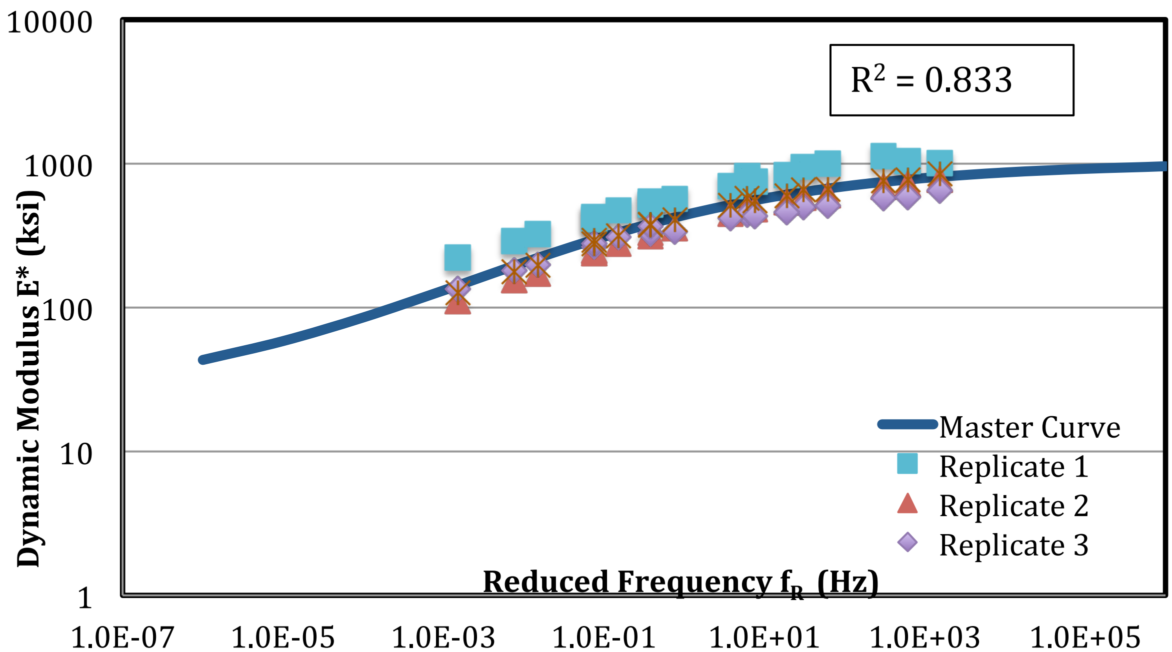

Figure A.I. 25. I-81 CCPR

8.2 <u>HMA mastercurves</u>

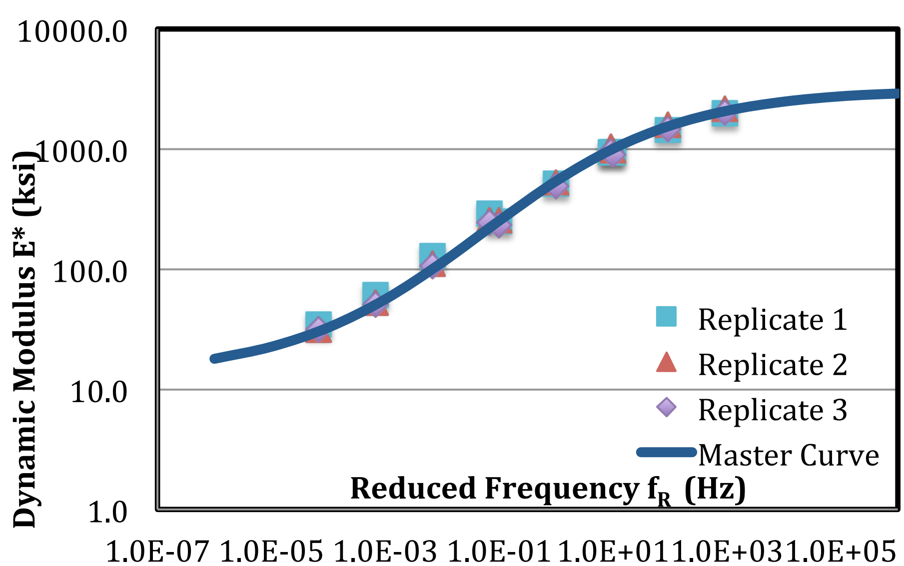

Figure A.I. 26. H160A09

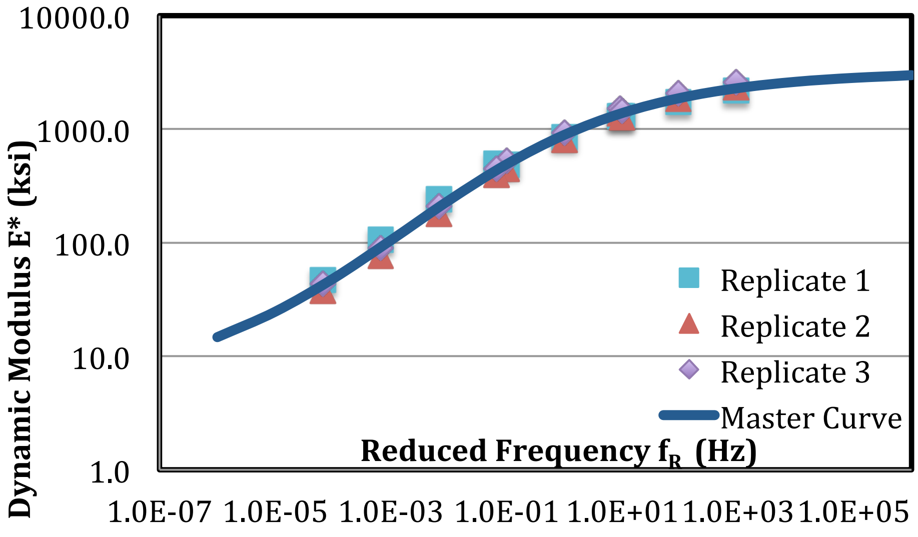

Figure A.I. 27. H151B19

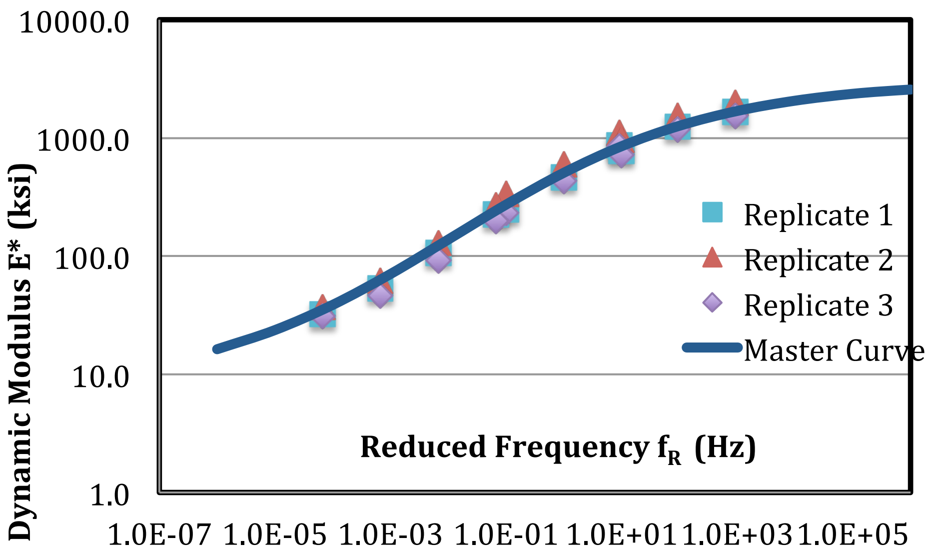

Figure A.I. 28. H135A19

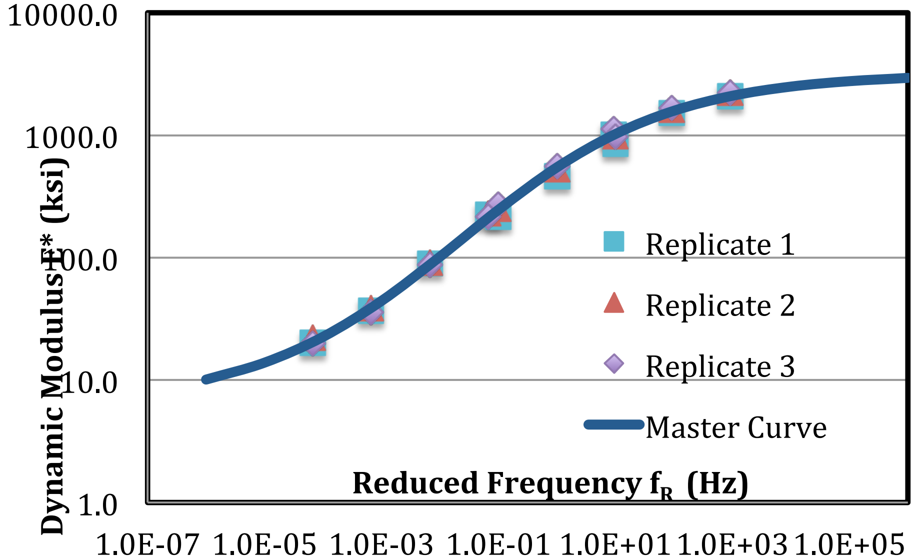

Figure A.I. 29. H077A09

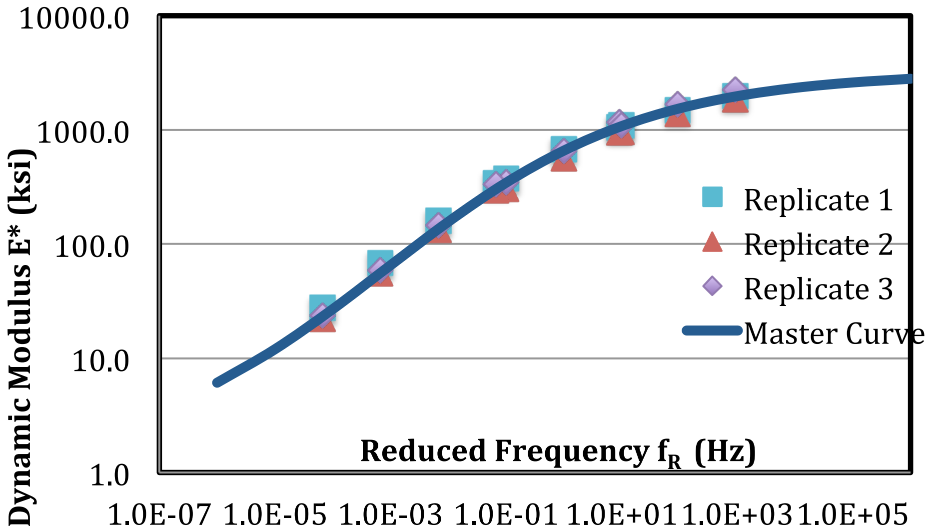

Figure A.I. 30. H083A12

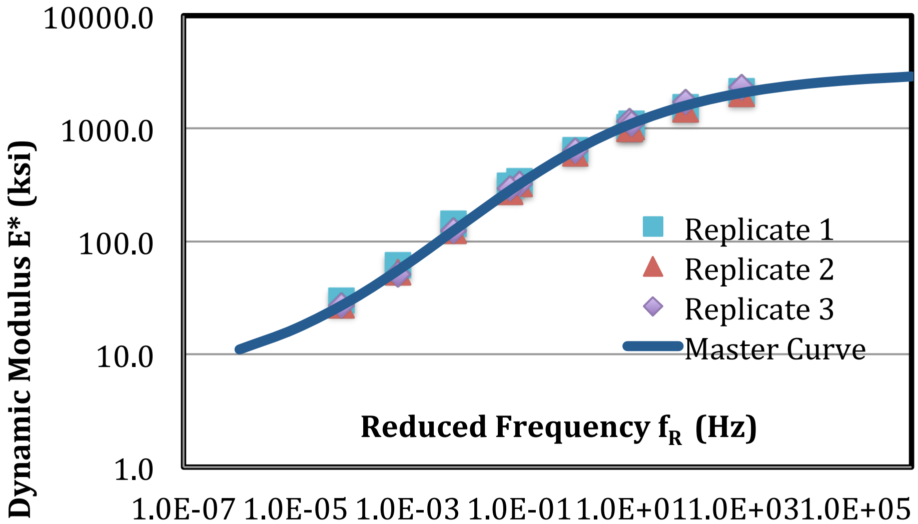

Figure A.I. 31. H127A12

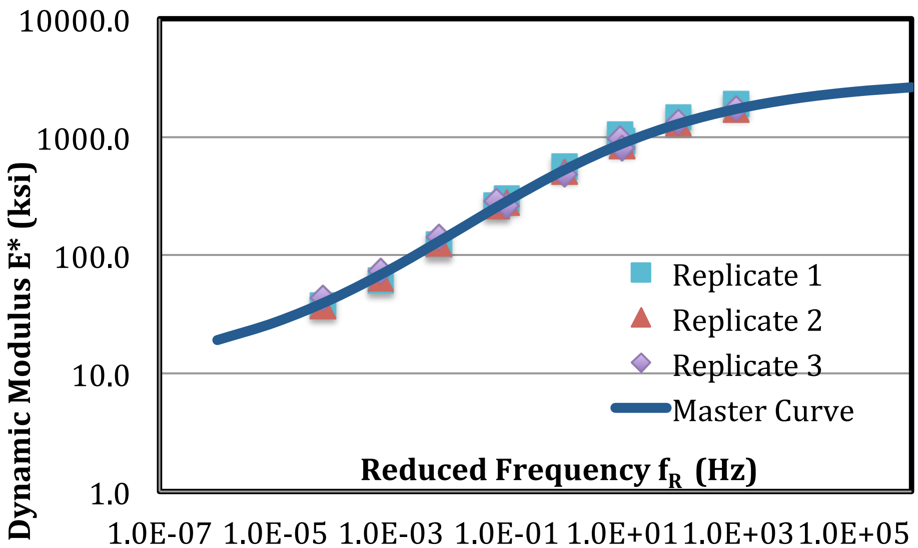

Figure A.I. 32. H135A12

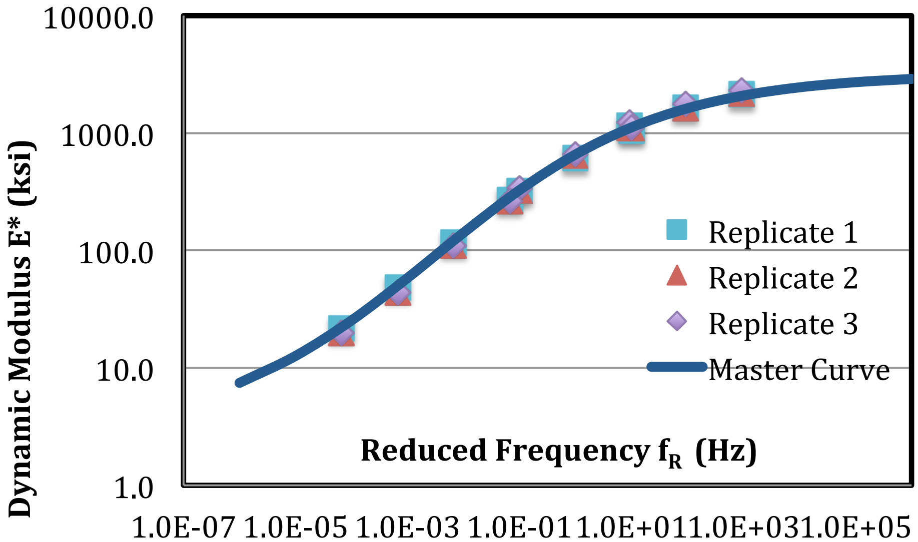

Figure A.I. 33. H168A09

Appendix II: RLPD graph of NCHRP 9-51 projects and HMA mixtures

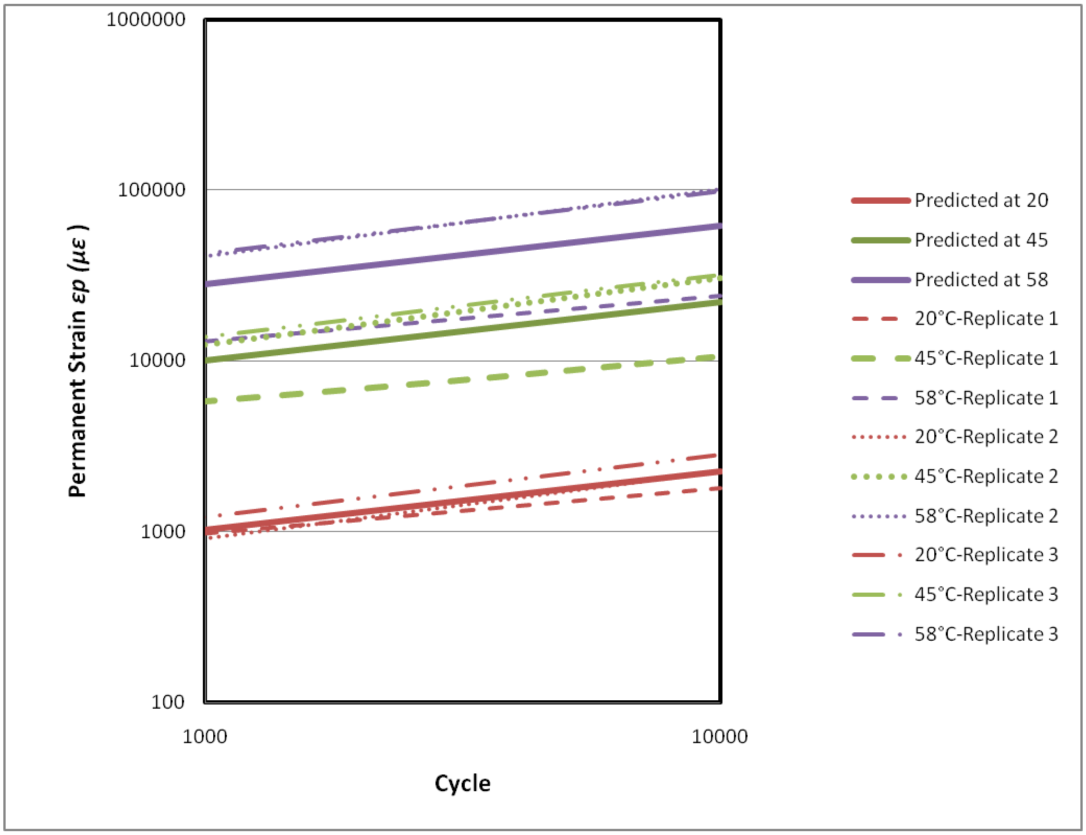

Figure A.II. 1. 13-1093 RLPD fitted graph

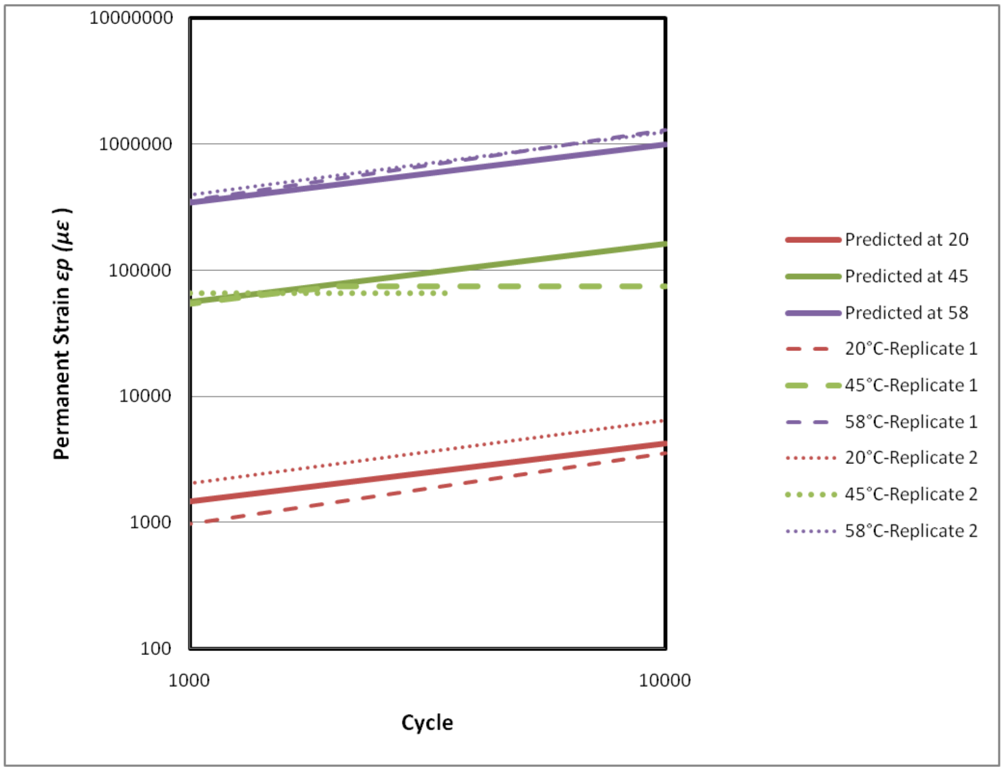

Figure A.II. 2. 13-1111 RLPD fitted graphs

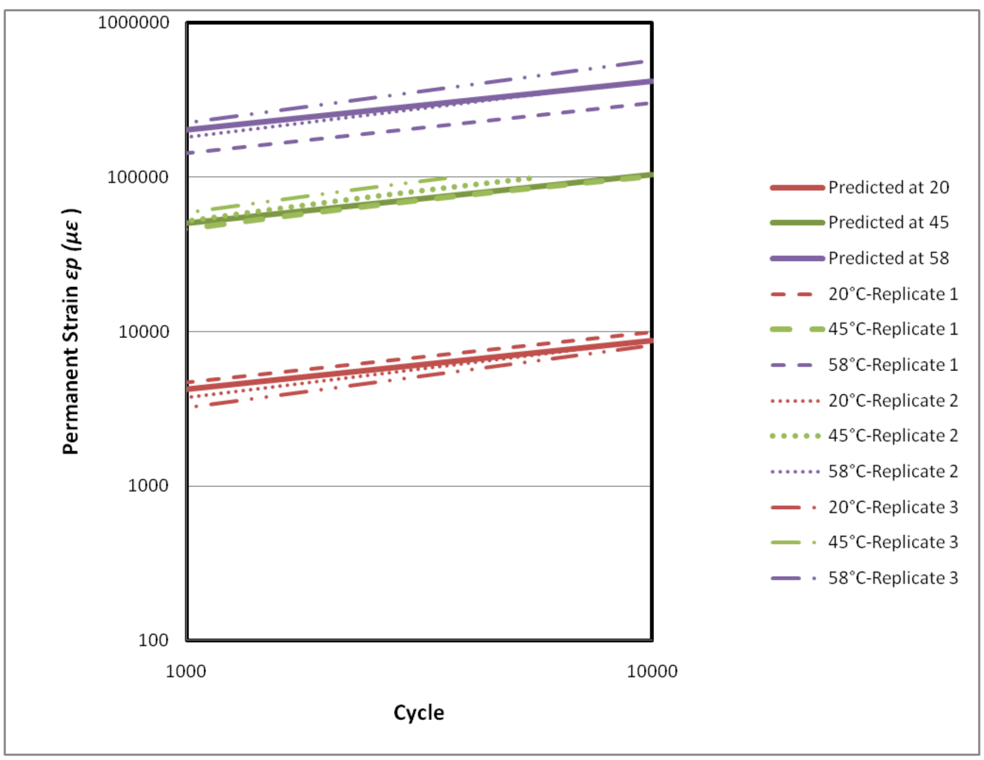

Figure A.II. 3. 13-1112 RLPD fitted graph

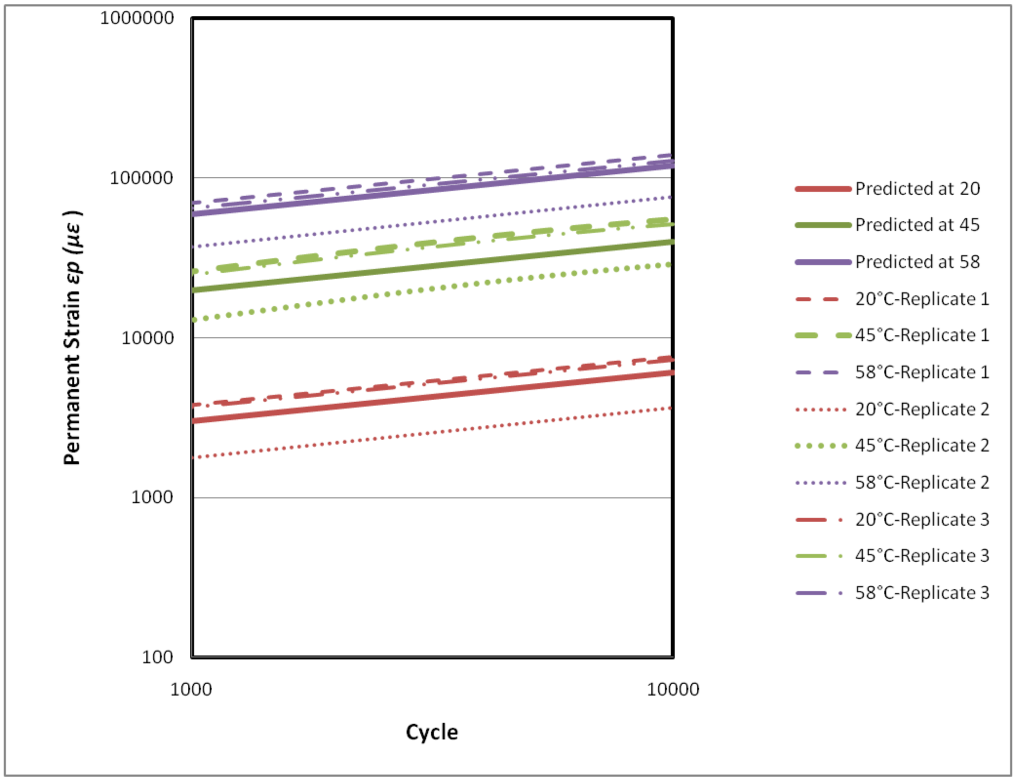

Figure A.II. 4. 13-1113

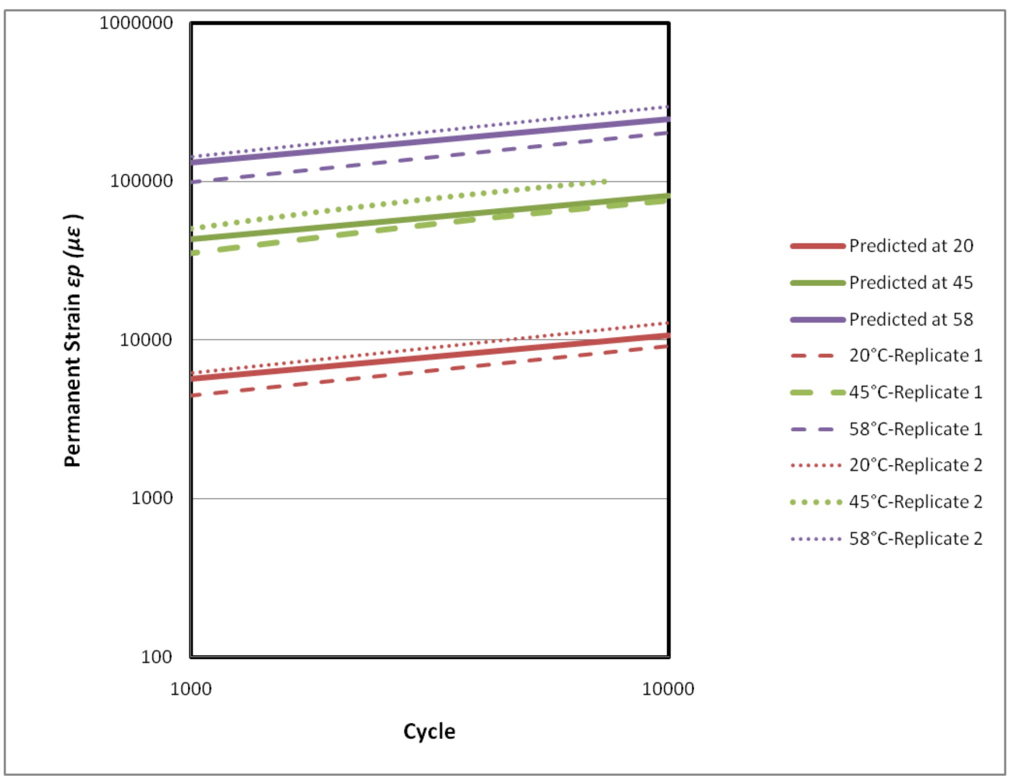

Figure A.II. 5. 13-1114

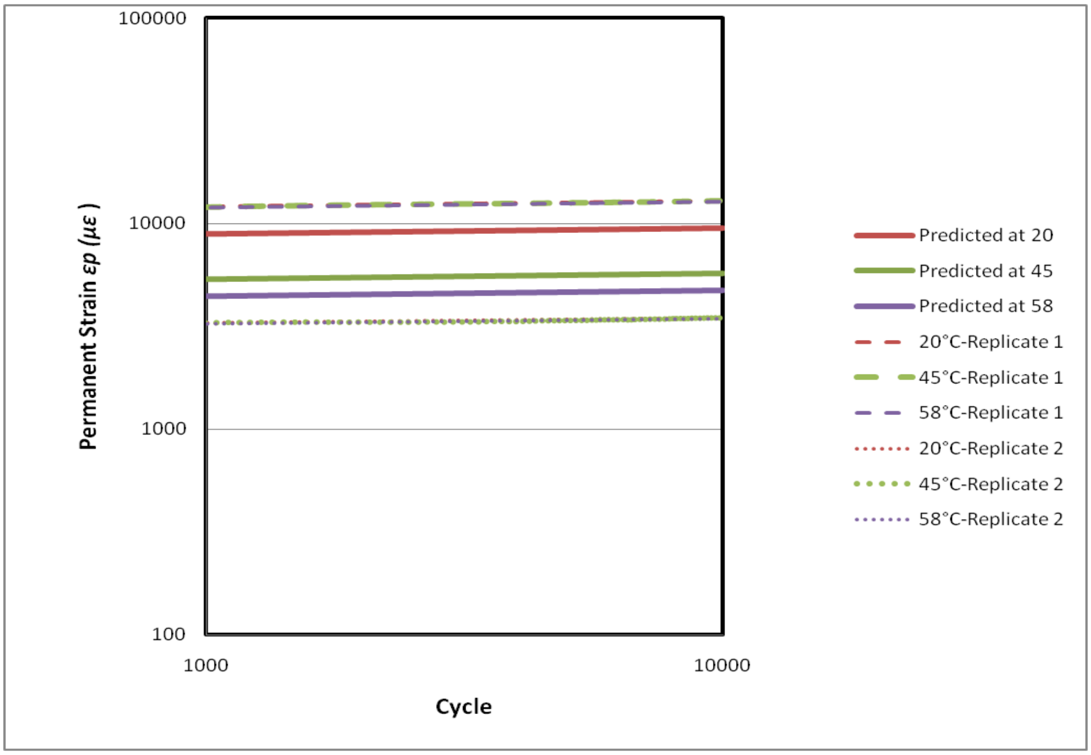

Figure A.II. 6. 13-1115

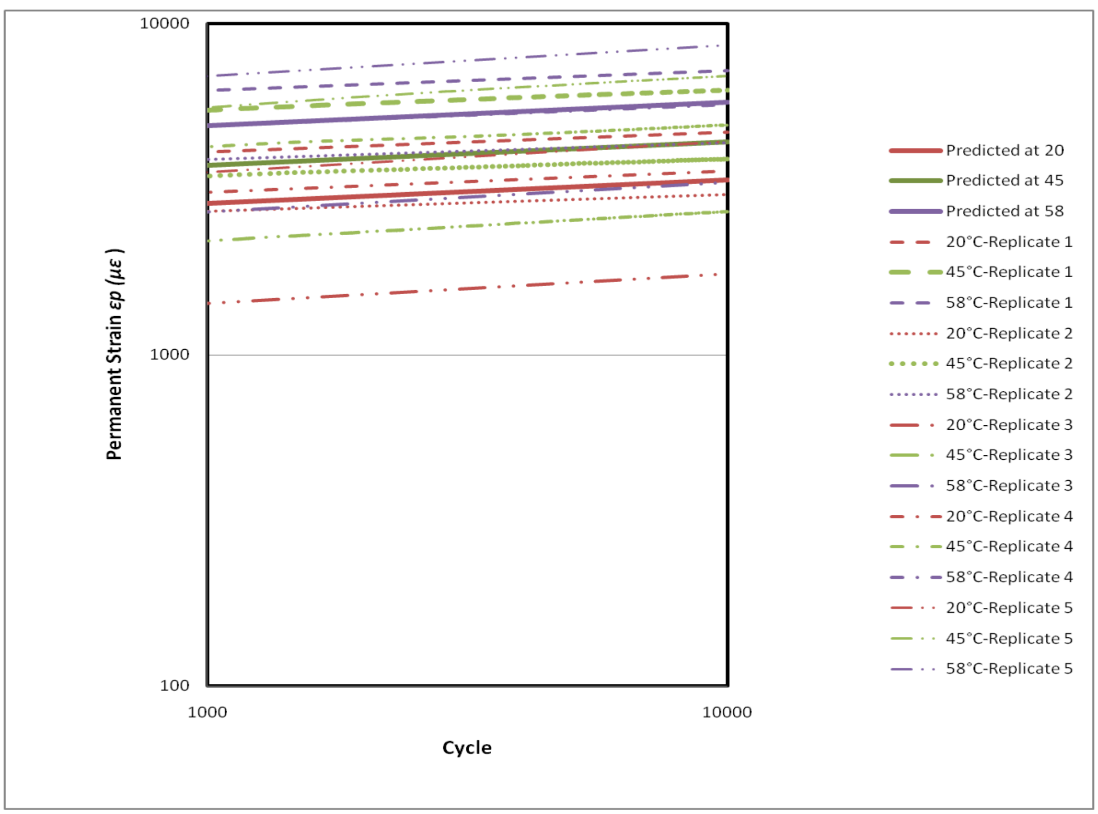

Figure A.II. 7. 13-1116

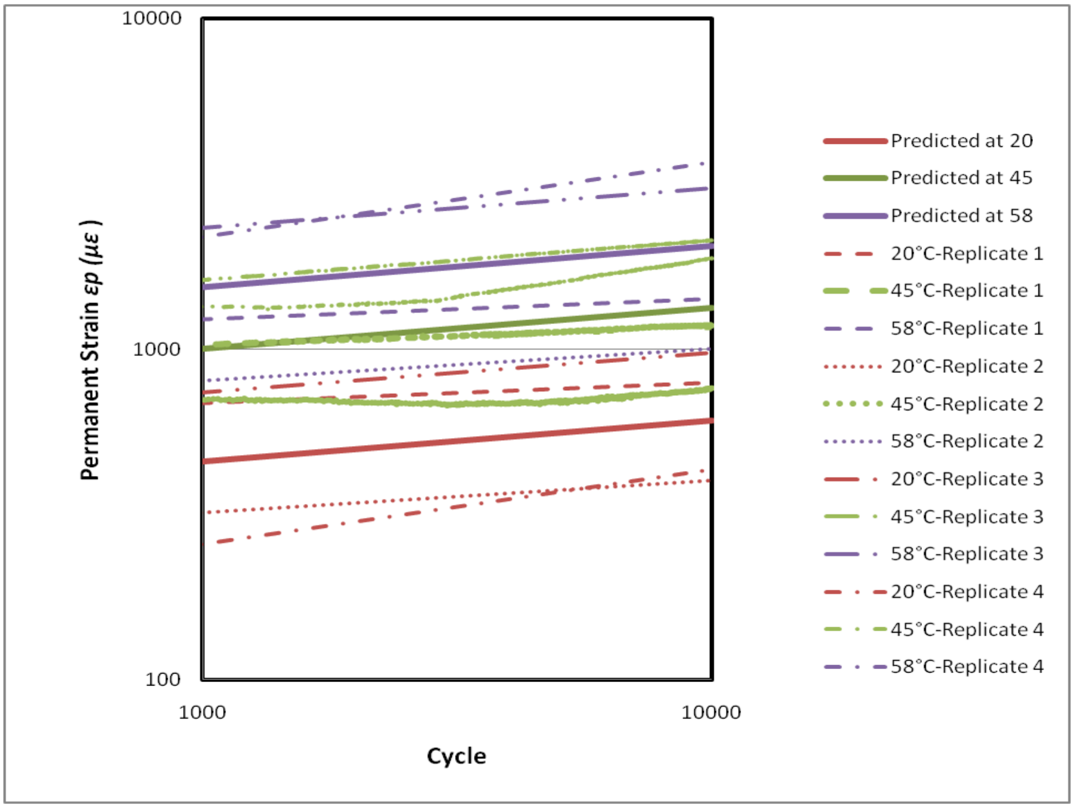

Figure A.II. 8. 13-1117

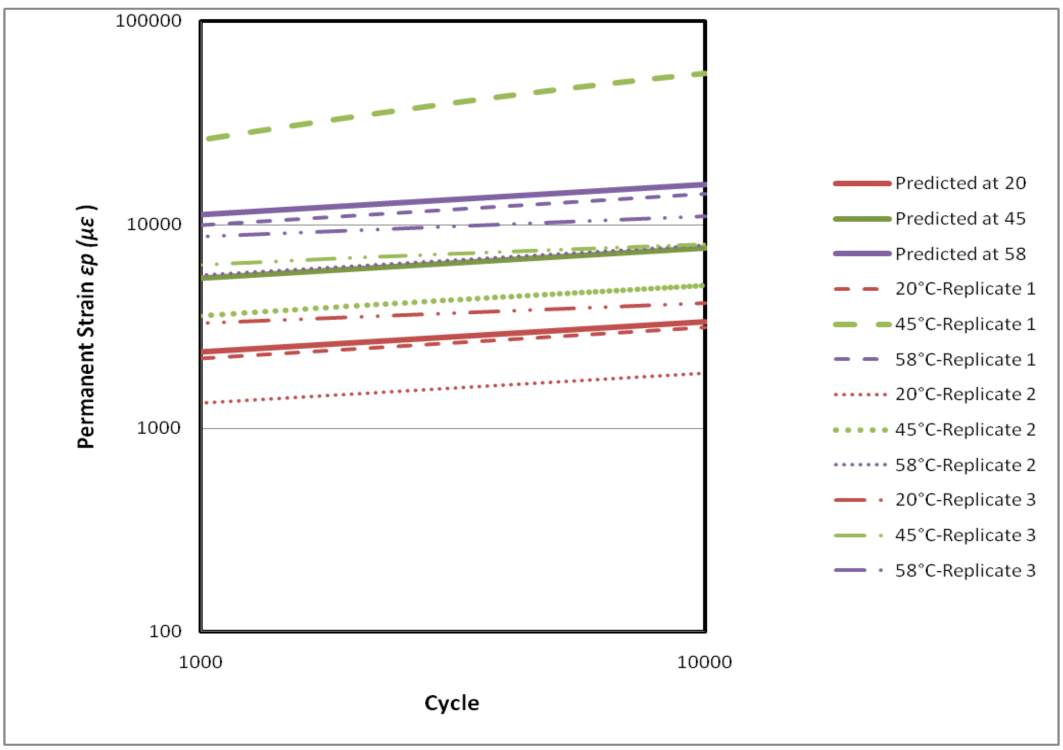

Figure A.II. 9. 13-1124

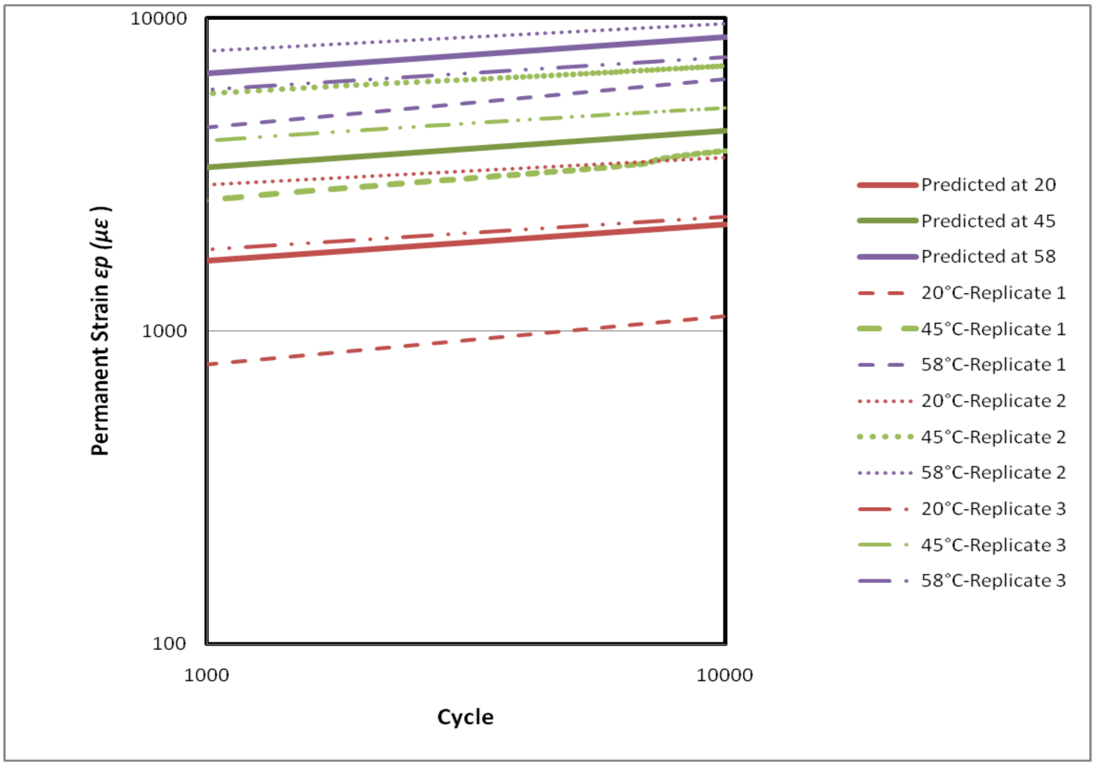

Figure A.II. 10. 13-1127

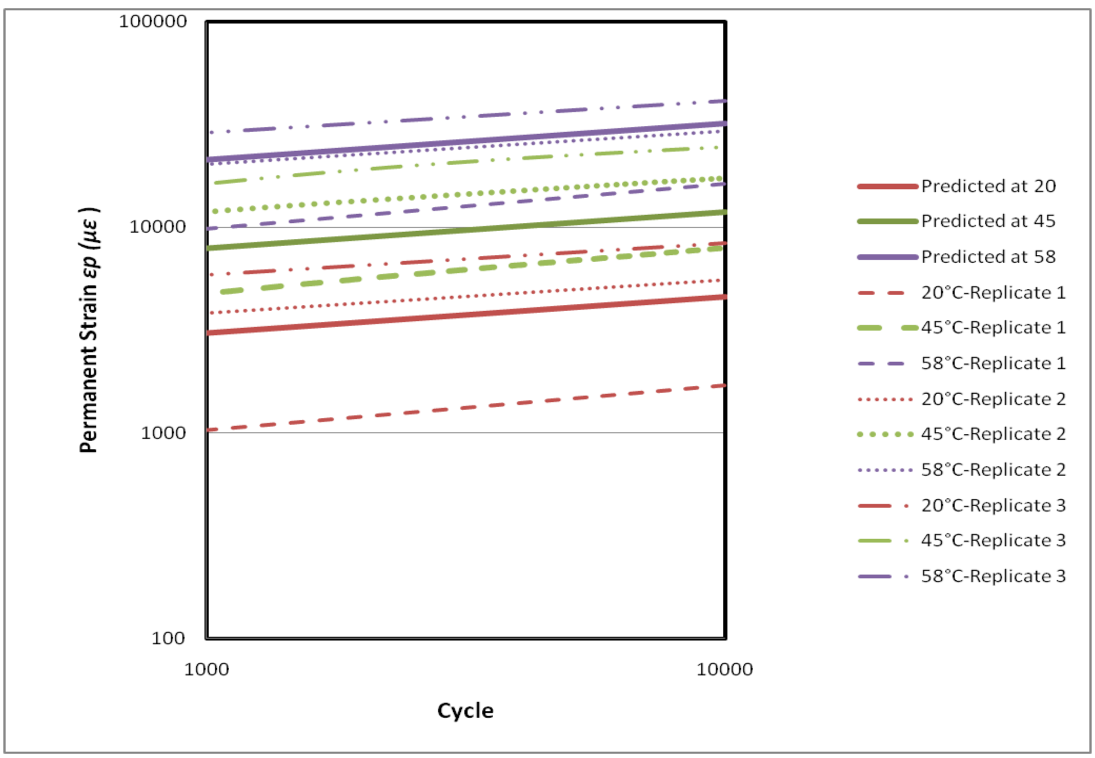

Figure A.II. 11. 14-1001

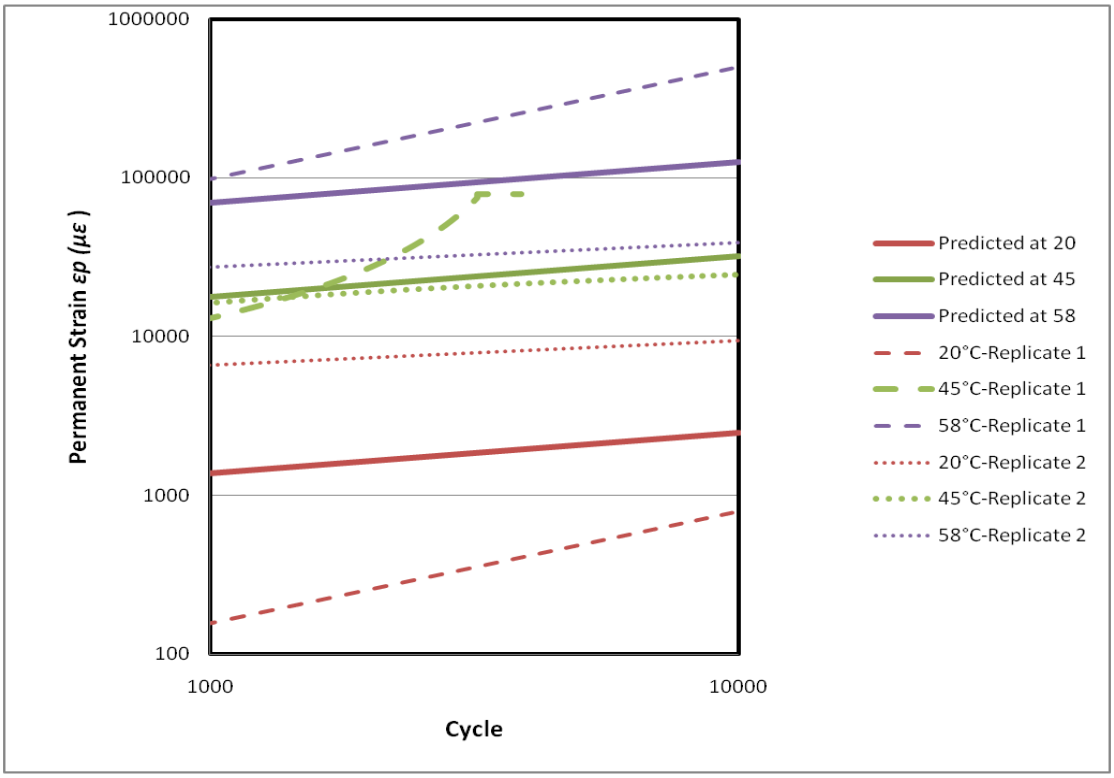

Figure A.II. 12. 14-1002

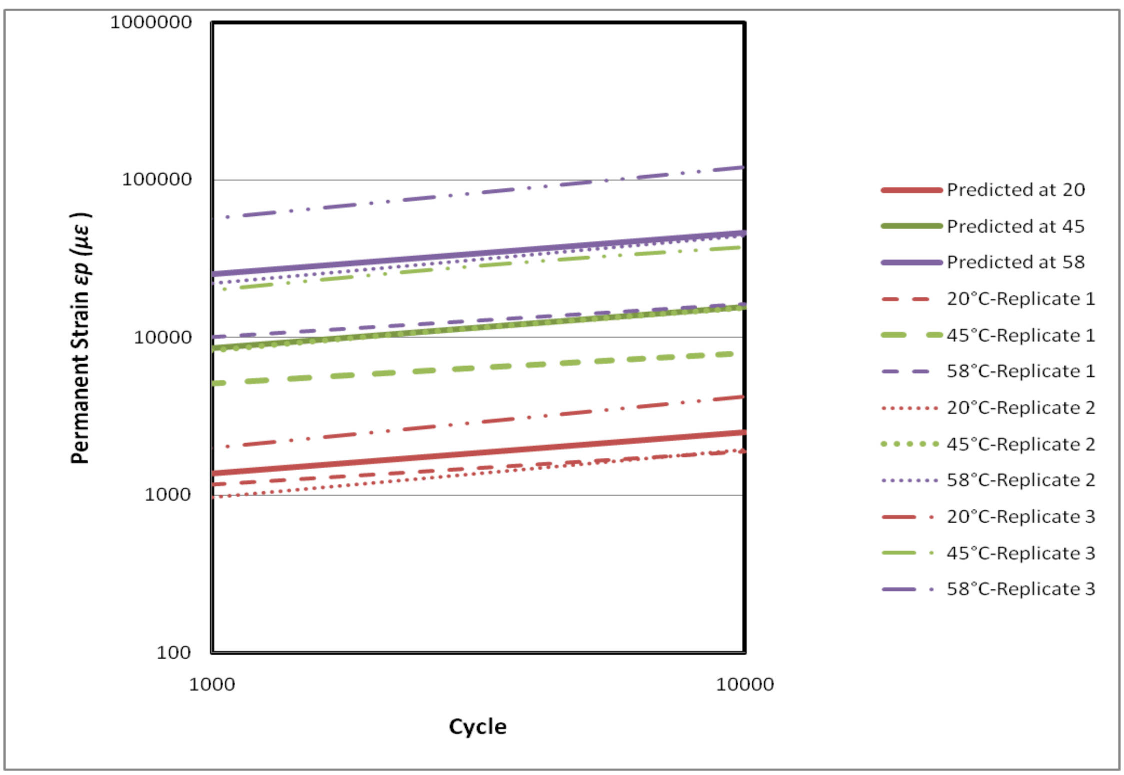

Figure A.II. 13. 14-1003

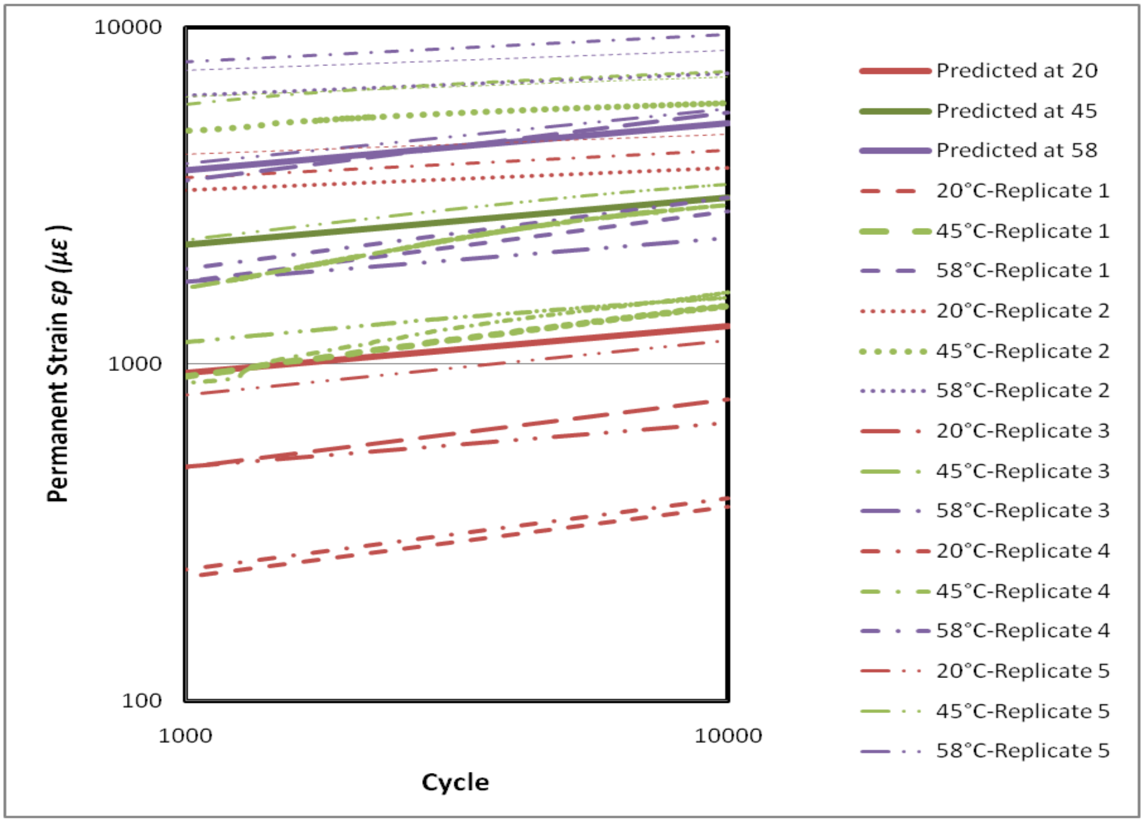

Figure A.II. 14. 14-1011

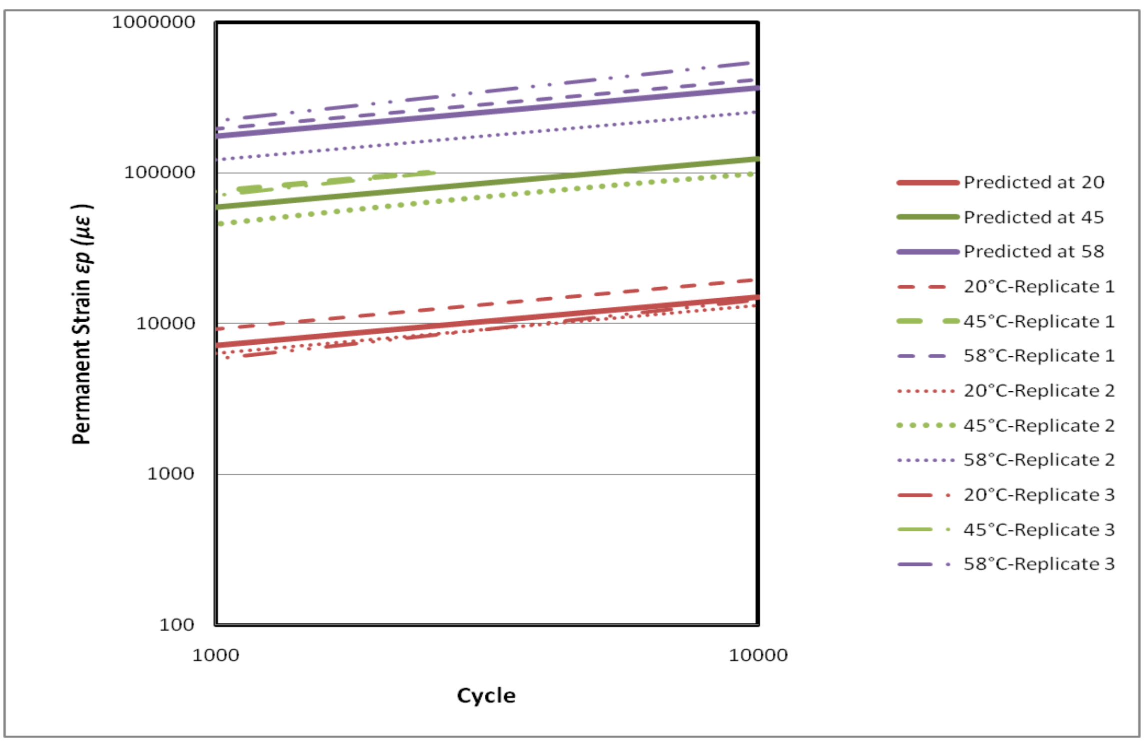

Figure A.II. 15. 14-1025

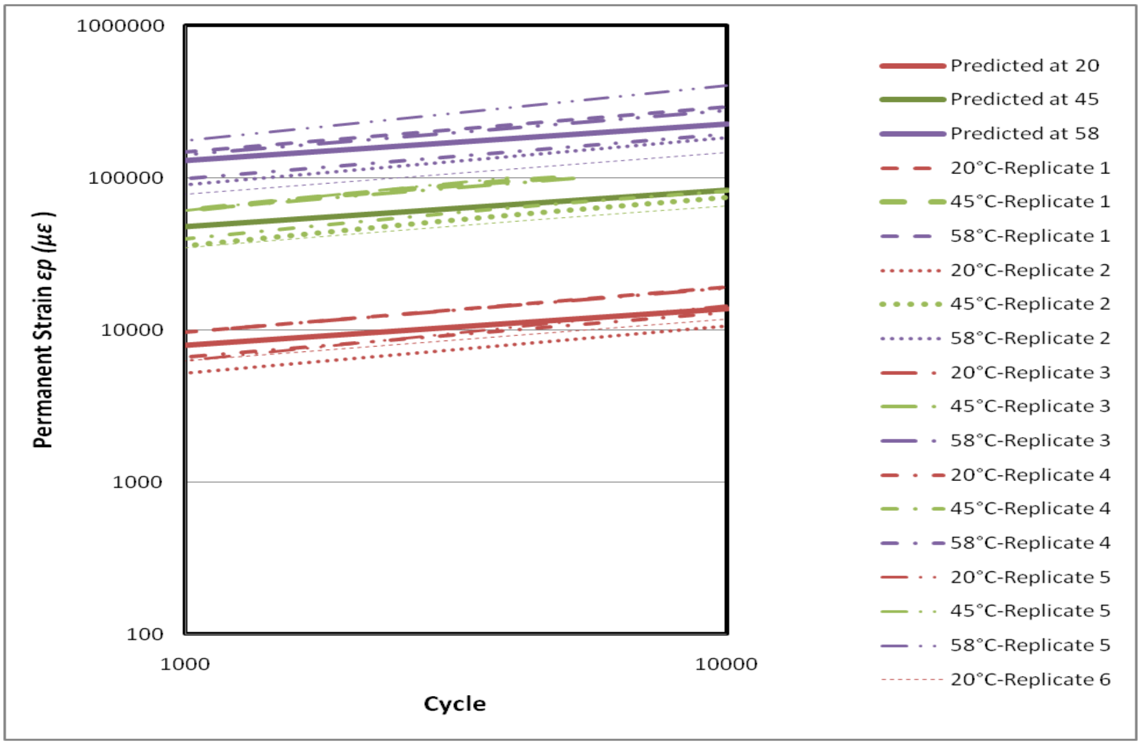

Figure A.II. 16. 14-1026

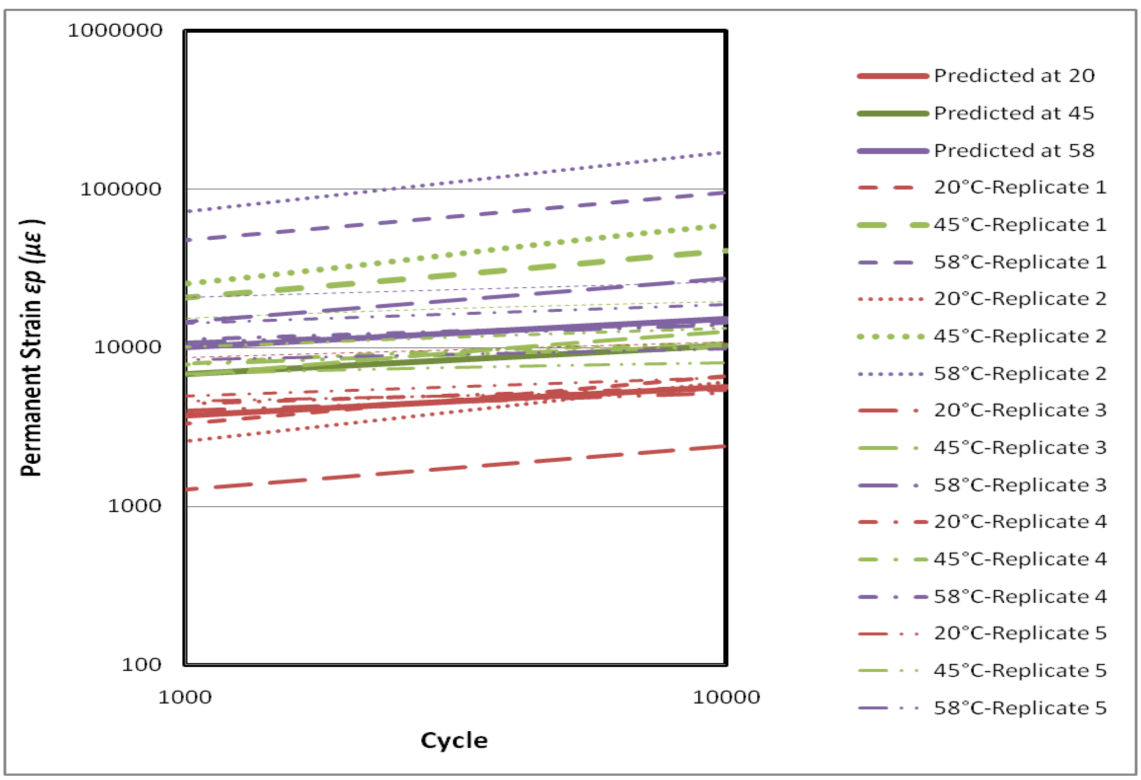

Figure A.II. 17. 14-1027

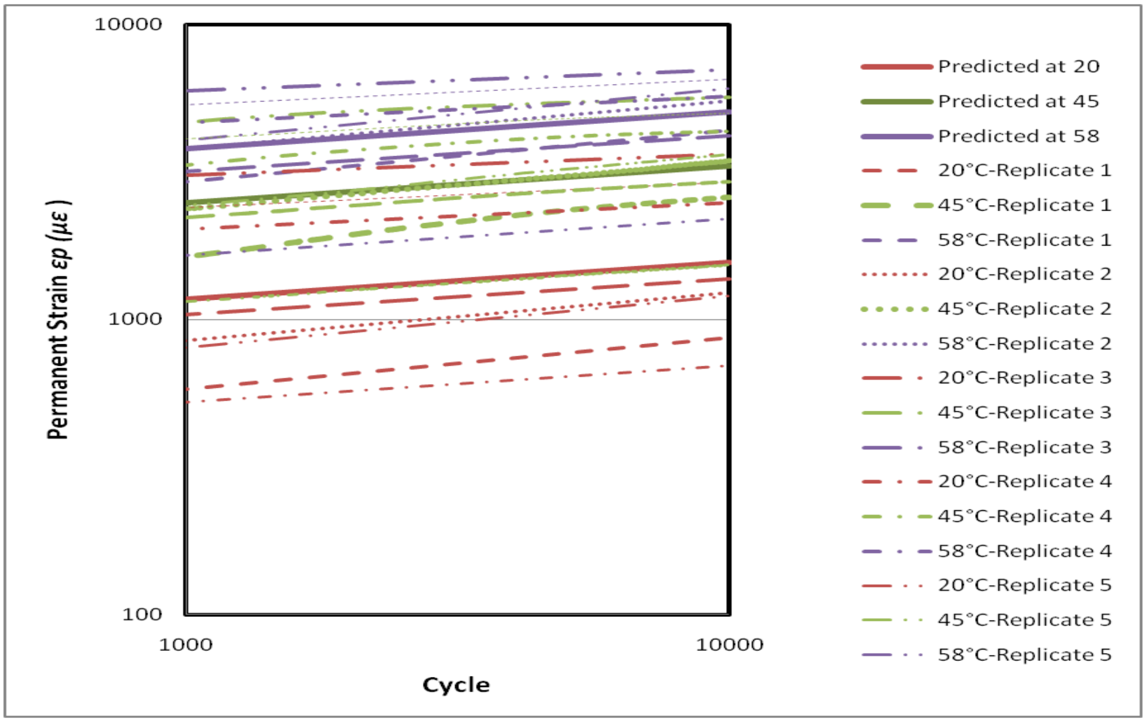

Figure A.II. 18. 14-1028

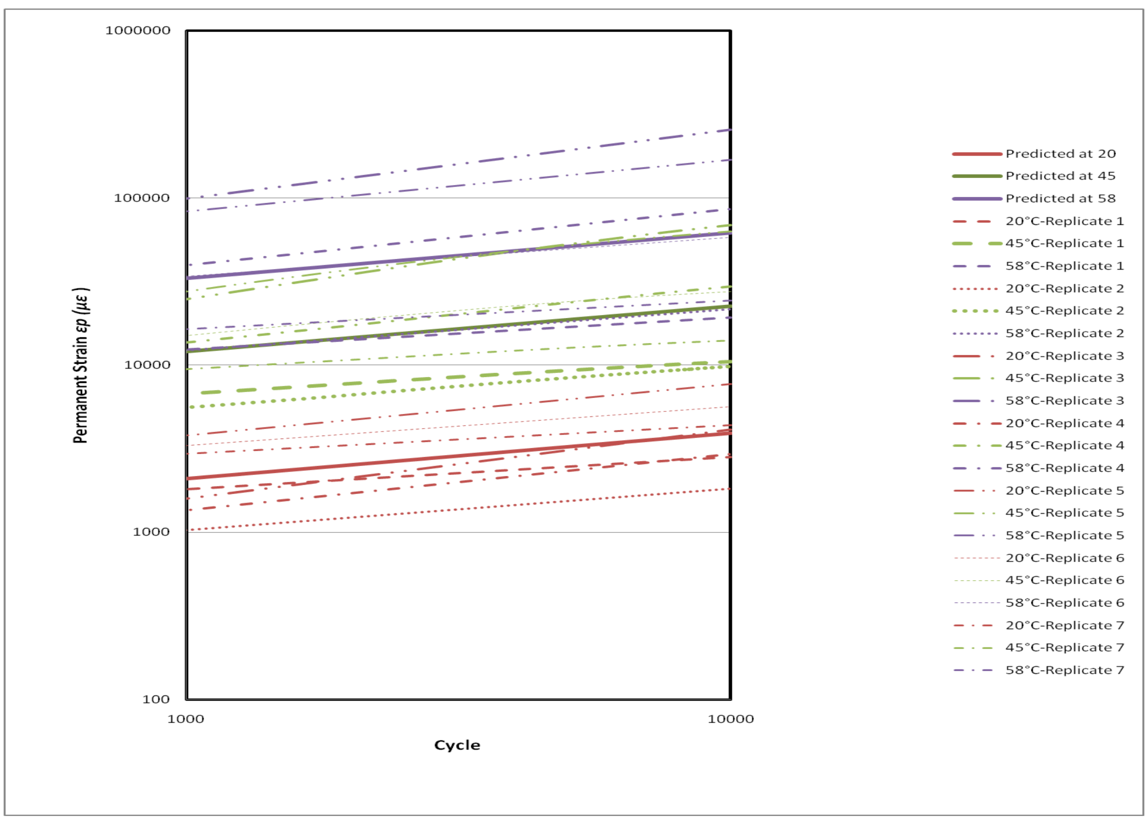

Figure A.II. 19. 14-1055

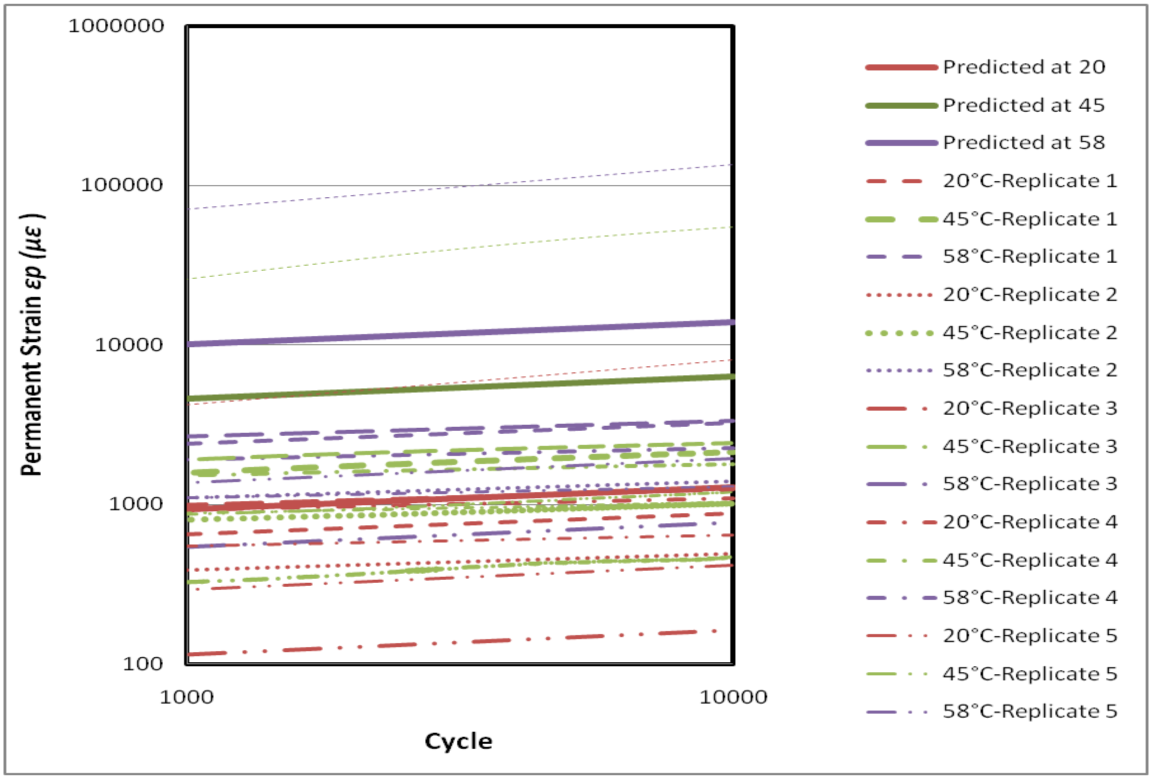

Figure A.II. 20. 10-1057

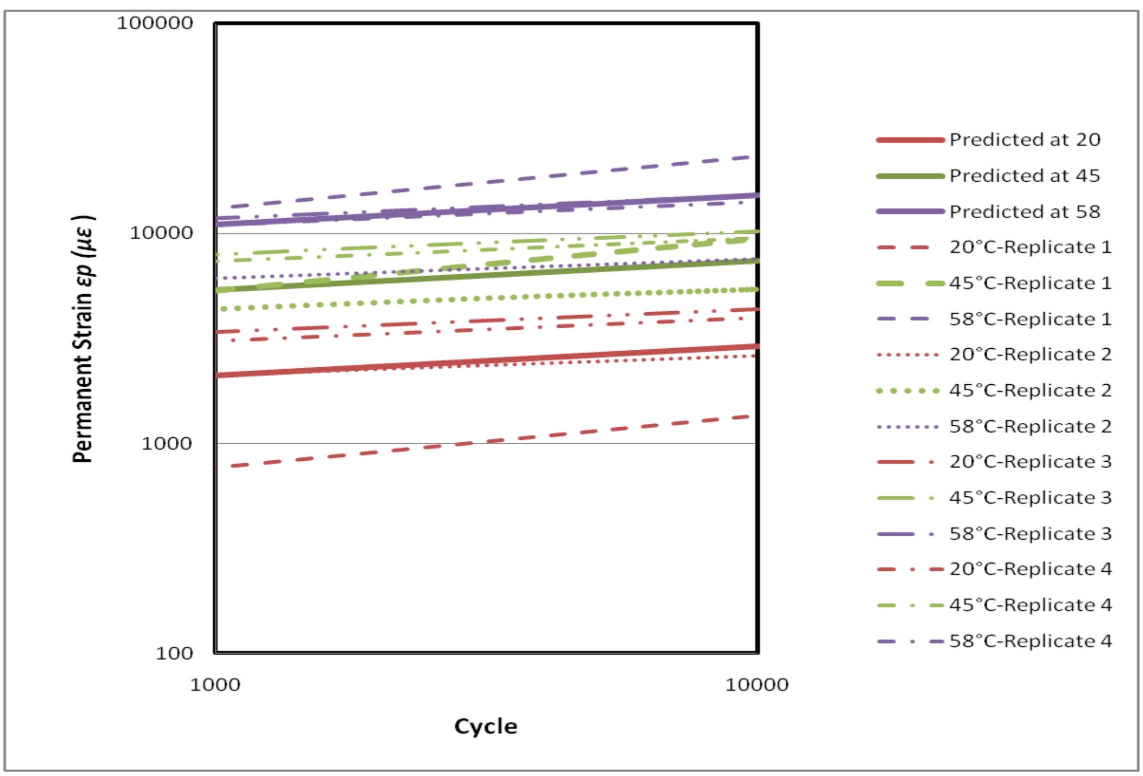

Figure A.II. 21. 14-1058

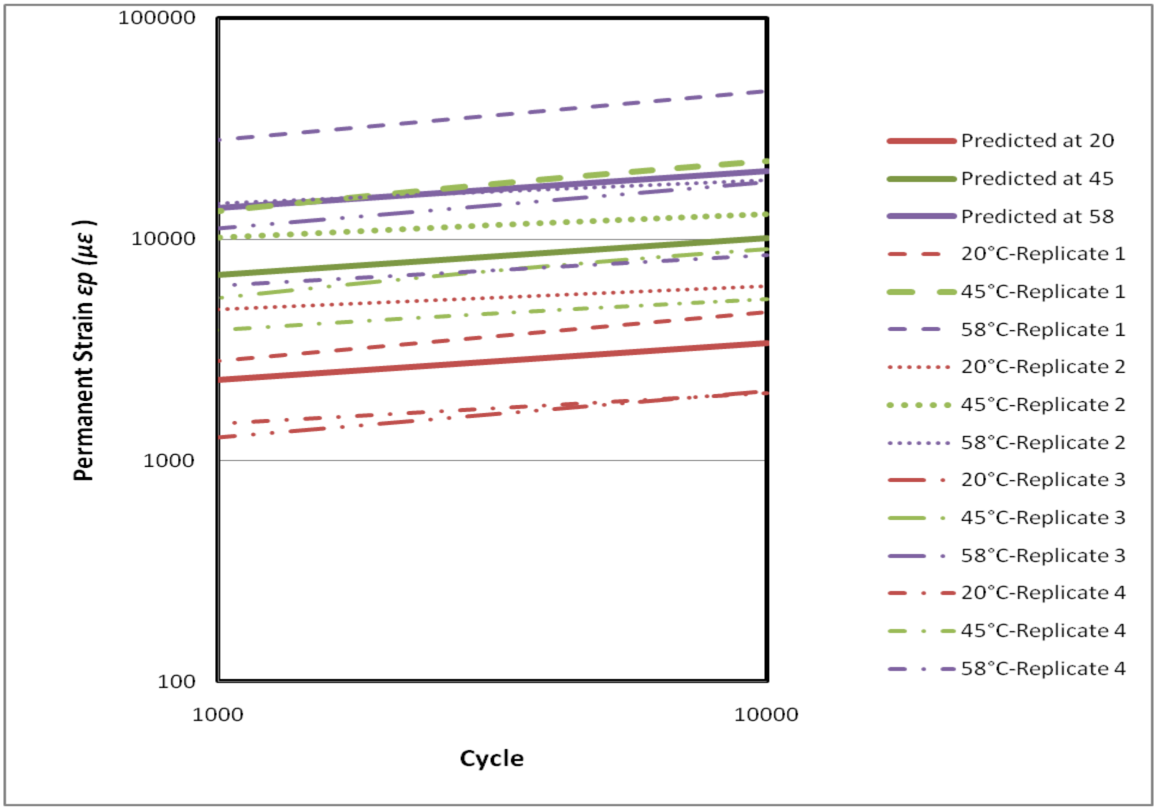

Figure A.II. 22. 14-1062

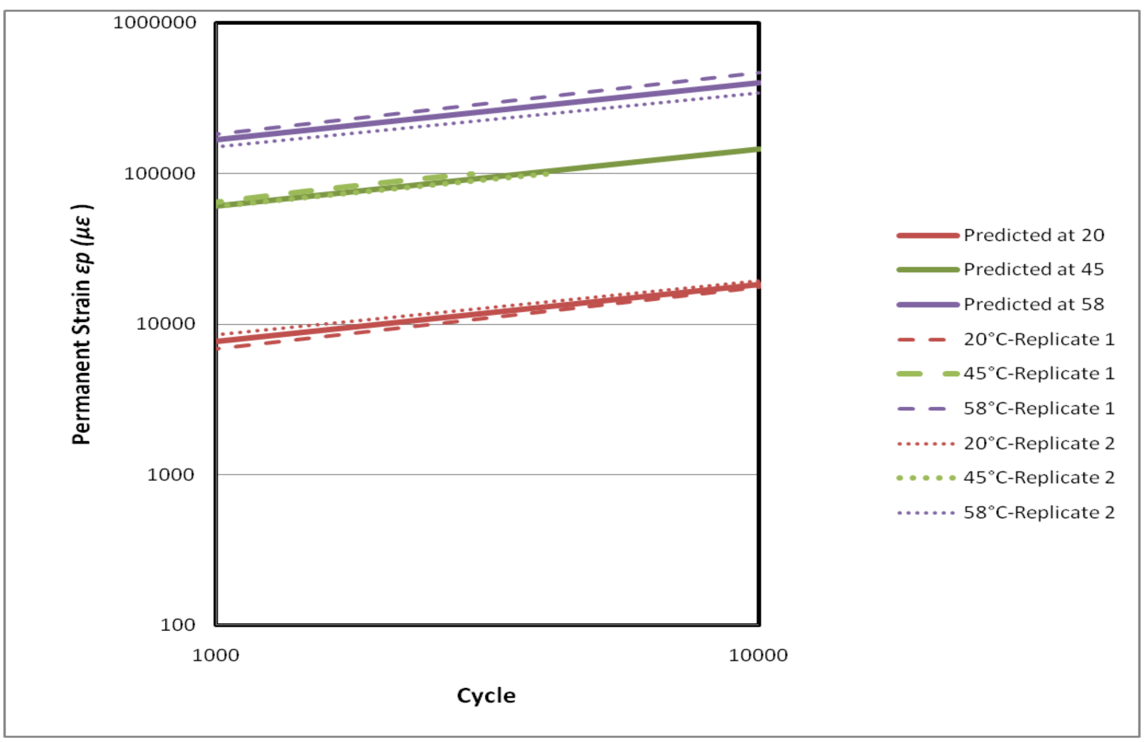

Figure A.II. 23. 15-1002

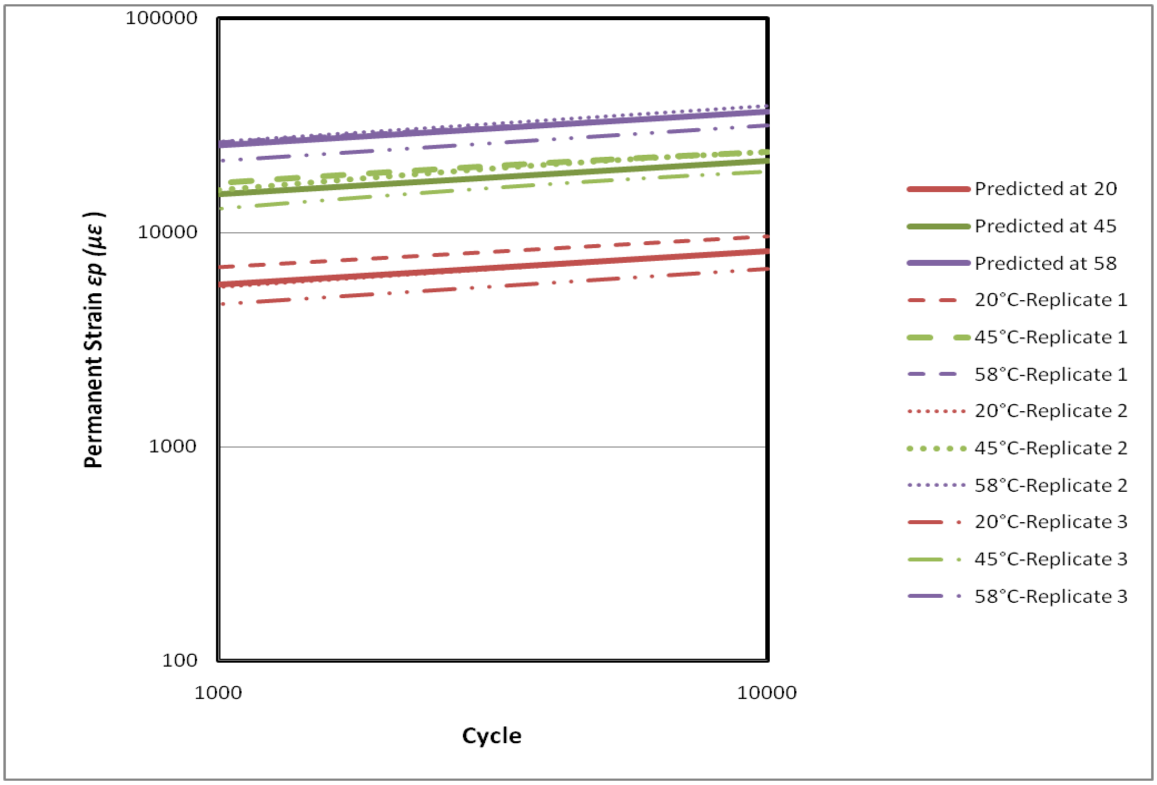

Figure A.II. 24. 15-1003

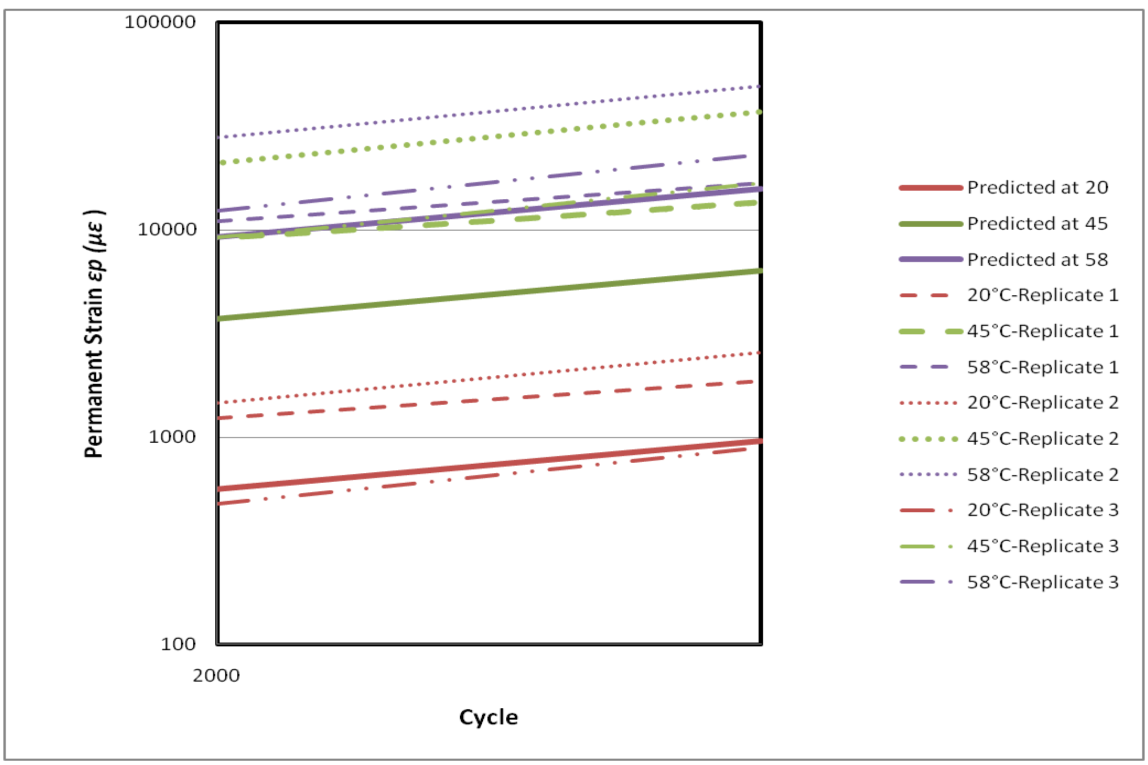

Figure A.II. 25. I-81CCPR

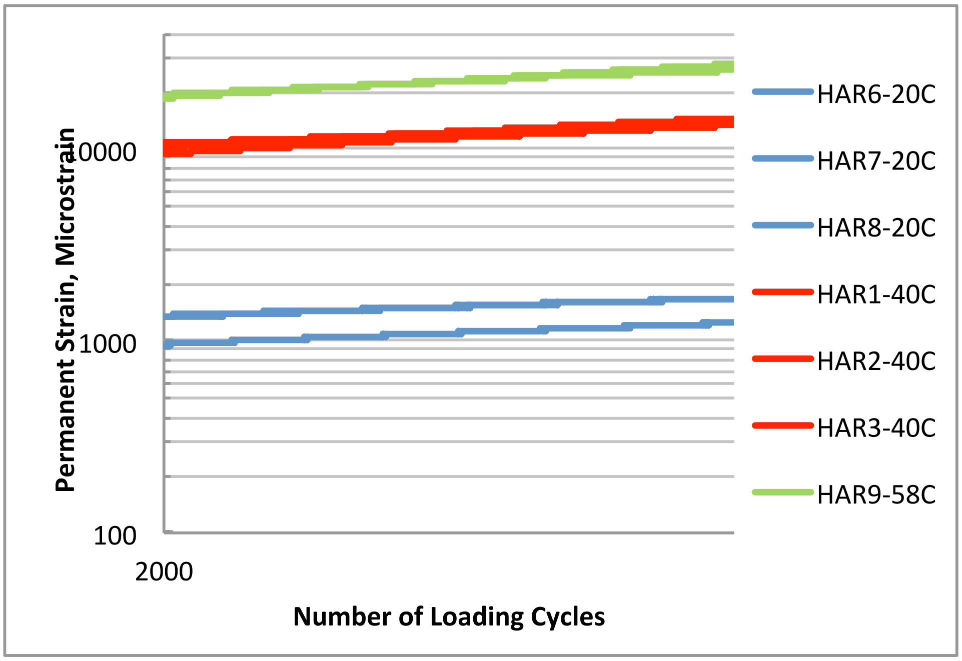

Figure A.II. 26. H160A09

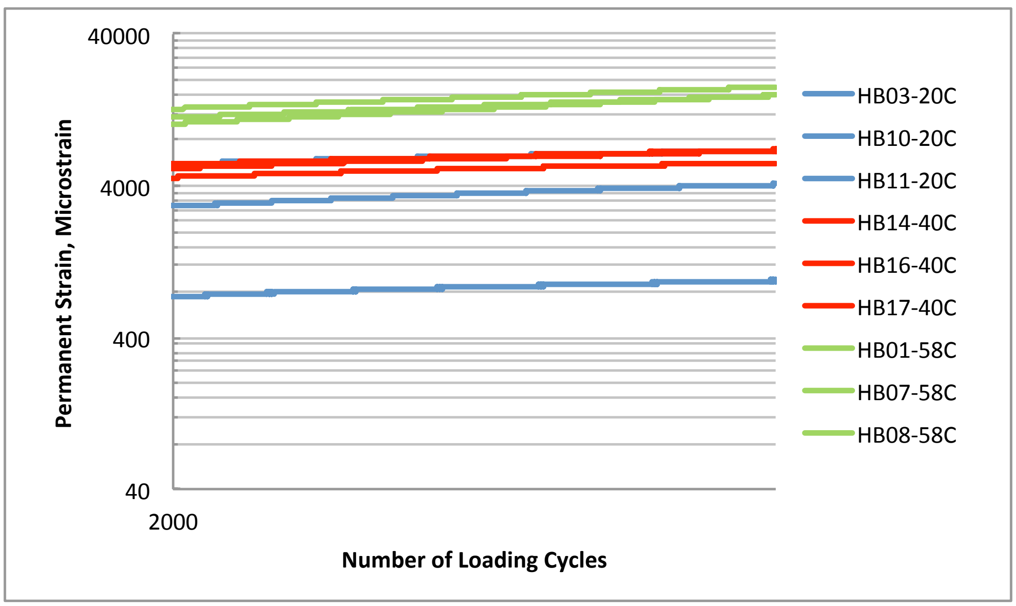

Figure A.II. 27. H151B19

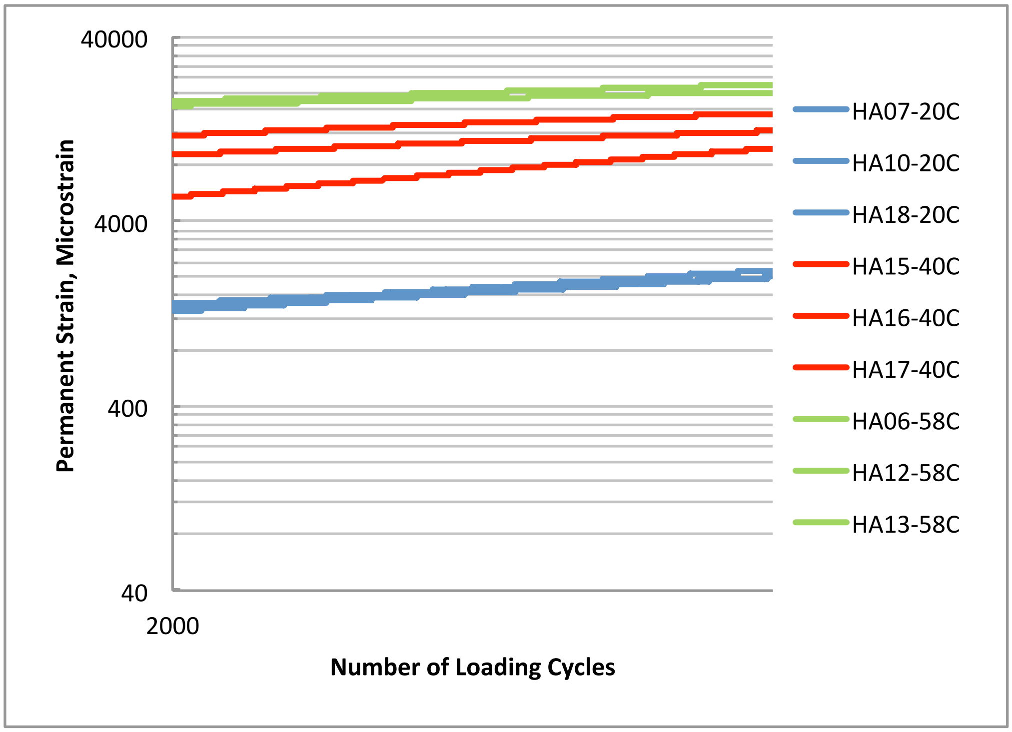

Figure A.II. 28. H135A19

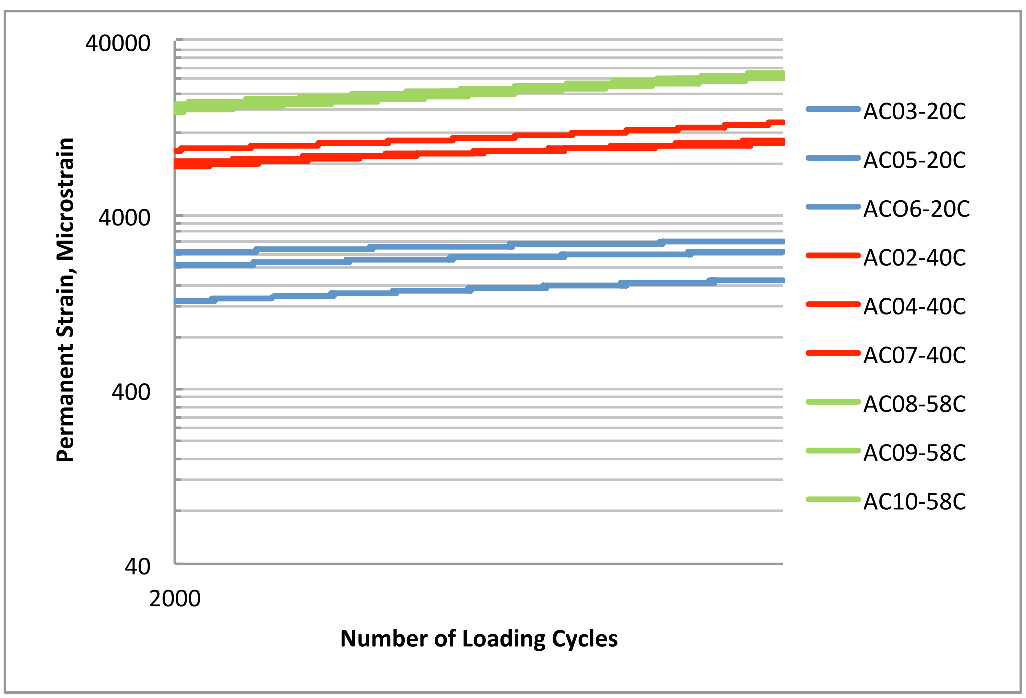

Figure A.II. 29. H077A09

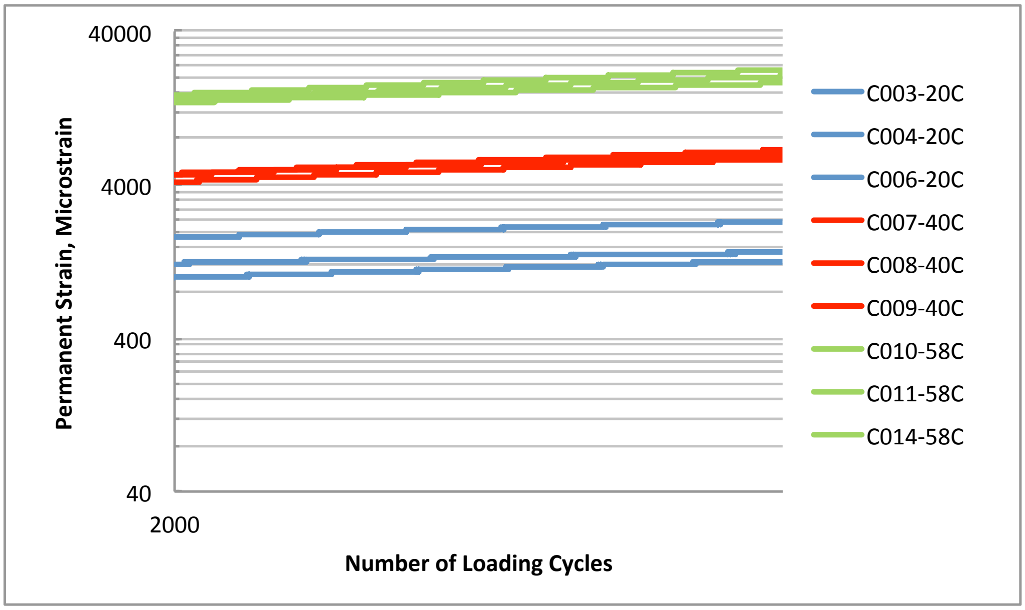

Figure A.II. 30. H083A12

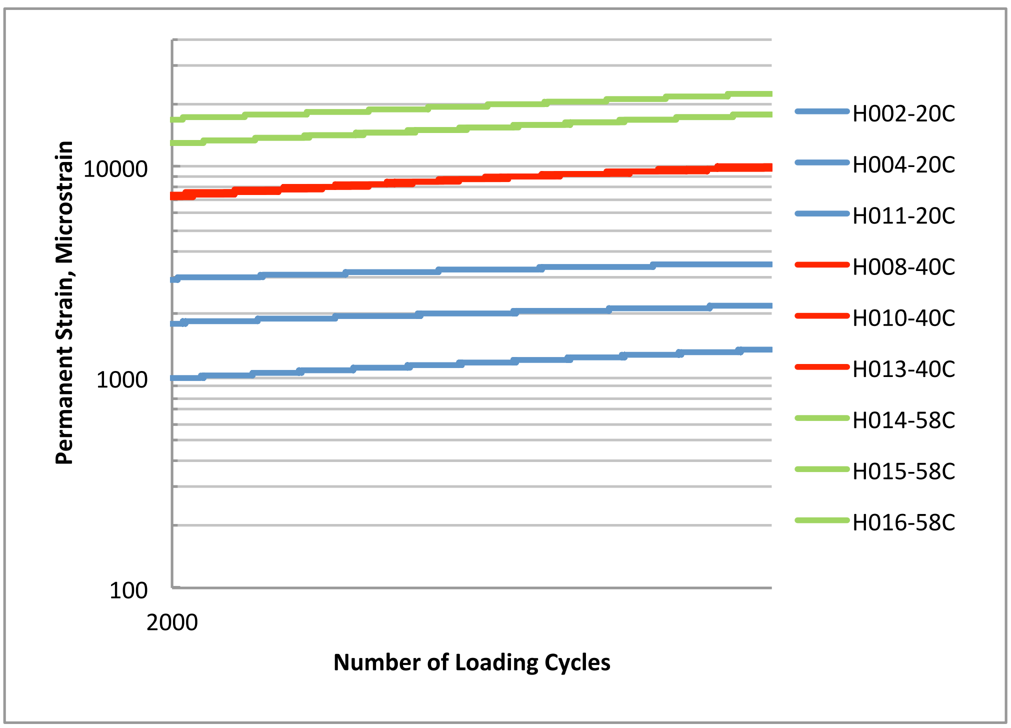

Figure A.II. 31. H127A12

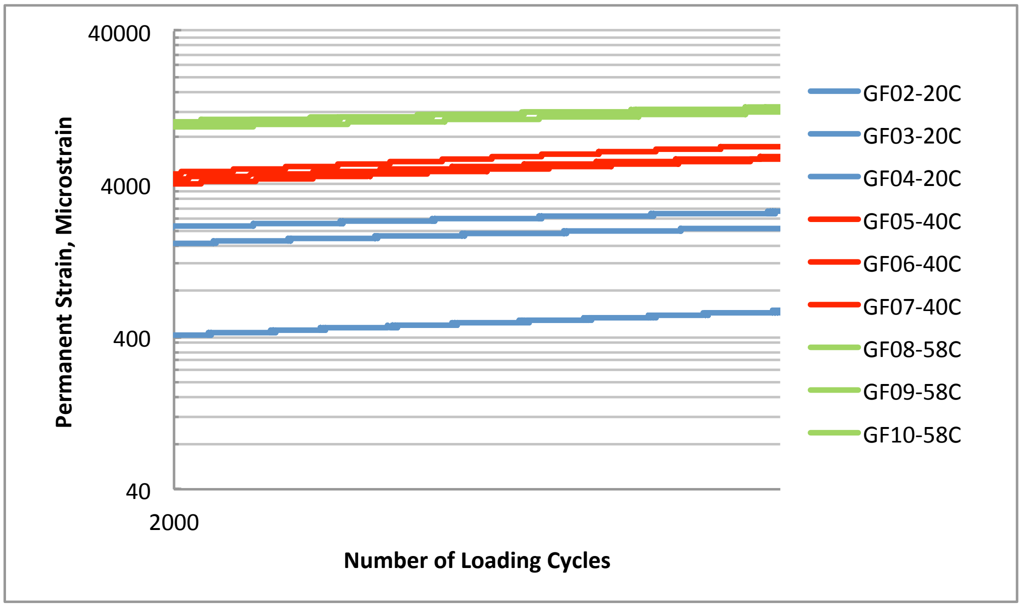

Figure A.II. 32. H135A12

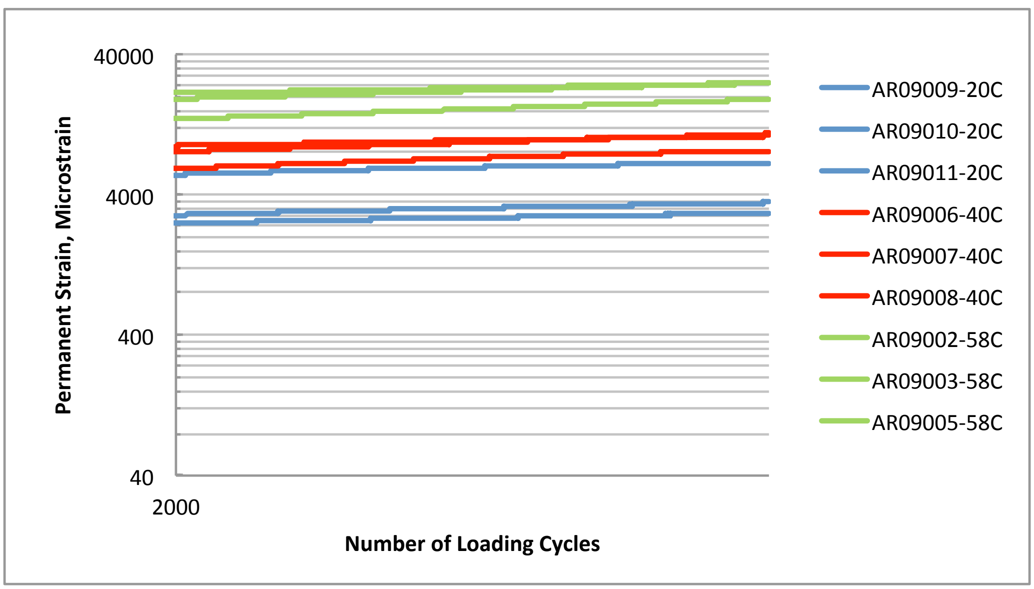

Figure A.II. 33. H168A09

Table A.II. 1Master curve fitting parameters for recycled projects

	Min	beta	gamma	EA	Max
13-1093	0.0016791	-1.8174	-0.21383	252000	2534.3
13-1111	0.084092	-1.4515	-0.33865	224000	2329
13-1112	0.038163	-1.4458	-0.32811	213000	3047.3
13-1113	0.12615	-1.3259	-0.33742	206000	2385.2
13-1114	0.56043	-1.0344	-0.39988	211000	2200.5
13-1115	11.941	1.4493	-0.17885	-9390.2	10600000
13-1116	12.424	-0.97124	-0.53211	152000	651.52
13-1117	1.9816	-2.1946	-0.25261	202000	1638.1
13-1124	0.084866	-1.9693	-0.34403	210000	1444.7
13-1127	0.000216	-2.3869	-0.25742	240000	1847.7
14-1001	0.0000033	-2.7805	-0.34169	219000	2213.7
14-1002	0.00013861	-2.538	-0.33434	194000	840.09
14-1003	0.88567	-1.5737	-0.37066	219000	1888.8
14-1011	0.73169	-1.5812	-0.26231	190000	1136.9
14-1025	0.78222	-0.8811	-0.39841	198000	2525.1
14-1026	0.52253	-0.98696	-0.36398	196000	3549.6
14-1027	2.1349	-0.86351	-0.26399	189000	4430.1
14-1028	81.242	-1.1424	-0.58093	197000	890.76
14-1055	0.57479	-1.2819	-0.33644	213000	2669.3
14-1057	1.1689	-1.7778	-0.25004	215000	1345.8
14-1058	3.0952	-1.5424	-0.34917	244000	2003.5
14-1062	0.20546	-1.56	-0.26679	222000	1722.3
15-1002	0.0073071	-1.2929	-0.24251	171000	1610.5
15-1003	3.9228	-0.66208	-0.33687	198000	1708.7
I-81CIR	0.1623	-1.5442	-0.3334	169000	1850.9
I-81CCPR	21.902	-1.2686	-0.46738	179000	1017.7

Appendix III: NCHRP 9-51 project information

Table A.III. 1. Dynamic modulus for recycled projects

	4C-25Hz	20C-10Hz	40c-1Hz
13-1093	0.13898	1009.8	486.79
13-1111	0.33242	1225.7	539.07
13-1112	0.33591	1421.4	592.7
13-1113	0.22686	1139.3	496.81
13-1114	0.76633	1147.3	447.61
13-1115	1.091	273.34	240.43
13-1116	4.586	488.38	317.01
13-1117	0.70209	1217	959.38
13-1124	1.8808	984.51	601
13-1127	0.23029	1092.9	640.84
14-1001	3.4249	1552	938.89
14-1002	0.21256	570.36	364.07
14-1003	1.0077	1278.6	723.65
14-1011	12.27	637.49	416.53
14-1025	0.16755	1169.8	435.12
14-1026	1.2413	1508.1	577.9
14-1027	0.65191	1423.7	683.9
14-1028	3.5244	805.64	619.81
14-1055	1.818	1398.9	660.33
14-1057	21.218	855.92	592.83
14-1058	1.1839	1433.4	857.73
14-1062	1.9236	890.58	492.33
15-1002	2.7471	399.84	182.03
15-1003	0.12023	732	332.94
I-81CIR	0.70796	964.42	535.98
I-81CCPR	0.6562	813.43	572.59

Table A.III. 2. Recycled projects information

	Bulk Density	Stabilizer Content	P200	Cu	Cz
13-1093	125.12	2.5	5.5	29.1824	1.747325
13-1111	136.93	1	5.5	16.31	0.56
13-1112	133.14	1.2	5.7	13.46	0.45
13-1113	135.86	1	8.4	19.48	0.72
13-1114	130.45	1.2	5.7	13.46	0.45
13-1115	119.09	2.5	7.8	43.85	1.94
13-1116	122.5	2	9.3	47.06	0.74
13-1117	130.4	2.5	7	22.06	2.26
13-1124	140.79	2.2			
13-1127	126.36	2.5	5.4	17.88	1.04
14-1001	130.83	3	4.5	26.32	1.14
14-1002	117.92	3	6.6	21.07	1.07
14-1003	139.55	3	6.5	29.48	1.26
14-1011	118.87	3.4	9.8	38.08	3.02
14-1025	135.9	3.5			
14-1026	135.03	3.5			
14-1027	133.24	3.5	7.2	39.7	2.02
14-1028	130.05	3.5	19.2	41.68	2.03
14-1055	133.6				
14-1057	127.4	2	7.6	22.55	2.73
14-1058	131.44	2	8	22.85	2.10
14-1062	131.05	3	8.9	60.91	2.25
15-1002	131.5	3			
15-1003	124	3.5			
I-81-CIR	-	2			
I-81-CCPR	-	2	5.95	16.8171	1.2748

Table A.III. 3. Recycled projects information

	OL thickness	Curing Time	Dry Additive	Depth of Recycling
13-1093	1.5	494	1	4
13-1111	0	507	0	4
13-1112	0	538	0	4
13-1113	0	447	0	4
13-1114	0	538	0	3
13-1115	2.9527	495	1	7.874
13-1116	2.9527	458	1.5	6.9
13-1117	2.9527	517	1	7.874
13-1124	2	426	1	4
13-1127	2.00	504.00	1.5	4.00
14-1001	1.50	707.00	0.00	3.00
14-1002	0.00	881	0.05	3.00
14-1003	2	1080	0.00	2.50
14-1011	2	718	1.00	-
14-1025	0	819	0.00	4
14-1026	0	773	0.00	4
14-1027	0	742	0.00	6
14-1028	0	742	0.00	6
14-1055	1	600	0.00	3
14-1057	2	756	3	8
14-1058	2.4	464	1.5	3.6
14-1062		541	1.5	4
15-1002		966	1	2
15-1003		966	1	1
I-81-CIR		420	1	5
I-81-CCPR	2	420	1	8

Table A.III. 4. Volumetric properties of HMA mixtures

MixDesignID	Gmm	Gmb	Gse	Pb	Pba	Pbe	Va	VMA	VFA	Percent RAP	Binder Grade
H077A09A2C3	2.567	2.385	2.785	5.2	0.6	4.6	7	15.1	73.3	-	64-22
H083A12C2C2	2.583	2.4	2.796	4.8	0.4	4.4	7	14.6	72.7	14.5	64-22
H127A12R2C2	2.578	2.393	2.775	5.1	0.2	4.9	7	15.7	74.5	19	64-22
H135A12G4F1	2.445	2.27	2.685	6.7	0.3	6.4	7	18.1	80.7	-	76-22
H135A19G4F1	2.435	2.252	2.686	6.5	0.1	6.4	7	18.1	80.7	-	76-22
H151B19R2C2	2.57	2.39	2.721	4.1	0.1	4	7	13.8	71.3	15	64-22
H16809R2C02	2.53	2.352	2.783	5.9	1.1	4.8	7	17.53	60.07	15	64-22

Table A.III. 5. Gradation of HMA mixtures

MixDesignID	37.5 mm	25 mm	19 mm	12.5 mm	9.5 mm	4.75 mm	2.36 mm	1.18 mm	0.6 mm	0.3 mm	0.15 mm	0.075 mm
H083A12C2C2	100	100	100	98	83	50	33	24	18	12	8	5.7
H127A12R2C2	100	100	100	98	90	62	34	22	15	12	10	7.5
H135A12G4F1	100	100	100	97	82	37	20	16	14	12	11	8.5
H135A19G4F1	100	100	100	82	43	22	16	13	12	11	10	9
H151B19R2C2	100	100	95	74	60	39	25	18	13	9	7	5.3
H16809R2C02	100	100	100	100	92	70	44	27	18	12	10	7.4

Bibliography

AASHTO, Guide. "'Guide for Design of Pavement Structures." American Association of State Highway and Transportation Officials, Washington, DC(1993).

AASHTO, Mechanistic-Empirical Pavement Design Guide. "A manual of Practice." Interim Edition, July (2008).

Bemanian, Sohila, Patty Polish, and Gayle Maurer. "Cold in-place recycling and full-depth reclamation projects by nevada department of transportation: State of the practice." Transportation Research Record: Journal of the Transportation Research Board 1949 (2006): 54-71.

Bemanian, Sohila, Patty Polish, and Gayle Maurer. "Cold in-place recycling and full-depth reclamation projects by nevada department of transportation: State of the practice." Transportation Research Record: Journal of the Transportation Research Board 1949 (2006): 54-71.

BOWERS, BENJAMIN F. "Asphalt Mixture Performance Characterization Using Small-Scale Cylindrical Specimens." Contract 2015 (2013).

Ceylan, Halil, Kasthurirangan Gopalakrishnan, and Sunghwan Kim. "Advanced approaches to hot-mix asphalt dynamic modulus prediction."Canadian Journal of Civil Engineering 35, no. 7 (2008): 699-707.

Chen, Don, Charles T. Jahren, Hosin "David Lee, R. Chris Williams, Sunghwan Kim, Michael Heitzman, and Jungyong "Joe Kim. "Effects of recycled materials on long-term performance of cold in-place recycled asphalt roads." Journal of Performance of Constructed Facilities 24, no. 3 (2009): 275-280.

Diefenderfer, Brian K., and Alex K. Apeagyei. Analysis of full-depth reclamation trial sections in Virginia. No. FHWA/VCTIR 11-R23. 2011.

Diefenderfer, Brian K., Benjamin F. Bowers, Charles W. Schwartz, Azadeh Farzaneh, and Zhuoyi Zhang. "Dynamic Modulus of Recycled Pavement Mixtures." Transportation Research Record: Journal of the Transportation Research Board 2575 (2016): 19-26.

Fu, Pengcheng, David Jones, and John T. Harvey. "Micromechanics of the effects of mixing moisture on foamed asphalt mix properties." Journal of Materials in Civil Engineering 22, no. 10 (2010): 985-995.

Jahren, Charles T., Bryan Cawley, Brian Ellsworth, and Kenneth L. Bergeson. "Review of cold in-place asphalt recycling in Iowa." Proceedings of the Transportation Research Board (1998).

Kazmierowski, Tom, Pamela Marks, and Stephen Lee. "Ten-year performance review of in situ hot-mix recycling in Ontario." Transportation Research Record: Journal of the Transportation Research Board 1684 (1999): 194-202.

Khosravifar, Sadaf, Intikhab Haider, Zahra Afsharikia, and Charles W. Schwartz. "Application of time–temperature superposition to develop master curves of cumulative plastic strain in repeated load permanent deformation tests." International Journal of Pavement Engineering 16, no. 3 (2015): 214-223.

Kim, Yongjoo, Hosin "David Lee, and Michael Heitzman. "Dynamic modulus and repeated load tests of cold in-place recycling mixtures using foamed asphalt." Journal of Materials in Civil Engineering 21, no. 6 (2009): 279-285.

Kim, Yongjoo, Soohyok Im, and Hosin "David Lee. "Impacts of curing time and moisture content on engineering properties of cold in-place recycling mixtures using foamed or emulsified asphalt." Journal of Materials in Civil Engineering 23, no. 5 (2010): 542-553.

Koehn, Philipp. "Combining genetic algorithms and neural networks: The encoding problem." (1994).

Long, F. M., and D. F. C. Ventura. "Laboratory Testing for the HVS Sections on the N7 (TR11/1)." CSIR Transportek, Contract Report CR-2003/56. Pretoria, South Africa (2003).

Manual, Basic Asphalt Recycling. "Asphalt recycling and reclaiming association." Annapolis, Maryland (2001).

Meier, Roger W., and Glenn J. Rix. "Backcalculation of flexible pavement moduli using artificial neural networks." Transportation research record 1448 (1994).

Mirzahosseini, Mohammadreza, Yacoub M. Najjar, Amir H. Alavi, and Amir H. Gandomi. "Next-Generation Models for Evaluation of the Flow Number of Asphalt Mixtures." International Journal of Geomechanics 15, no. 6 (2015): 04015009.

Mohammad, Louay, Ananda Herath, Masood Rasoulian, and Zhang Zhongjie. "Laboratory evaluation of untreated and treated pavement base materials: Repeated load permanent deformation test." Transportation Research Record: Journal of the Transportation Research Board 1967 (2006): 78-88.

Mohammad, Louay, Murad Y. Abu-Farsakh, Zhong Wu, and Chris Abadie. "Louisiana experience with foamed recycled asphalt pavement base materials." Transportation Research Record: Journal of the Transportation Research Board 1832 (2003): 17-24.

Morian, Dennis, Jeffrey Oswalt, and Akshay Deodhar. "Experience with cold in-place recycling as a reflective crack control technique: Twenty years later."Transportation Research Record: Journal of the Transportation Research Board 1869 (2004): 47-55.

Moulthrop, J., and M. Witczak. "NCHRP report 704: a performance-related specification for hot-mixed asphalt." Transportation Research Board, Washington (DC) (2011).

Sanjeevan, Selvaratnam, Murugaiyah Piratheepan, Elie Hajj, and Anita Bush. "Cold In-Place Recycling in Nevada: Field Performance Evaluation over the Past Decade." Transportation Research Record: Journal of the Transportation Research Board 2456 (2014): 146-160.

Sebaaly, Peter, Gabriel Bazi, Edgard Hitti, Dean Weitzel, and Sohila Bemanian. "Performance of cold in-place recycling in Nevada."Transportation Research Record: Journal of the Transportation Research Board 1896 (2004): 162-169.

Seo, Youngguk, Omar El-Haggan, Mark King, S. Joon Lee, and Y. Richard Kim. "Air void models for the dynamic modulus, fatigue cracking, and rutting of asphalt concrete." Journal of Materials in Civil Engineering 19, no. 10 (2007): 874-883.

Witczak, M., C. Schwartz, and H. Von Quintus. "NCHRP Project 9-19: Superpave support and performance models management." Interim Report, Federal highway administration and the national cooperative highway research program (2001).

Yun, Taeyoung, B. Shane Underwood, and Y. Richard Kim. "Time-temperature superposition for HMA with growing damage and permanent strain in confined tension and compression." Journal of Materials in Civil Engineering 22, no. 5 (2009): 415-422.

Zhao, Yanqing, Hui Liu, and Wanqiu Liu. "Characterization of linear viscoelastic properties of asphalt concrete subjected to confining pressure."Mechanics of Time-Dependent Materials 17, no. 3 (2013): 449-463.